Experimental Validation of New Vacuum Bag Only Processing Techniques for Co-bonded Composite Repairs

Andrew MACLEAN
Department of Mechanical Engineering
MCGILL UNIVERSITY, MONTREAL
August 2017

A thesis submitted to McGill University in partial fulfillment of the requirements of the degree of Master of Engineering

Abstract

In service damage is inevitable for commercial aircraft structures. Although carbon fibre reinforced thermoset polymers are now extensively used, inefficient bolted repair techniques are still relied on for their structural repair. Improved mechanical property recovery, reduced weight and reduced drag are offered by co-bonded scarf repairs, in which a prepreg or wet layup composite patch and adhesive are cured simultaneously to a scarfed damaged structure. However, co-bonded repair processing is a challenge, with several quality and inspection issues currently precluding their use in structural repairs. In particular, robust procedures are needed to reduce their high void content which has led to reduced strength, durability and inspectability.

When cold temperature storage is inconvenient, wet layup repair materials are used. There has been little research into wet layup repair processes, which currently yield very high void contents of 5-10 %. Therefore the primary objective of this work will be **to develop an improved understanding of the wet layup repair process**, and then **to propose improved procedures and validate these on a decommissioned aircraft structure**. A secondary objective will be **to validate semi-impregnated prepreg with an air breathable adhesive film on this structure**. This material combination recently demonstrated improved quality and robustness relative to established prepreg methods, but has yet to applied to a real structure.

Firstly, to assess the effect of several processing variables on void content, many wet layup repair patches were manufactured according to a Taguchi design of experiments test matrix. These lab scale experiments permitted more robust, low void content wet layup repair processes to be designed. These processes were confirmed to yield reduced void content as well as significantly improved short beam strength.

Compared to controlled laboratory conditions, repairing a real structure introduces process deviations such as pre-bond moisture and thermal gradients due to one-sided heating. Therefore both the improved wet layup repair methods developed in this work, as well semi-impregnated prepreg with air an breathable adhesive film, were applied to repair a decommissioned A320 elevator. Overall the improved wet layup and prepreg co-bonded repair materials and processes led to significant quality improvements relative to established methods.

Sommaire

Présentement, on compte sur les réparations boulonnées pour rétablir la résistance mécanique des pièces aéronautiques en polymères thermodurcissables renforcés de fibres de carbone endommagés en service. Par contre, les réparations co-collées en biseau, employant des matériaux composites pré-imprégnés ou *wet layup* ainsi qu'un film adhésif, offrent une meilleure performance mécanique avec moins de poids et de traînée. La mise en œuvre de ces réparations est cependant un défi, avec plusieurs problèmes de qualité et d'inspection empêchant leur application structurelle. En particulier, des procédés robustes sont nécessaires pour réduire leur taux de porosité, qui est nuisible à la récupération de résistance mécanique, la durabilité et l'inspection.

Les matériaux *wet layup* sont utilisés lorsque l'entreposage au congélateur est inconvénient. Il y a eu peu de recherche sur la qualité de ces procédés; ils mènent donc à des taux de porosité élevés de 5-10 %. Comme premier objectif, **une meilleure compréhension du procédé *wet layup* serait recherchée**, et ensuite **des procédés améliorés seront proposés ainsi que validé sur une structure d'avion décommissionnée**. Un deuxième objectif serait **de valider les matériaux semi-imprégnés et un procédé de texturation de film adhésif sur cette structure**. Dans la littérature, cette combinaison de matériaux a démontré une forte réduction de taux de porosité relative aux réparations pré-imprégnées typiques, mais n'a jamais été appliqué sur une pièce réelle.

Premièrement, plusieurs réparations *wet layup* ont été fabriquées selon un plan d'expériences Taguchi. Ces expériences en laboratoire ont permis de déduire l'effet de plusieurs variables du procédé sur la porosité et de formuler un procédé amélioré. Des réductions remarquables dans le taux de porosité ont été confirmées dans des tests de suivi, avec une augmentation importante dans la résistance au cisaillement inter-laminaire.

Comparé aux conditions de laboratoire contrôlées, la réparation d'une structure réelle entraine des défis additionnels tels que l'humidité dans la pièce à réparer et les gradients de température. Les techniques améliorées de réparation *wet layup* développées à l'échelle de laboratoire, ainsi que les matériaux semi-imprégnés et un procédé de texturation de film adhésif, ont donc été appliquées sur une gouverne de profondeur A320 décommissionnée. Globalement ces procédés et matériaux innovants ont démontré une amélioration considérable relativement aux méthodes existantes.

Acknowledgements

I would like to express my sincere gratitude to my thesis advisor Pascal Hubert. Often I focus too much on details: through your guidance I viewed my research work in a broader context that helped me to interpret results, draw conclusions and communicate effectively.

This project was made possible thanks to financial support, materials and access to equipment from the Consortium for Research and Innovation in Aerospace in Quebec (CRIAQ); the Natural Science and Engineering Research Council (NSERC); the Centre de Recherche sur les Systèmes Polymères et Composites à Haute Performance (CREPEC); Bombardier Aerospace; the National Research Council (NRC); L3-MAS; McGill University; Henkel Aerospace, Huntsman Advanced Materials and Lincoln Fabrics. I'd also like to thank Delta Airlines for generously donating the decommissioned A320 elevator.

For the many insightful discussions, friendship and support I'd like to thank all members of the Structures and Composite Materials Laboratory. In particular many thanks to my friend and closest collaborator Daniele Casari. We developed a great synergy working together, accomplishing far more in less time than would have been possible working separately. I would also like to thank Paul Bruneau for his help with short beam shear testing and the demonstrator. Special thanks go to Mathieu Préau for his generous mentorship throughout my Master's. I am also grateful to Lucie Riffard for training and assistance.

I am grateful to CFP des Moulins, particularly Stéphane Roy, Marc Boisvert and Jacques André for the scarfing and use of the hot bonder for the demonstrator repairs.

I would like to express my gratitude to Julien Walter and his team at the Centre Technologique en Aérospatiale for the NDT and related analysis of the demonstrator.

I am thankful to the industrial partners for sharing their expertise in composite repairs, in particular David Wilson, Hasan Salek, Marie-Josée Landry, Chun (Lucy) Li and Étienne Bélanger.

I am also thankful to the other academic partners in the CRIAQ COMP 507 project, for their feedback and collaboration on the demonstrator, notably Emna Ghazali and Justine Bertrand from Université Laval, and Omar Laamoumi from École Polytechnique.

Finally I would like to thank my family for their constant support.

Contributions of the Author

The work presented herein was fully carried out by the author, with the following exceptions:

Chapter 2: Daniele Casari, a McGill/École Polytechnique Fédérale de Lausanne Master's student, helped with the manufacturing of the DOE study wet layup repair patches as well the analysis of the DOE study results. Paul Bruneau, a McGill summer undergraduate research student supervised by the author, helped with the glass tool plate visualization of the random blob process, as well as with the manufacture, testing and optical microscopy of the short beam shear specimens. The DOE study results for void content were also presented in a conference paper at the SAMPE Technical Conference in Long Beach, CA in May 2016 [1]. I am the primary author of this publication.

Chapter 3: Stéphane Roy and his team at CFP des Moulins in Terrebonne, Quebec scarfed the demonstrator. Paul Bruneau helped with the processing of the demonstrator repairs. Marie-Josée Landry and her team at Bombardier Aerospace helped with the processing for two of the demonstrator repairs. Several other graduate students assisted with the processing of two of the demonstrator repairs: Mathieu Préau from McGill, Emna Ghazali and Justine Bertrand from Université Laval, and Omar Laamoumi from École Polytechnique. Julien Walter and his team at the Centre Technologique en Aérospatiale in St-Hubert, Quebec performed the NDI and analysis of the NDI results.

Contents

List of Figures

List of Tables

Chapter 1

Introduction

1.1 Motivation

1.1.1 Composite Aircraft Structures

Since the 1970s there has been a strong push to increase the fuel efficiency of commercial airliners, driving weight reduction efforts [2]. To this end carbon fibre reinforced epoxy composites were gradually introduced into commercial airliners, starting with secondary structures such as elevators and rudders in the late 1970s [2], [3]. Compared to aluminum alloys, the conventional airframe materials, these composites can offer reduced weight due to better specific strength and stiffness, as well as improved fatigue and corrosion resistance. Double digit, 20-40 % weight reduction has been demonstrated for composite primary and secondary structures relative to aluminum [4]. For modern commercial airliners such as the Boeing 787 and the Airbus A350XWB, these materials now account for over 50 % of the airframe by mass and have replaced aluminum in primary structures such as the fuselage and wings [5], [6]. A further advantage is reduced airframe maintenance costs due to the absence of corrosion and fatigue. For the Boeing 787, 30 % lower maintenance costs are anticipated relative to a comparable aluminum airframe [5].

1.1.2 Composite Damage

Before an aircraft enters service, manufacturing defects or incidents at the factory may require repair. Aircraft structures also experience unexpected in-service damage: in-flight due to lightning, hail, bird strike and runway debris as well as on the ground due to impact from airport ground vehicles, maintenance operations and even collisions with other aircraft [6]. Due to the large number of ground vehicles around an aircraft, impacts from these vehicles were recorded to account

for half of all in service damage on the Airbus A320 family [6], mostly around doors. Therefore as composites become the predominant airframe material, there is a growing need for structural composite repairs [7].

Composite sandwich structures with honeycomb core, often used in secondary structures such as elevators, are also susceptible to damage from liquid water ingress. For commercial aircraft with non-metallic honeycomb cores, such liquid water ingress can cause (1) node bond failures and skin to core bond failures due to freeze-thaw cycles and (2) blown core or skin disbonds if the assembly is heated above 100 °C such as during a repair [8], [9].

1.1.3 Composite Repair

If damage is detected, and exceeds the allowable damage limit (ADL), a structural repair is required. The Original Equipment Manufacturer (OEM) provides instructions for damage assessment and repair in the Structural Repair Manual (SRM) for a given aircraft. Either bolted or bonded repairs are performed as described next.

Bolted Repair

Bolted repairs are the traditional method of repairing metallic aircraft structures, and naturally were the first method applied to repair composites [10]. After grinding to remove damaged material and any sharp edges or corners, a metal or (cured) composite plate is attached by mechanical fasteners in a single or double lap joint configuration. Most often metallic plates are used for practical reasons. These repairs are advantageous as they are quick to implement, and technicians require minimal additional training as they are already familiar with these techniques for metal structures. While there is minimal process sensitivity compared to bonded repairs, proper hole drilling is critical [11]. Bolted repairs also need to be considered in the aircraft structure's initial design to accommodate fastener bearing loads and stress concentration effects around holes [12], [13]. Currently, bolted repairs are the only method used for structural repairs of load bearing primary structures, such as the fuselage of the Boeing 787 and Airbus A350XWB [5], [14].

Bonded Repair

Alternatively, composite or metal repairs can be bonded, negating the need for stress raising holes and providing more uniform load transfer between repair and parent structure. If metallic repair

materials are used, stiffness mismatch and coefficient of thermal expansion mismatch effects need to be considered [11]. A metal or pre-cured composite plate can be bonded in a lap joint configuration, or the parent structure can be stepped or scarfed for a composite patch. Composite repair materials can be cured prior to bonding, or co-cured with the adhesive: the *hard* and *soft patch* approaches respectively. Soft patch repairs are also referred to as *co-bonded*. Compared to bolted or bonded lap repairs, scarf and step bonded repairs will yield the highest stiffness and strength recovery, as they add virtually no eccentricity to the load path and induce negligible peel stresses [11]. Further advantages of scarf or step bonded repairs over bolted are reduced weight and aerodynamic drag.

The most common type of bonded repair is the soft patch scarf repair, illustrated schematically in Figure 1.1, cured *in-situ* by means of a heat blanket under a vacuum bag. To minimize expensive aircraft downtime, or due to the impossibility of removing some components, they are performed *in-situ*: at the flight line or a field station with minimal equipment and uncontrolled ambient conditions. While hard patch repairs can offer better quality [15], such patches require either custom tooling to be made and/or accurate machining which requires specialized equipment, training and takes much more time to implement. Step repairs, in which the parent structure is stepped, have two serious manufacturing difficulties: precisely grinding steps into the parent structure, and getting the repair plies to fit the steps without gaps or overlaps [10]. Therefore, for being advantageous to *in-situ* application and its ease of implementation, soft patch scarf repairs will be the focus herein.

Bonded Scarf Repair Process

The general soft patch scarf repair process starts with damage assessment, followed by cleaning [16] and paint removal from the repair area. Damaged laminate and core are then removed. The parent structure is then scarfed, which is usually done manually with a die grinder to an angle of 3° or less [17]. The bonding surface is prepared by solvent cleaning and/or by light sanding followed by a dry wipe with a silicone/lint free cloth [16], [18]. The repair area is then dried [19].

An adhesive is then typically laminated onto the repair area, followed by the repair plies. Repair plies consist of uncured composite: usually carbon fibre fabric impregnated with epoxy resin. See the next section (section 1.1.3) for details on the composite and adhesive materials.

The repair area is then vacuum bagged, vacuum is applied, and the repair is cured by means of a heat blanket as shown by Figure 1.1 [20], [21]. The repair is then inspected and finishing operations are performed.

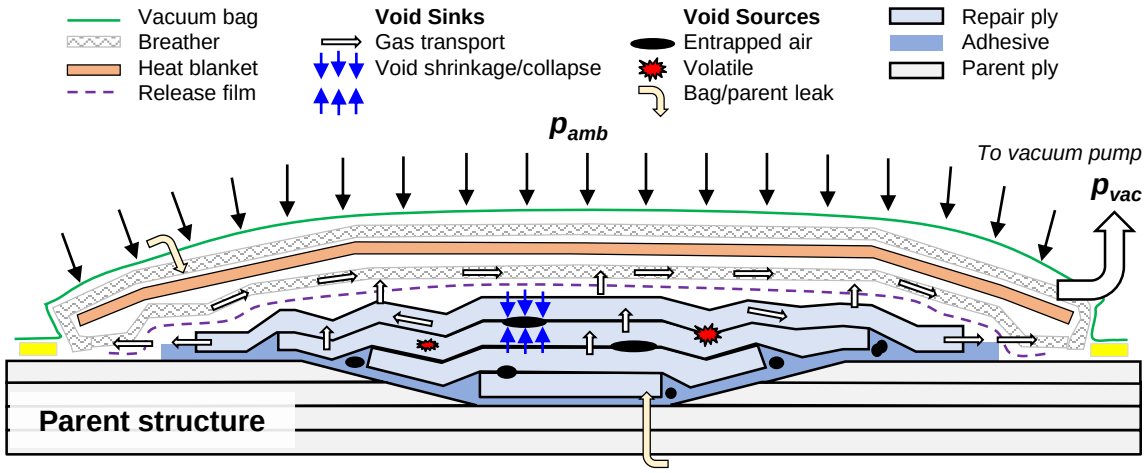

FIGURE 1.1: *In-situ* soft patch bonded scarf repair processing schematic. The repair is cured using a heat blanket under consolidation pressure provided by a vacuum bag only. Adapted from [22].

Soft Patch Repair Materials

The repair patch consists of plies of either **prepreg** or **wet layup** impregnated fabric, the latter when cold storage of prepreg is impractical [23].

For a **wet layup** repair, a dry fibrous reinforcement, such as plain weave carbon fibre fabric, is manually impregnated with a low viscosity liquid resin [13]. Two part epoxy resins consisting of a resin and hardener are used. The two parts are stored separately and mixed manually just prior to use [24]; thus they may be stored at room temperature for 6 months or more [13]. Usually a large piece of fabric is impregnated, from which all the plies for a given repair are cut [25]. Additional laminating resin is also brushed onto the repair area prior to collation of the impregnated plies [25].

Prepreg refers to any fibrous reinforcement material that has been pre-impregnated with catalyzed resin by a material supplier. The reinforcement can be fully impregnated: these are typically referred to as **autoclave prepregs**. The reinforcement can also be semi-impregnated so that dry areas or openings exist for gas extraction [26], and these materials will be referred to herein as **semipregs**. Consolidation pressure and heating during the cure cycle causes the resin to flow and saturate the dry regions. Between the repair area and prepreg patch, an epoxy **film adhesive** is used. Both prepreg resins and film adhesives are *B-staged*: the degree of cure is slightly advanced so that the resin viscosity is high at room temperature, but drops again upon heating during the

cure cycle [13]. Prepregs and film adhesives must thus be stored in a freezer near $-18\,^{\circ}\mathrm{C}$ to slow advancement in degree of cure. They have a shelf life of ≈ 12 months at $-18\,^{\circ}\mathrm{C}$ and room temperature out life of 10 to 30 days [13].

Bonded Repair Quality Issues

The quality (minimal voids, high fibre volume fraction, etc.) and therefore the anticipated mechanical properties of soft patch bonded repairs are highly process dependent. Firstly, they are susceptible to human error, and this is compounded by a current lack of technician certification requirements. Inadequately trained technicians are often cited as the cause of non-conforming repairs [27]. Note that efforts to standardize training and certification for bonded repair technicians are ongoing and are led by the Commercial Aircraft Composite Repair Committee (CACRC) [10], [28].

Secondly, the **vacuum bag only** (VBO) process, necessitated by the *in-situ* nature of such repairs, creates several quality issues, chiefly voids in the patch and bondline. As shown in Figure 1.1, the repair is cured under a vacuum bag sealed to the parent structure. In a VBO process the consolidation pressure, which is the pressure difference between the bag and ambient, is limited to the local atmospheric pressure. This is unlike the autoclave process with which the aircraft structure would have been originally made [13], for which $\approx 7\,\mathrm{bar}$ of positive pressure is applied. Sources of voids include air entrapped between plies during layup or within the resin (wet layup repairs), volatiles such as moisture from the uncured materials or parent structure and leaks in the bag or parent structure [22], [29]. If these entrapped gases cannot be evacuated by the applied vacuum or collapsed/dissolved by the consolidation pressure before the resin gels, they will be locked in as voids in the cured repair. Hence due to the reduced consolidation pressure available in the VBO process, such processes yield higher void contents and are far less robust than autoclave processes.

These two effects, operator variability and deficiencies of the VBO process, were investigated in a round robin (soft patch) bonded scarf repair study [30]. In this study identical sandwich panels with typical instructions for repair were sent to many different repair field stations and OEMs. Repaired panels were tested statically under elevated temperature wet conditions, and varied widely in strength from 38 % below the undamaged strength to 7 % above. Weaker repairs were associated with high void contents of up to 11 % in the patch. This high variability highlights

the need for more robust bonded repair procedures that lead to low void content in the patch and bondline.

NDI and Certification Issues

There is currently no non-destructive inspection (NDI) method that can reliably assess the strength of a bonded joint [31]. Due to this lack of inspection capability and the high sensitivity to processing, bonded repairs are currently only acceptable to certification authorities if limit load or better can be maintained with the patch departed [31]. Consequently, only bolted repairs are acceptable when damage exceeds the limit load capability, limiting most bonded repairs to essentially cosmetic or aerodynamic purposes. Therefore bonded scarf repair procedures that yield high quality and are robust to process deviations are needed to help make such repairs certifiable for load bearing applications.

1.2 Thesis Objectives and Outline

There is currently a need for more consistent, high quality (anticipated strength) bonded soft patch scarf repair processes, particularly for wet layup repairs. Therefore the primary objective of this work will be to find robust methods to reduce patch void content in wet layup repairs. This objective will be met by lab scale material and process development, and by validating improved procedures on an aircraft demonstrator part. As a secondary objective, recently developed prepreg repair techniques will also be validated on the demonstrator. The systematic approach that will be followed is outlined in Figure 1.2.

Laboratory scale experiments in Chapter 2 will lead to an understanding of the effect of wet layup repair processing variables on patch void content. The effect of void content on static strength will also be investigated. This understanding will be used to design improved wet layup repair procedures, which will then be validated by repairing a decommissioned aircraft structure in Chapter 3.

Highlighted in beige, Figure 1.2 also shows repair development work performed by other authors that this work will help to complete. Prepreg repair process development was performed in the works indicated, for semipregs and a breathable adhesive film. While the prepreg repair process developed led to a considerable reduction in patch and bondline void content for laboratory

scale panels and fixtures, it has not yet been tested on a real structure. Presented in Chapter 3, this prepreg repair process will also be validated alongside wet layup repairs on a decommissioned aircraft structure and the resulting quality assessed by several means. The lessons learned from the demonstrator implementation will be readily applicable to improve robustness and quality of aircraft composite bonded repairs.

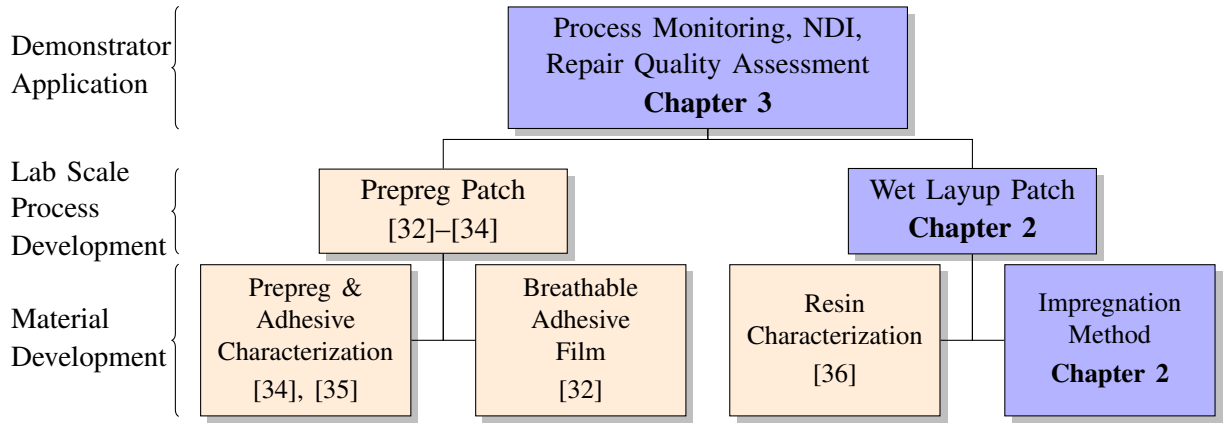

FIGURE 1.2: Task organization for development of robust co-bonded repair processes.

1.3 Literature Review

A brief review of relevant literature follows, including past work on prepreg and wet layup repair processing.

1.3.1 Composite Repair Materials

Prepreg Repair Materials

In Chapter 3 prepreg repairs performed with several different epoxy based materials from Cytec Engineered Materials (now Cytec Solvay Group) are analyzed. Two different carbon plain weave fabric prepregs were used: a semipreg and a conventional autoclave prepreg. The motivation for using these materials follows.

Semipregs are ideal repair materials as they are designed for VBO processing. These materials are partially impregnated, to extract air either through the thickness or in the plane of the ply during room temperature vacuum holds prior to cure [26], [37], [38]. Entrapped air is the main source of voids with such materials as they have lower volatile release and lower cure temperatures than autoclave prepregs [39]. Of particular concern however to repairs which are performed in uncontrolled environments, the un-cured resin can also absorb significant moisture (up to 1 wt %) from ambient air which was also shown to promote void growth in VBO processes [40]. There is a large amount of literature on semipreg processing, also known as Out-of-Autoclave (OoA) processing, but very little relating to composite repairs except for the work of Bernetich [41] and Préau [18], [32], [42] who both investigated co-bonded repairs with Cytec Cycom® 5320 semipreg.

To help validate the work performed by Préau the semipreg chosen used Cycom® 5320 resin, impregnated at 36 wt % resin content into a 196 $\mathrm{g\,m^{-2}}$ 3k plain weave with Cytec T650-35 carbon fibres [43]. This 5320 semipreg is impregnated in the manner illustrated by Figure 1.3a, in which a continuous resin film is partially impregnated into both sides of the fibre bed [44]. This semipreg morphology leads to good in-plane permeability to air, but through thickness permeability is two orders of magnitude lower [45]. This is problematic for scarf repairs, as the bondline normally blocks off in-plane air evacuation pathways [18] as shown by Figure 1.1.

The autoclave prepreg used was Cycom® 977-2 impregnated into a $\approx 196\,\mathrm{g\,m^{-2}}$ 3k carbon plain weave [46]. This toughened epoxy resin is used in several modern aircraft such as the Boeing 787 and Airbus A380 [47]. Since the preferred repair material is often that with which the structure was originally made, it was therefore of interest to test this autoclave prepreg. Since autoclave prepregs tend to be fully impregnated, it is difficult to extract air and volatiles from such laminates and hence under VBO cures they tend to yield high (≈ 5 %) porosity [13].

The film adhesive used was FM® 300-2M, with 293 $\mathrm{g\,m^{-2}}$ weight, 0.25 mm nominal thickness and a non-woven polyester carrier [48]. This 121 °C curing adhesive was also chosen to validate previous work on bonded repairs in honeycomb structures by Préau [32], [42]. In particular Préau developed a technique to texture this film adhesive to create an air evacuation pathway along the bondline, as illustrated in Figure 1.3b. The embossed film adhesive was shown to be effective at both removing entrapped air and moisture from the bondline and 5320 semipreg repair plies [18], [42]. The addition of perforations by means of a porcupine roller in the film also permitted air extraction from the core, either through the bondline or through the thickness of the plies [42]. Using the combination of adhesive perforation and embossing with semipreg, when repairing lab

scale sandwich panels Préau dramatically reduced bondline porosity from over 10 % to near 0 % even with high levels of pre-bond moisture in the core [32], [42].

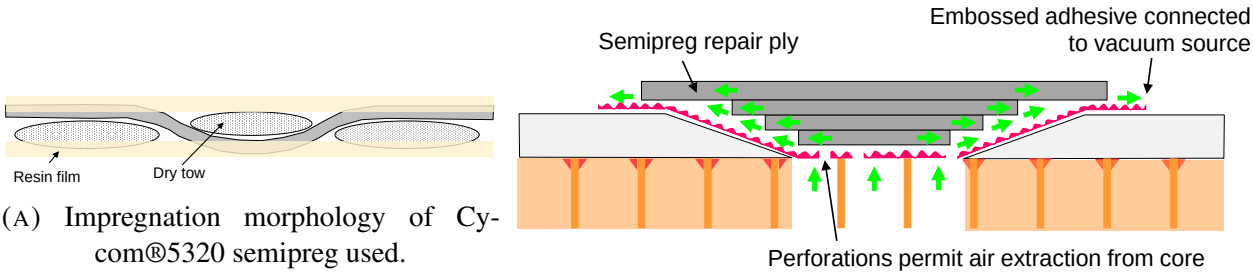

(A) Impregnation morphology of Cycom®5320 semipreg used.

(B) Air evacuation pathways (green) with embossed/perforated adhesive and semipreg plies.

FIGURE 1.3: Semipreg and embossed/perforated film adhesive.

Wet Layup Repair Materials

Two wet layup resins designed for repair will be studied in Chapter 2: Huntsman Epocast 52 A/B [49] and Henkel EA 9390 [50]. When freezer storage of prepreg is not practical wet layups are performed: for example EA 9390 can reportedly be stored as hot as 38 °C for 300 days with no adverse effects on cure [51]. Another important advantage of these two resins over most aerospace prepregs is that they have manufacturer recommended cure cycles in the range of 93 °C to 149 °C, while still offering good hot/wet properties at elevated temperature [51]. This is ideal firstly for avoiding warpage as a result of heating near the original cure temperature of the part, and secondly repairing honeycomb structures for which heating above the boiling point of water (100 °C) could risk causing skin to core disbond [51]. The cure kinetics and viscosity of these two resins are well understood thanks to experiments and models developed by Casari [36].

Epocast 52 A/B was chosen as it meets the CACRC's AMS 2980 [52], an effort to standardize wet layup repair resins and carbon fabric materials. This standard specifies storage requirements, processing methods and minimum mechanical properties, which are published for this particular resin and the standard plain weave carbon fabric in [53]. Interestingly the published void contents were in the range of 2.9 % to 3.9 %, with widely varying fibre volume fractions of 44 % to 60 % suggesting there is room for process optimization [53]. This standardization effort minimizes the certification work that OEM's will have to do to employ this repair material. The second resin,

EA 9390, was chosen as it is commonly used for composite aircraft repair in conjunction with the DVD process discussed next.

1.3.2 Double Vacuum Debulk (DVD)

Efforts by the Naval Air Warfare Centre in the 1980s to develop a high quality, robust *in-situ* field bonded repair method requiring minimal equipment led to the development of the Double Vacuum Debulk (DVD) technique [54], [55]. The goal was to achieve autoclave quality prepreg or wet layup patches, in terms of minimal void content and high fibre volume fraction. It was realized that in a VBO process, the one atmosphere of consolidation pressure is enough to close off air evacuation pathways, but not enough to collapse voids. For instance it has been reported that at least 2 bar to 3 bar of positive pressure are required to achieve low porosity laminates in an autoclave prepreg process [56]. A method was therefore devised to degas a laminate with vacuum, but without compaction pressure.

A schematic of the DVD process is shown in Figure 1.4. The technique involves first laminating either a prepreg or wet layup patch onto a flat tool. The patch is then sealed in an *inner* vacuum bag, and placed inside a rigid, airtight chamber. Vacuum is pulled simultaneously in the inner bag and the chamber, usually with just slightly higher vacuum in the inner bag to avoid rupturing it. Then, heat is applied so that the resin reaches its minimum viscosity for the most efficient degassing as shown in Figure 1.4a. After a certain dwell time at constant temperature the vacuum in the rigid chamber is removed, allowing atmospheric pressure to compact the patch as shown in Figure 1.4b. The patch is then removed, inspected, laminated onto the damage structure, and cured using a normal vacuum bag only process with a heat blanket. Dedicated chambers to perform this DVD process are commercially available, such as from Heatcon®, and they can also be fabricated with basic materials such as wood [57] as done in Chapter 2. See Figure 2.8 and 3.15 of Chapters 2 and 3 respectively for additional examples.

A good knowledge of the resin's cure kinetics and rheology are required: the dwell time and temperature in the DVD chamber must maximize the removal of air and volatiles from the patch, while not advancing its degree of cure substantially [56]. This way debulked patches can still be applied to highly curved structures [56]. Viscosities of 25 Pa s or lower are effective for the degassing stage [56], [58].

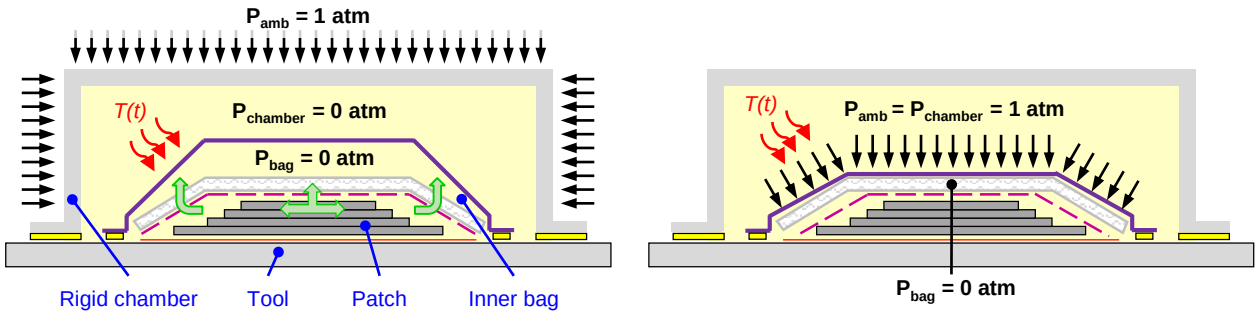

(A) Degassing stage. (B) Compaction stage.

FIGURE 1.4: Double Vacuum Debulk (DVD) process.

The DVD method can also be applied directly on the damaged structure, possibly allowing bondline porosity to be reduced as well [59]. After a patch is laminated and vacuum bagged on the parent structure, a rigid box is placed over it and then sealed in a second, outer vacuum bag. The drawbacks are that this technique is difficult or impossible for curved structures, the patch cannot be inspected after debulking and pulling vacuum in a rigid box in this way places significant bending loads on the damaged structure.

While DVD has mostly been associated with US Naval aircraft repair, its becoming more common for repair of commercial transport aircraft: it is now specified in the 787 SRM with instructions for fabricating a wooden DVD box [5].

DVD with EA 9390 Resin

Two processing studies were found for Henkel EA 9390 used in conjunction with the DVD technique [51], [57]. For both, flat 8 ply laminates were manufactured with carbon fabrics using a manual impregnation technique (see Chapter 2), and degassed in DVD chambers for 60 min to 90 min, at either 54 °C [57] or a proprietary temperature [51]. Average void contents of 1 to 3 % were reported, with fibre volume fractions of 54-62 %. For a non-DVD process, a void content of 7 % was found, with a 50 % fibre volume fraction and a 64 % decrease in short beam strength [51]. Thus a clear improvement was demonstrated in quality and mechanical properties for the DVD technique with EA 9390.

1.3.3 Wet Layup Repair Void Mitigation

Aside from wet layup repairs performed using the DVD technique, there is little scientific literature on the effect of processing on wet layup porosity, whether for repair or manufacturing. This is perhaps because in production, experience based, labour intensive wet layup techniques are used for their low material and tooling costs in very low volume applications such as for prototypes [13] and home built aircraft [60], racecars or boats [61]. The process is highly dependent on operator skill [13]. For such applications the high void content, reaching 10 % in some cases [62], and low fibre volume fractions inherent to the process are acceptable [63].

The main differentiation from prepreg processes are the resin mixing and impregnation operations: as they are performed manually there is less control over the resin content and there is the chance for mixing errors. Considerable air can become entrapped in the resin during mixing, unless it is degassed [29]. To investigate the effect on void content, one study compared individually degassing plies to degassing the entire laminate by the DVD technique: it was concluded that most of the entrapped air in a laminate (80 %) is due to ply layup [64]. DVD is likely far more effective than degassing mixed resin because it removes both intra and inter-ply air.

One paper demonstrated that wet layup quality can be significantly increased with process optimization, without adding significant process complexity [62]. Since wet layup resins have very low viscosities, this paper explored whether increasing the resin viscosity at the time of VBO consolidation pressure application would improve laminate quality. The idea came from autoclave prepreg processing, for which excessive bleed is known to lead to porosity, as a result of the associated drop in resin pressure and resin starvation [29]. The interesting conclusion was that to optimize both void content and fibre volume fraction, the resin viscosity at the time of vacuum application should be in the range of 7.5 Pa s to 16.5 Pa s regardless of resin type or fibre architecture. With this process, void contents of 1 % to 2 % were achieved, with fibre volume fractions of 58 % for non-crimp reinforcement and 50 % for plain weave fabric. For non-optimal processes void contents of 7 % or higher were measured, therefore this represents as significant quality improvement. Micrographic evidence and measurements of resin bleed suggested that when vacuum pressure was applied at too low a viscosity, inter-ply voids occurred due to excessive resin bleed, suggesting a trade-off between fibre volume fraction (resin bleed) and void content. Intra-tow micro-voids were also observed, but it was unclear if they were due to overbleed or entrapped air. Another conclusion, from tests on varying the initial resin content and number of bleeder plies, was that neither of these factors could be used to control fibre volume fraction. Also no reduction

in void content was found for degassing the resin after mixing.

1.3.4 Bonded Repair Standards

The Commercial Aircraft Composite Repair Committee (CACRC) is an ATA/IATA/SAE technical committee whose membership includes mainly industry: OEMs, maintenance, repair and overhaul companies (MROs) and airlines. The committee's mission statement is: "To reduce the cost of maintaining composite structures, through standardization of materials, techniques and training" [65].

Different CACRC task groups produce standards related to all aspects of composite repair, including bonded repair processing. The standards are based on current industry best practices as the group does not conduct research [65]. These standards include all aspects of the wet layup repair process, including cleaning and bondline surface preparation [16], drying [19], core restoration [66], resin mixing [24], ply impregnation and layup [25], vacuum bagging [20], cure with a heat blanket [21] and non-destructive inspection [67]. There are also specifications for wet layup [52] and prepreg [68] repair materials. These standards are relatively new, with the first issues appearing between 1996 and 2011. Further standards are under development for the prepreg repair process, such as for ply collation.

There are relatively few published studies to validate CACRC wet layup and prepreg procedures and materials. The only work found was performed by NIAR (Wichita, KS). One study compared OEM prepreg repair techniques to CACRC wet layup repair techniques, and tasked different airline depots and OEMs with repairing identical sandwich panels [69]. Similar strength restoration was found for both methods, however the wet layup method used twice the scarf length and an additional ply. A similar study compared CACRC prepreg and wet layup techniques and materials [30]. Only the prepreg results have been presented so far, and show a large variation in static strength recovery (62 % to 107 % of pristine strength) between different depots. Poor strength recovery corresponded to higher porosity levels (up to 11 %), while the best repairs had 3.8 % porosity or lower. Both of these studies also showed a strong dependence between strength recovery and technician skill.

1.3.5 Summary

A summary of the state of the art processing technologies discussed in this literature review for both prepreg and wet layup VBO co-bonded repairs is presented in Table 1.1. A common limitation of all processing studies was that repairs were performed only on laboratory scale panels and fixtures.

Promising void content reduction was obtained for semipreg repairs with embossed and perforated adhesive. The only two wet layup repair processing studies found simply manufactured flat laminates rather than repair patches for scarfed panels. So far low void content laminates utilizing wet layup repair materials have been demonstrated only with DVD processing. There appears to be some promise in optimizing cure cycles (resin viscosity) to reduce void content as well [62]. Thanks to the viscosity models available for the wet layup repair materials selected these two factors can be further explored. There are many other process variables in wet layup repair processing, such as the impregnation technique, and currently a complete understanding of their effect on void content is lacking.

Lastly the CACRC has published standards for wet layup processing which require further validation. These standards also make a good starting point for further wet layup repair process improvement.

TABLE 1.1: VBO Co-Bonded Repair Lab Scale State of the Art

Author	**Repair**	**Material**		**Parent**	**Void Content** (%)	
	Technology	**Ply**	**Adhesive**	**Structure**	**Patch**	**Bondline**
[41]	Semipreg, dry fabric in bondline	3k PW / CYCOM® 5320-1	Unknown	Monolithic	< 5.7	–
[41]	Prepreg with DVD	3k PW / 3501-6	Unknown	Monolithic	< 2.0	–
[18]	Semipreg, embossed adhesive	3k PW / CYCOM® 5320	FM® 300-2M	Monolithic	< 0.5	< 0.1
[42]	Semipreg, embossed/perforated adhesive	3k 8HS / CYCOM® 5320	FM® 300-2M	Sandwich	< 1.5	< 1.2
[51]	Wet layup DVD	3k 5HS/ EA 9390	–	None	< 3.0	–
[57]	Wet layup DVD	3k PW / EA 9390	–	None	3.0	–

Chapter 2

Experimental Study of the Wet Layup Repair Process

Wet layup repair procedures currently lack a thorough scientific basis. Current vacuum bag only (VBO) wet layup repair processes yield high void contents (5-15 %) and there can be large variations in porosity both within patches and between repairs. Further, there exists no standard wet layup repair process, with different original equipment manufacturers (OEMs) and repair depots following different procedures.

To improve the quality of wet layup repair patches, and to help move towards standardization, a better understanding of the wet layup repair process is needed. To this end the relationship between processing variables and repair patch quality is investigated in this chapter. This chapter expands on work previously presented at SAMPE 2016 [1].

Void growth, nucleation and transport mechanisms are both difficult to model and observe experimentally [70]. Instead of modeling this physics problem, the effects of many different process variables on porosity were first determined experimentally through Taguchi Design of Experiments (DOE). This study allowed the most important process factors to be determined, as well as the optimal factor levels for both porosity and fibre volume fraction. To study a broad number of factors, only porosity within the patch and not the bondline was assessed. Additional experiments were then carried out to both validate and better understand these results.

Finally, to emphasize the importance of reducing porosity in the patch, short beam shear tests were performed.

2.1 Effect of Processing Variables on Void Content: DOE Study

2.1.1 Experimental Procedure

Wet Layup Repair Patch Manufacturing

To investigate the quality within wet layup repair patches, patches were manufactured on a monolithic parent structure, with ambient conditions between 20 °C to 26 °C and 20 to 26 % relative humidity. According to the test matrix outlined in the Test Matrix section, they were processed in the following steps: (1) resin mixing, (2) impregnation of dry fabric with resin, (3) lamination of impregnated plies on the scarfed parent structure, (4) vacuum bagging (completed before 80 % of the resin's pot life had elapsed), (5) room temperature debulk and (6) cure in a convection oven.

Since the objective of this work was to investigate only the quality of the patch, and not the bondline, the parent structure was chemically sealed and released so that it could be re-used. In this way the repair patches were removed from the parent structure once cured, allowing all tests to be performed on the same parent structure. Prior to gelation of the patch's resin, this approach provides the exact same processing conditions for the patch. Once the patch's resin resin has gelled, air and volatiles could theoretically escape along the scarf since it is released. However, at gelation, voids are essentially stable and no further growth or dissolution occurs as the resin is no longer liquid [29]. This approach has also been used previously in the study of prepreg bonded scarf repair processing [42].

The parent structure consisted of 16 plies of Cytec CYCOM 5320 Out-of-Autoclave prepreg featuring a plain weave (carbon) fibre architecture (T650-35 3K PW, 196 gsm, 36 % resin content) in a quasi-isotropic $[+45/0/-45/90]_{2S}$ configuration. A layer of epoxy surfacing film (Cytec Surface Master 905M) was also co-cured on the top and bottom of this panel. Figure 2.1 shows a cross-section of this parent laminate. The parent included a 76 mm diameter circular hole in the 5^{th} ply, and all subsequent plies up to the top surface were scarfed at an angle of 1.8°. To create the scarf, the parent laminate was initially manufactured with circular holes cut out of the prepreg plies, with a 6.35 mm step size as shown in Figure 2.2a. Then, the steps were sanded smooth to a scarf with a pneumatic die grinder, finishing with P120 grit silicone carbide disks.

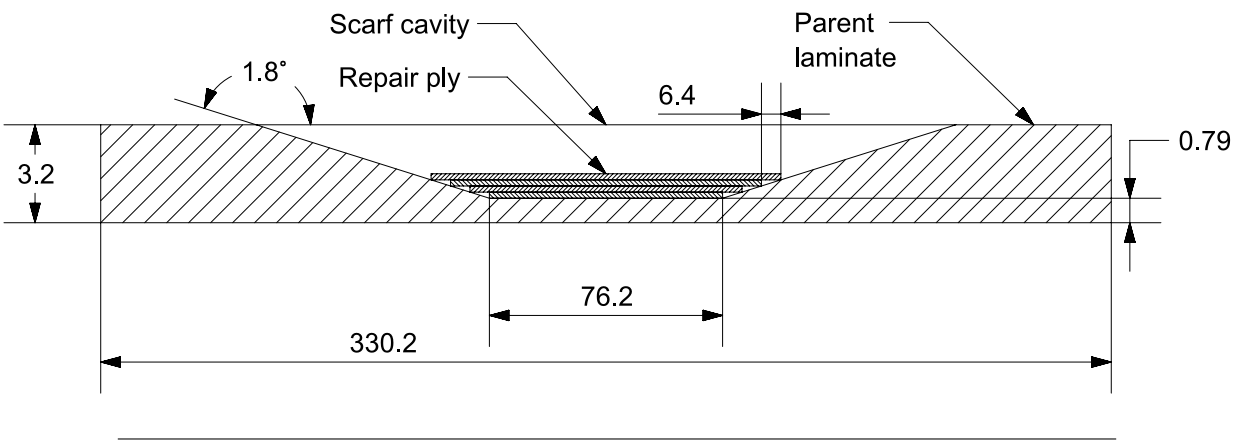

FIGURE 2.1: Cross-section of the parent laminate tool, dimensions in mm. Not to scale.

Test Matrix

Eight processing factors that were thought to affect patch quality were chosen for study. These factors are listed in Table 2.1 along with their chosen levels.

TABLE 2.1: Processing Factors and Levels

	Factor	Level 1	Level 2	Level 3
A	Resin Type	EA 9390	Epocast 52 A/B	-
B	Impregnation Technique	Random Blob	Manual	Vacuum
C	Bagging Arrangement	Vertical Bleed	No Bleed	DVD
D	RT Debulk Time	0 min	30 min	120 min
E	Fibre Architecture	PW	4HS	Twill 2x2
F	Repair Thickness	4 plies	8 plies	12 plies
G	Level of Vacuum	>96 kPa (28.5 inHg)	74 kPa (22 inHg)	50 kPa (15 inHg)
H	Cure Cycle	2 °C/min	5 °C/min	Two dwells

A **main effect** of a factor at a given level is its effect on the dependent variable with the effects of all other factors averaged across their levels. Here the dependent variable is patch quality, see the Quality Characteristics section for how this was quantified. Main effects are defined mathematically later in terms of Equation 2.16. To determine main effects with the least number of experiments, patch configurations to manufacture were selected from an L_{18} Taguchi orthogonal

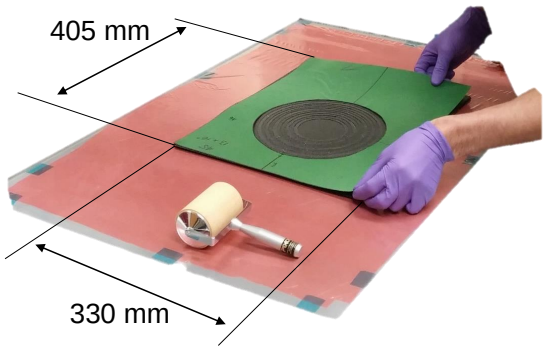

(A) Parent laminate ply collation.

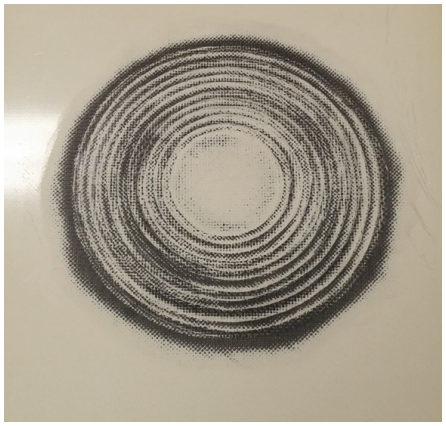

(B) Closeup of parent after scarf sanding.

FIGURE 2.2: Parent laminate tool.

array, Table 2.2 [71]. This array requires 18 trials, in contrast to the 4374 ($2 \cdot 3^7$) that would be required for a full factorial experiment.

The effect of interactions between factors was neglected by this experimental design. This is a common practice for preliminary studies [72], to permit the overall effects of a broad number of factors to be considered with a reasonable number of trials. With 18 trials, studying all two factor interactions would leave only enough degrees of freedom to study two three level factors [72].

For the array in Table 2.2, each trial represents a column and is numbered from 1 to 18. Each row represents a factor, labelled A-H, corresponding to the factors in Table 2.1. The values in the array represent levels for each factor. For example, in trial 1 all factors are at level 1. From Table 1, the configuration for trial 1 is EA 9390, random blob, vertical bleed, 0 min, PW, 4 plies, >96 kPa and 2 °C/min. Additionally, one replication was performed for each trial to account for noise, so a total of 36 wet layup repair patches were manufactured. Performing at least one replication permits effects of factors to be determined not only on the mean of the quality characteristic, but also on its standard deviation; in this way an optimal process can be determined that yields the targeted patch quality in a robust way.

Factors

A. Resin Type Two resins designed for wet layup repair were chosen: Epocast 52 A/B from Huntsman [49] and Loctite EA 9390 Aero from Henkel [50].

TABLE 2.2: Taguchi L_{18} Orthogonal Array

Factor	Trial																	
	1	2	3	4	5	6	7	8	9	10	11	12	13	14	15	16	17	18
A	1	1	1	1	1	1	1	1	1	2	2	2	2	2	2	2	2	2
B	1	1	1	2	2	2	3	3	3	1	1	1	2	2	2	3	3	3
C	1	2	3	1	2	3	1	2	3	1	2	3	1	2	3	1	2	3
D	1	2	3	1	2	3	2	3	1	3	1	2	2	3	1	3	1	2
E	1	2	3	2	3	1	1	2	3	3	1	2	3	1	2	2	3	1
F	1	2	3	2	3	1	3	1	2	2	3	1	1	2	3	3	1	2
G	1	2	3	3	1	2	2	3	1	2	3	1	3	1	2	1	2	3
H	1	2	3	3	1	2	3	1	2	1	2	3	2	3	1	2	3	1

B. Impregnation Technique The resin impregnation technique determined both the method of wetting out the fabric with resin, and ply lay-up.

The **manual impregnation technique** was inspired by the CACRC's method 2 in ARP 5319 [25]. A rectangular piece of fabric was cut first, large enough to fit all of the repair plies. Referring to Figure 2.3a, release film (red line) was taped to a tool plate (grey) 75 mm larger than the fabric. A mass of resin equal to approximately 67 % the fabric mass was mixed according to the CACRC's ARP 5256 [24], and spread evenly over the release film where the fabric would be placed. Then, the fabric (dashed black line) was placed on top, and pressure was applied gently with a spatula to impregnate the fabric. After waiting 5 min for air to escape, the fabric was covered with one ply of vacuum bag (green) with ply outlines drawn on it. The plies were then cut with scissors, keeping them covered with the release film/vacuum bag on both sides as shown in Figure 2.3b.

Since the parent was used as a tool to manufacture patches, it was not coated with resin. Each ply was laminated onto the parent, by first peeling off the release film on one side and placing that side on the parent. The ply was oriented to match the ply orientation in the parent. A spatula was used to remove wrinkles and entrapped air by squeezing the ply gently from the center outwards, as shown in Figure 2.4. The vacuum bag on the exposed side was then removed and the remaining plies added in the same fashion.

The **vacuum impregnation technique** was inspired by the CACRC's method 3 in ARP 5319 [25]. Release film was taped to a tool plate and a rectangular piece of fabric large enough to fit all of the

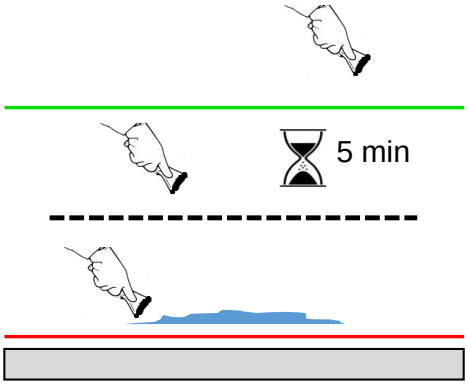

(A) Manual impregnation.

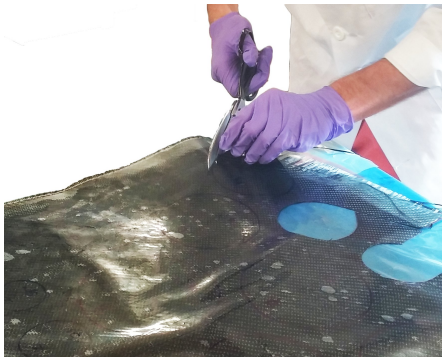

(B) Cutting manually impregnated plies.

FIGURE 2.3: Manual impregnation and ply cutting.

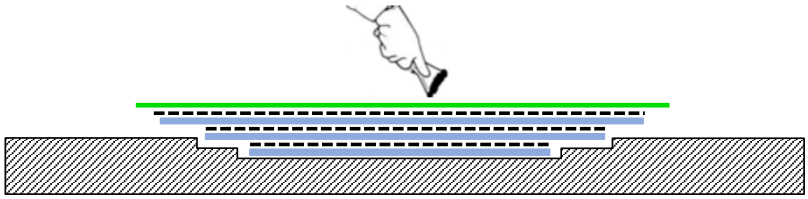

FIGURE 2.4: Ply layup for manual and vacuum impregnation methods.

repair plies was placed on top. Approximately 75 mm wide strips of breather were placed on all sides, butted against the edges of the fabric. A mass of resin equal to the fabric mass was mixed according to the CACRC's ARP 5256 [24]. The resin was poured in a line across the center of the fabric as shown in Figure 2.5a. Then, the fabric was covered in release film and a vacuum bag was sealed to the outer edges of the tool plate. Full vacuum was pulled and squeegees were used to spread the resin, until no pools of resin or dry areas remained as shown in Figure 2.5b. Note that due to the high viscosity of the resins at room temperature, ranging from 5.5 Pa s to 10 Pa s [49], [50], very little flow occurred once vacuum was pulled, so it was by applying pressure with a squeegee on the vacuum bag that the resin was spread to wet the dry fabric.

After the fabric was fully impregnated, the vacuum bag was removed, keeping the release film in place. Vacuum bag with ply outlines was placed on top and the plies were cut. The lay-up followed the same steps as the manual impregnation technique.

(A) Line of resin. (B) Vacuum impregnation.

FIGURE 2.5: Vacuum impregnation method.

The **random blob impregnation technique** is not based on any existing method, but rather was devised for this study in an effort to maximize the transverse permeability to air of the wetted plies. It aims to minimize the degree of impregnation prior to vacuum application and heating, so that air may be removed transverse to the plies through the dry regions, similar to the USCpreg presented in the background [26]. Contrary to the other techniques, each ply was first cut from the dry fabric. Resin was mixed according to ARP 5256 [24]. The first ply was then placed on a scale, as shown in Figure 2.6a, and resin was added in small blobs, dispersed uniformly over the area of the ply. A typical impregnated ply is shown in Figure 2.6b. A mass of resin equal to 56 % and 54 % the fabric mass was added depending on whether EA 9390 or Epocast 52 A/B resin was used respectively. This proportion was calculated to yield a 55 % fibre volume fraction based on the resin and fibre densities, for a laminate with no bleed and no voids. The ply was then placed with the resin blobs facing the parent structure as per Figure 2.6c. The ply was not compacted after lamination, so as to minimize the degree of impregnation. This was repeated for each ply.

C. Bagging Arrangement Three vacuum bagging arrangements were considered. The vacuum bagging arrangement is important as it affects the amount of resin that can be bled, as well as the air evacuation from the patch. Two bagging arrangements were directly inspired by the CACRC's ARP 5143 [20]. These were the **bleed** and **no-bleed** bagging arrangements, which were inspired by *Method 1 Vertical Bleed* and *Method 2 No-Bleed* respectively from ARP 5143 [20]. They are both shown schematically in Figure 2.7.

A **double vacuum debulk** (DVD) bagging arrangement as shown in Figure 2.8 was the third

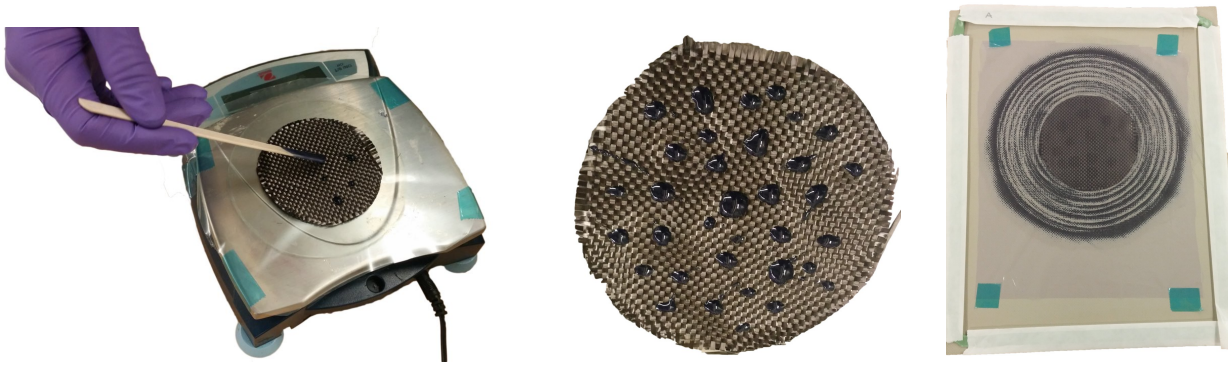

(A) Random blob application. (B) Impregnated ply. (C) Layup.

FIGURE 2.6: Random blob impregnation method.

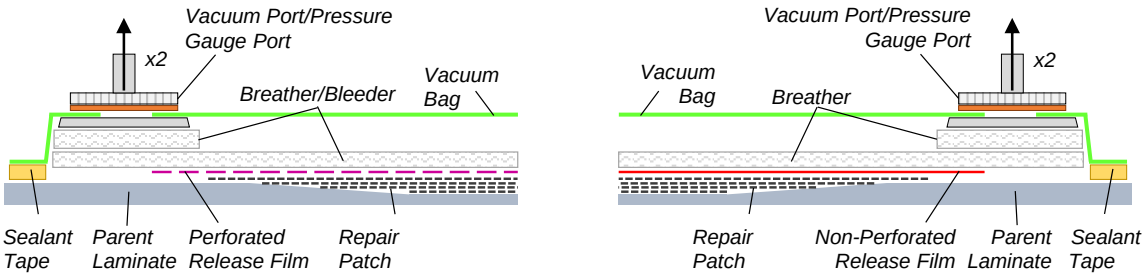

(A) Vertical bleed. (B) No-bleed.

FIGURE 2.7: Bleed and no-bleed vacuum bagging arrangements.

configuration used. The inner bag is identical to the vertical bleed bag used in this study, however it was sealed to a large tool plate, with the parent structure inside. A rigid wooden box was placed on top of the inner bag, so that it enclosed the parent structure. Then, a second outer vacuum bag was made over the box and sealed to the inner bag. Equal vacuum was pulled in both the inner and outer bag during the room temperature debulk, based on the level of vacuum specified for that trial (50 kPa, 74 kPa or >96 kPa). After the specified room temperature debulk was complete, the whole assembly was placed in an oven. For the single dwell cure cycles, the outer bag was vented to atmosphere when the oven air temperature reached 60 °C. For the cure cycle that included an intermediate dwell at 60 °C, the outer bag was vented after the oven air temperature had been at 60 °C for 15 min. Figure 2.9 shows the cure cycles and the point at which the DVD was vented. When the outer bag was vented, compaction of the laminate began as shown in Figure 2.8b.

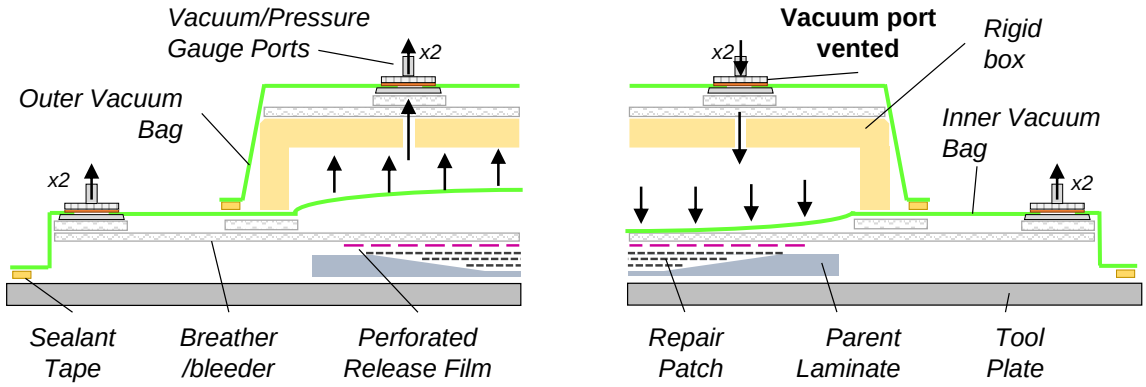

(A) Debulk stage. (B) Compaction stage.

FIGURE 2.8: DVD vacuum bagging arrangement.

D. RT Debulk Time Room temperature debulks help to extract air prior to cure, but lengthen the process. Also, the viscosities of wet layup resins increase quickly after mixing, limiting the permissible length of room temperature debulks. For instance, the Epocast 52 A/B has a 3.5-5.5 hour gel time at 25 °C [49]. So, three levels were considered: 0 min, 30 min and 120 min. It was chosen to consider only debulks after the entire layup was complete to minimize process complexity.

E. Fibre Architecture The fibre architecture and weight influences the wetting behaviour, air extraction capability and drapeability [25]. Carbon fabrics with a 3k tow size, 200 g/m^2 areal weight were chosen in three different architectures: plain weave, four harness satin and 2 x 2 twill.

F. Repair Thickness Three repair thicknesses were investigated: 4, 8 and 12 plies, to represent thin and thicker repairs.

G. Level of Vacuum Vacuum pressure inside the bag is necessary for the removal of volatiles and to create a pressure differential which allows ambient pressure to consolidate the laminate. Since reduced vacuum pressure might potentially yield a better quality repair, and since full vacuum may not be available for all field repairs, three vacuum levels were chosen: >96 kPa, 74 kPa and 50 kPa.

H. Cure Cycle The cure cycle influences several variables critical to patch quality, including the resin viscosity and volatile pressure. The three cure cycles considered are shown in Figure 2.9. The final hold temperature of all three cure cycles was set to 93 °C for the Epocast 52 A/B and 121 °C for the EA 9390. This was done because at these temperatures, the resin datasheets recommend similar hold times (2 hours and 2.5 hours respectively), as the Epocast 52 A/B is more reactive at lower temperatures [49], [50]. The single dwell level 1 and 2 cure cycles assess the difference between a 2 °C/min and faster 5 °C/min ramp rate. The level 3 cycle aims to increase the time for which both resins are near their minimum viscosity with an intermediate dwell at 60 °C, before ramping up to the final hold temperature of each resin.

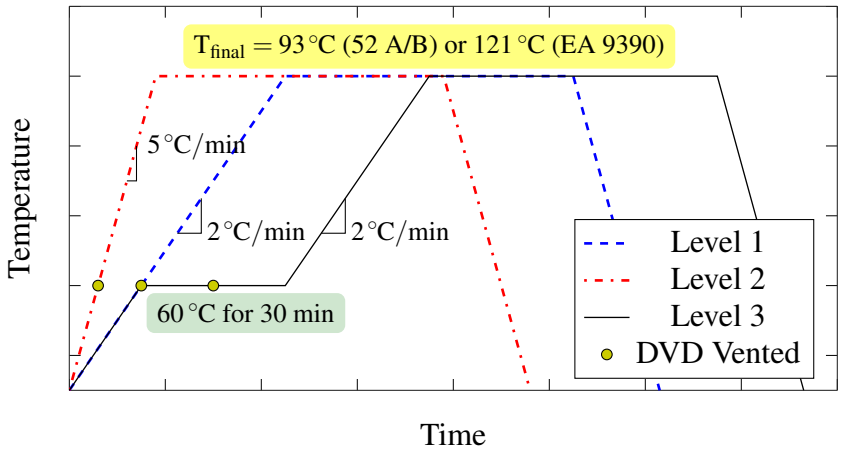

FIGURE 2.9: Cure cycle levels. If the DVD bagging arrangement was used, the point at which it was vented is indicated.

Quality Characteristics

Void Content Three 38 mm long specimens were cut within the boundary of the smallest repair ply for each patch at 0°, 45° and 90°. Specimens were cast in epoxy resin blocks and polished up to 0.3 µm with a Forcipol variable speed grinder/polisher equipped with a Forcimat automatic head. An up-right Nikon Eclipse L150 optical microscope with a 100 × 100 mm Märzhäuser motorized stage was used along with Clemex Captiva to capture images of each sample.

Void content was calculated as per Equation 2.1 for each optical micrograph, by thresholding using the image processing software ImageJ. In Equation 2.1, A_{void} represents the total area of voids in a cross-section, while $A_{cross-section}$ represents the total cross-sectional area. Void content

was determined in this way for each 38 mm sample, for a total of three porosity measurements for each patch. Since two patches were processed for each trial, 6 measures of voidage were available per trial.

$$\text{Void Content } (\%) = \frac{A_{void}}{A_{cross-section}} \tag{2.1}$$

Fibre Volume Fraction Since the mass of fibre could be estimated from the known fabric areal weight and ply areas, Equation 2.2 was used to estimate the fibre volume fraction v_f for each patch using its cured mass. This calculation was corrected for the measured void content, which affects the calculated composite volume.

$$V_c = \frac{V_f + V_r}{1 - v_v},\ V_r = \frac{m_c - m_f}{\rho_r},\ V_f = \frac{m_f}{\rho_f} = \frac{A(FAW)}{\rho_f}, v_f = \frac{V_f}{V_c} \tag{2.2}$$

where:

v_f is the fibre volume fraction

v_v is the void volume fraction

V_c, V_f, V_r are the composite, fibre and resin volume respectively (m^3)

m_c, m_f, m_r are the composite, fibre and resin mass respectively (g)

ρ_f, ρ_r are the fibre and resin density respectively ($g\,m^{-3}$)

A is the total area of the repair plies (m^2)

FAW is the fabric areal weight ($g\,m^{-2}$)

This technique of measuring v_f is approximate; more accurate and time consuming methods were not used as the focus of the study was porosity. This calculation yields an average v_f for the entire patch, however in-plane v_f gradients probably exist, with v_f being higher towards the outside of the patch where it gets thinner.

2.1.2 Void Content Results

Void Content

The average void content for each trial was determined from 6 samples as described above and is presented in Figure 2.10, with error bars representing the (sample) standard deviation. There is a

very wide variation in quality: the average void content of each trial ranged from 2.2 % (Trial 10) to 15.9 % (Trial 8), with an overall average of 6.3 %. The standard deviation for each trial shows a similar scatter, ranging from 0.4 % (Trial 10) to 2.4 % (Trial 4).

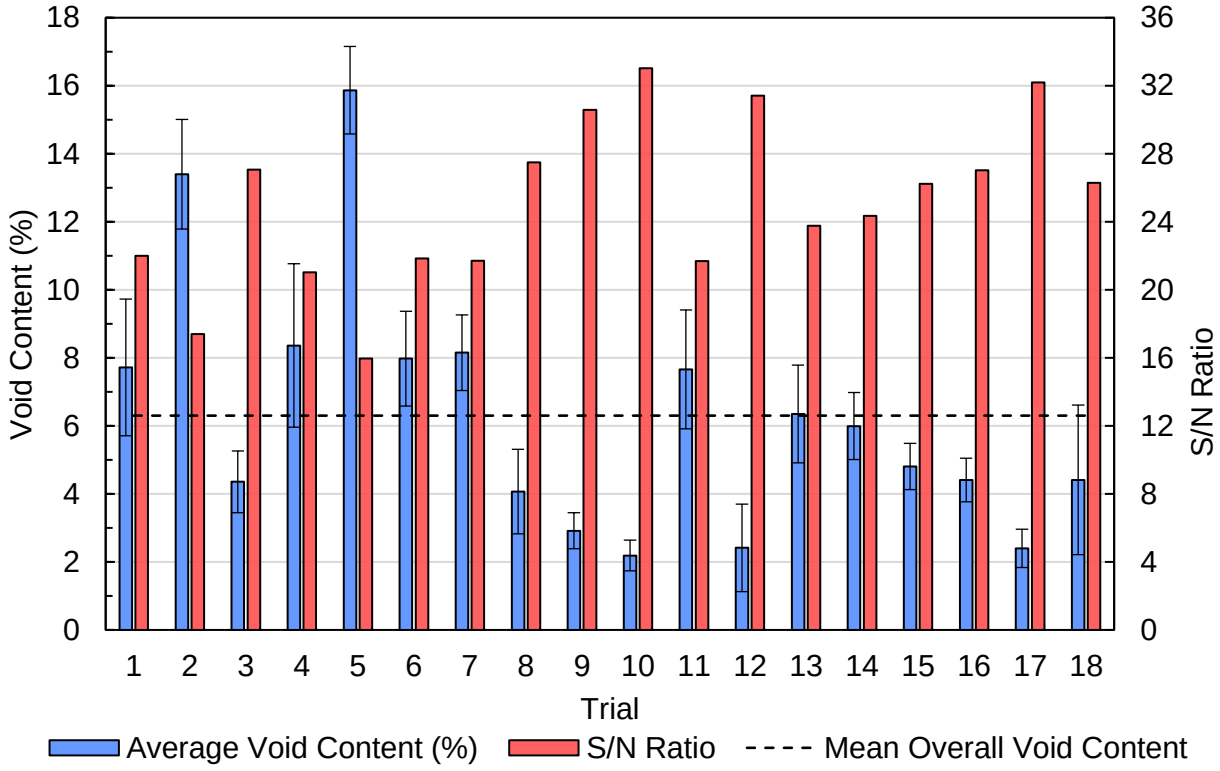

FIGURE 2.10: Void content.

S/N Analysis of Void Content

In analyzing these void content results, the parameters which had the greatest influence on both the void content and the variability (standard deviation) observed within each trial result were sought. This is because an improved wet layup repair process requires not only a minimal void content, but must also be repeatable. This dual objective was met by analysis of variance (ANOVA) techniques using a variance index known as the signal-to-noise (S/N) ratio.

Each trial was assigned a single S/N ratio. This ratio was computed from its six void content samples in two steps. First, for each trial the mean square deviation (MSD) was calculated from the six void content results, denoted by R_i in Equation 2.3.

$$MSD = \frac{1}{6}\sum_{i=1}^{6} R_i^2 \tag{2.3}$$

MSD depends on both the average and standard deviation of the results for a trial [71]. Further, Equation 2.3 is specific to our smaller is better criteria for void content (there is a target value of 0) [71]. The S/N ratio is computed from the base ten logarithm of the MSD as per Equation 2.4.

$$S/N = -10\log_{10}(MSD) \tag{2.4}$$

The logarithmic transformation to an S/N ratio linearizes any non-linear behavior that is present. The S/N ratio for each trial is plotted in Figure 2.10, for comparison with the average void content. For each trial, a larger S/N ratio is desirable. For instance, Trial 10 had both the lowest average void content and standard deviation, as indicated by the error bars. Consequently, it had the highest S/N ratio of 33.04. Trial 12 and Trial 17 had the same average void content (2.4 %), however Trial 17 had a lower standard deviation (0.6 %) than Trial 12 (1.3 %). This explains why the S/N ratio of Trial 17 (32.20) is higher than that of Trial 12 (31.41). So clearly the S/N ratio allows quantifying which results are closest to the quality characteristic (smaller is better) and which have the least amount of variability.

S/N Ratio ANOVA

An ANOVA table was prepared from the S/N ratios using standard ANOVA techniques [71]. This analysis allowed the significance, optimal levels, and percent contribution to be determined for each factor, as well as the expected void content for the optimal process. A description of the process and results follows.

Using Equation 2.5, the correction factor (CF) is first computed from the sum of all deviations from the target value T and the total number of observations n (which equals the number of trials since there is one S/N value per trial). Here $(S/N)_i$ represents the S/N ratio for trial i.

$$CF = \frac{T^2}{n} = \frac{(\sum_{i=1}^{n}(S/N)_i)^2}{18} = 11305.22 \tag{2.5}$$

The sum of squares for a factor is computed as per Equation 2.6, where, for factor A, S_A is the sum of squares, L is the number of levels and n_k is the number of results that contain level k. For factor A in this experiment (resin type), $L = 2$ and $n_k = 9$ for $k = 1, 2$.

$$S_A = \sum_{k=1}^{L} \frac{1}{n_k} \left[\sum_{i=1}^{n} \begin{cases} (S/N)_i & \text{if factor A at level k} \\ 0 & \text{otherwise} \end{cases} \right]^2 - CF \tag{2.6}$$

The total sum of squares S_T is computed as per Equation 2.7.

$$S_T = \sum_{i=1}^{n} (S/N)_i^2 - CF = 403.81 \tag{2.7}$$

The sum of squares of the error, S_e, is computed in Equation 2.8, where any pooled factors are not subtracted from S_T.

$$S_e = S_T - S_A - S_B \cdots - S_H, \text{ excluding S for pooled factors} \tag{2.8}$$

The degrees of freedom (DOF) of the total, error and individual factor sum of squares terms, f_T, f_e and $f_A \cdots f_H$ respectively, are necessary to find the variance. These are defined in Equations 2.9 and 2.10.

$$f_T = n - 1, \; f_A = L - 1 \tag{2.9}$$

$$f_e = f_T - f_A - f_B \cdots - f_H, \text{ excluding pooled factors} \tag{2.10}$$

It can be seen that the DOF of the error increases as factors are pooled. Variance, V, is the ratio of sum of squares to DOF, Equation 2.11.

$$V = S/f \tag{2.11}$$

Significance (F ratio and p-value) The variance ratio F is the ratio of a factor's variance to the variance of the error, defined by Equation 2.12 for factor A. It can be used to determine whether a factor has a statistically significant effect on the results, e.g. that the null hypothesis can be rejected [73]. For factor A, the null hypothesis is that there is no difference in average S/N ratio between each of A's levels.

If $F_A \approx 1$, then the null hypothesis is very likely true, which occurs when $V_A = V_e$ [73]. In this case, F_A follows an F distribution of the form $F(f_A, f_e) = F(1,4)$. If F_A is sufficiently large, the null hypothesis is very likely false. The question of how large F_A must be to reject the null

hypothesis can be interpreted instead as a probability, p. Mathematically, this can be expressed as $P(F(f_A, f_e) \geq F_A) = p$, and p is commonly referred to as a p-value. The p-value is the probability the observed effect of a factor was due to random sampling error, *assuming truth of the null hypothesis* [74]. Often cutoff values for p, such as 0.05, are chosen in advance, and if $p < 0.05$ the null hypothesis is rejected. This is referred to as a p-value test. Note however that p is not the probability that the null hypothesis is true; in fact this can be much larger than p [74]. So, rather than choose an arbitrary cutoff value for p in advance, p was calculated for each factor and is presented in Table 2.3.

When factor G (Level of Vacuum) was initially included, it yielded a value of $p = 0.876$, meaning that it was very insignificant, and so it was pooled (namely its variation was added to the error). Pooling this factor caused the other factors to become more significant. Of the remaining factors, only A (Resin Type) and B (Impregnation Tech.) have $p \leq 0.05$. Factors C (Bagging Arrang'mnt), D (RT Debulk Time) and E (Fibre Architecture) all had $p \approx 0.08$, making them less likely to be significant. Factors F (Repair Thickness) and H (Cure Cycle) both had $p \geq 0.1$, so it is even more likely for these factors that their observed effects were a result of random sampling error.

$$F_A = \frac{V_A}{V_e} \tag{2.12}$$

Percent Contribution The pure sum of squares for a factor, such as S'_A for factor A, is defined by Equation 2.13, and similarly the pure sum of squares of the error, S'_e, by Equation 2.14. This quantity is used to determine the percent contribution, P, of each factor, defined next. The results of these calculations for are presented in Table 2.3.

$$S'_A = S_A - f_A V_e \tag{2.13}$$

$$S'_e = S_e + (f_A + f_B + \cdots + f_H)V_e, \text{ excluding DOF of pooled factors} \tag{2.14}$$

The percent contribution of each factor is the ratio of pure sum of squares to the total sum of squares, Equation 2.15. This value quantifies how much each factor contributes to the average S/N ratio, and hence provides the percent contribution of each factor to void content and variability in void content. The percent contribution for each factor is plotted in Figure 2.11. Note that factors F

TABLE 2.3: Void Content ANOVA Table Using S/N Ratios

Source of Variation	DOF	Sum of Squares S	Variance V	Variance Ratio F	Pure Sum of Squares S'	p-value
A. Resin Type	1	92.97	92.97	19.13	88.11	0.012
B. Impregnation Tech.	2	87.08	43.54	8.96	77.36	0.033
C. Bagging Arrang'mnt	2	50.09	25.04	5.15	40.37	0.078
D. RT Debulk Time	2	51.95	25.97	5.35	42.23	0.074
E. Fibre Architecture	2	50.84	25.42	5.23	41.12	0.076
F. Repair Thickness	2	31.48	15.74	3.24	21.76	0.146
G. Level of Vacuum	(2)	(2.41)	Pooled			
H. Cure Cycle	2	19.97	9.99	2.05	10.25	0.243
All other/error	4	19.44	4.86	-	1887.21	-
Total	17	403.81				

(Repair Thickness) and H (Cure Cycle) are included in this plot, despite likely being insignificant due to their high p-values as previously discussed.

$$P = \frac{S'}{S_T} \tag{2.15}$$

Predicted Optimum and Confirmation Test

Optimal Levels The main effect of each factor at a given level can be assessed by Equation 2.16, which computes the average S/N ratio for a factor (X) at a given level (k), $(\bar{S/N})_{Xk}$. These values are plotted in Figure 2.12. The most desirable level for a factor is the one that yields the highest average S/N ratio. For example, from the main effects plot (Figure 2.12), it is clear that level 2 is the most desirable level for factor A (Resin Type), as level 2 yields a much higher average S/N ratio of $(\bar{S/N})_{A2} = 27.3$ compared to $(\bar{S/N})_{A1} = 22.8$ for level 1. The optimal levels for each factor determined in this way are presented in Table 2.4.

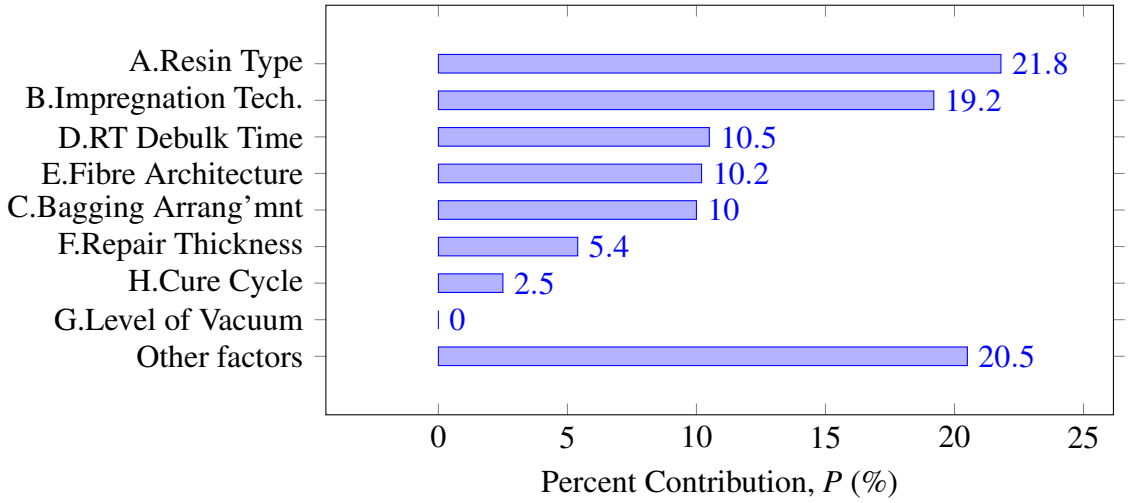

FIGURE 2.11: Percent contribution of each factor to void content.

TABLE 2.4: Optimal Condition for Minimum Void Content

	A. Resin Type	**B. Impreg. Technique**	**C. Bagging Arrangement**	**D. RT Debulk**	**E. Fibre Arch.**	**F. Repair Thick.**	**G. Level of Vac.**	**H. Cure Cycle**
Optimal Level	Epocast 52 A/B	Vacuum	DVD	120 min	Twill 2x2	4 plies	–	Two dwells
Percent Cont. (%)	21.8	19.2	10.0	10.5	10.2	5.4	0	2.5

$$\text{Average S/N for factor X at level k} = (\bar{S/N})_{Xk} = \frac{L}{n}\left(\sum_{i=1}^{n}\begin{cases}(S/N)_i & \text{if X at level k}\\ 0 & \text{otherwise}\end{cases}\right) \tag{2.16}$$

It was noted that factors C, D and E had $0.1 \geq p \geq 0.05$, and in particular F and H had $p > 0.1$. In Table 2.4, the optimal levels for these factors based on the main effects observed were nonetheless presented. However, with such high p-values, it should be noted that these factors may statistically have no effect on the outcome.

Void Content at Optimum Condition The void content for the optimal configuration of Table 2.4 may be estimated using the methods from [71], using only the factors which were not pooled.

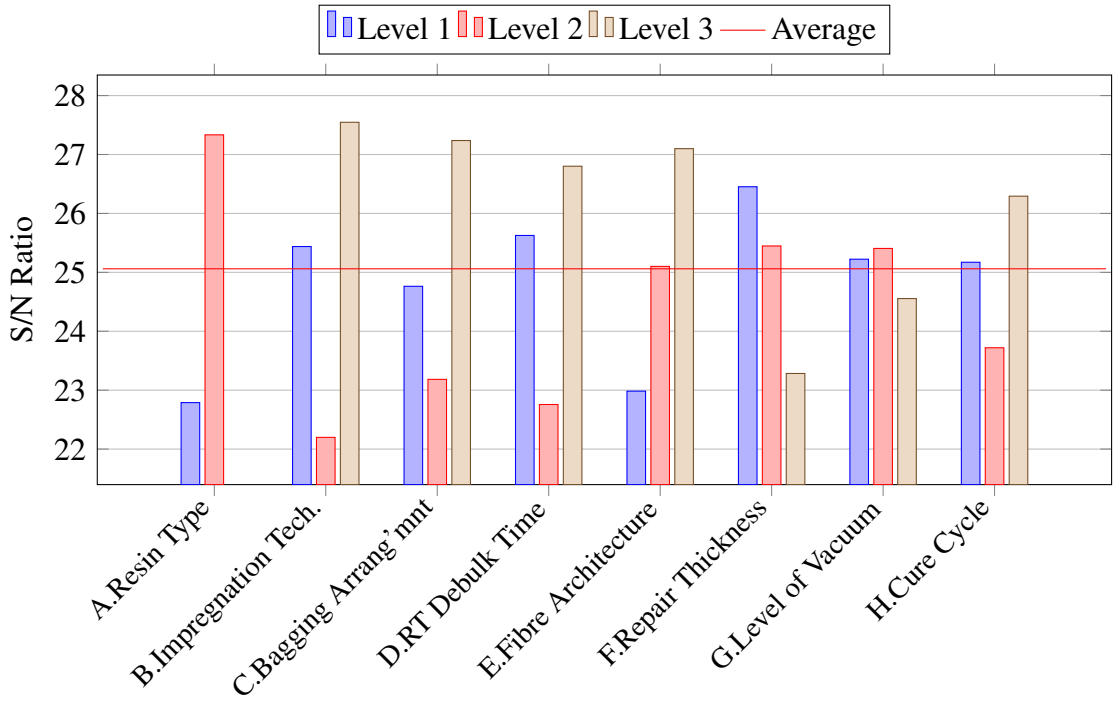

FIGURE 2.12: Main effects of each factor on the S/N ratio for void content.

First the average S/N ratio of all trials, $(\bar{S/N})$, is found from Equation 2.17. The contribution of each factor to the S/N ratio is determined by Equation 2.18. Finally, the S/N ratio for the optimal condition is found from Equation 2.19, and then converted to % void content by Equation 2.20. The expected standard deviation for the optimum condition was found in terms of S/N ratio from Equation 2.21 [75], and then converted to % void content by Equation 2.20. The predicted void content for the optimal configuration is 1.2 % with a standard deviation of 0.8 %.

$$(\bar{S/N}) = \frac{1}{n}\sum_{i=1}^{n}(S/N)_i = 25.1 \tag{2.17}$$

$$\begin{matrix}\text{S/N contribution of} \\ \text{factor X at level k}\end{matrix} = \Delta(S/N)_{Xk} = (\bar{S/N})_{Xk} - (\bar{S/N}) \tag{2.18}$$

$$(S/N)_{desired} = (\bar{S/N}) + \sum_{X=A,B,\ldots,H} \max\left[\Delta(S/N)_{Xk}, \text{for k} = 1, \ldots, \text{L}\right] \tag{2.19}$$

TABLE 2.5: Optimal Condition for Minimum Void Content: Estimated vs Tested

Sample	Void Content (%)	S/N
Estimated	1.2 ± 0.8	38.4
Tested	1.1 ± 0.5	38.8

$$\text{Void Content } \% = (100\%)\sqrt{10^{\frac{-(S/N)_{desired}}{10}}} \tag{2.20}$$

$$\sigma_{optimum} = \sigma_{avg} 10^{-\left[(S/N)_{desired} - (\bar{S/N})\right]/20} \tag{2.21}$$

Confirmation Test The optimal configuration of Table 2.4 was different from all trials in the Taguchi orthogonal array, so up to this point no "optimal" patches had been manufactured. Therefore to confirm that the optimal process will provide the lowest void content, one "optimal" patch was manufactured using the same parent laminate tool and equipment. Void content was assessed by optical microscopy in the same way, resulting in an average void content of 1.1 % $\pm$ 0.5 % as shown in Table 2.5. This is in good agreement with the expected value of 1.2 % $\pm$ 0.8 %, and is less than the lowest void content achieved of 2.2 % $\pm$ 0.4 % for Trial 10.

The objective in assessing main effects from the S/N ratios was to determine processing levels that minimize both average void content and its variation (minimal standard deviation). More than one patch would need to have been manufactured with the optimal process to determine if this process is indeed robust.

Factor Interaction The estimate of the optimal condition, using Equation 2.19, assumed the effect of each factor was additive. It therefore neglects the effect of any interactions between factors. As mentioned previously, a larger orthogonal array would be required to assess interactions, and consequently include such terms in the regression model of Equation 2.19. The good agreement obtained between the regression model and the confirmation test does however suggest that interactions were not significant compared to the main effects for the range of selected factors and levels.

2.1.3 Sample Micrographs

Representative micrographs are presented in Figures 2.13 and 2.14, with the average void content for the corresponding trial. All images are oriented with the bag side on top, and use the same scale. The fibre volume fraction, v_f, was estimated from the average specimen thickness t measured from the micrograph as per Equation 2.22. See the discussion in [76] for the applicability of this formula; it is noted that it is valid in the range $v_f = 0.45$ to 0.65 for which t and v_f vary linearly.

$$v_f = \frac{n_{plies} FAW}{t \rho_f} \tag{2.22}$$

where:

v_f is the fibre volume fraction

n_{plies} is the number of plies

FAW is the fabric areal weight ($\mathrm{g\,m^{-2}}$)

t is the average specimen thickness from the micrograph (m)

ρ_f is the fibre density ($\mathrm{g\,m^{-3}}$)

A sample micrograph for Trial 10, which had the lowest void content of all trials and used the random blob impregnation process, is shown in Figure 2.13. For comparison, a micrograph for one of the lowest void content vacuum impregnation patches (Trial 9) is shown in the same figure. The vacuum impregnation patch has almost no intra-tow porosity, while the random blob impregnation patch has some intra-tow porosity. However, the vacuum impregnation patch does seem to have more inter-ply voids. Note also that both of these patches had 8 plies of twill. As both micrographs are at the same scale, it is clear that Trial 10, with $v_f = 56\%$, is much thicker than Trial 9, with $v_f = 66\%$. Additional resin is visible in between the plies, particularly at tow crossover points, for the more resin rich Trial 10, which was typical for all of the more resin rich patches.

Two examples of the manual impregnation method are in Figure 2.14, representative of the lowest and highest porosity patches produced by this technique. Trial 5 in Figure 2.14 also demonstrates the worst porosity observed of all trials, at 15.9 %. Significant intra-tow micro voids and inter-ply macro voids were present in all manual impregnation patches.

Void Morphology A distinction can be made between intra-tow micro voids, which tended to have areas on the order of $1000\,\mu\mathrm{m}^2$, and inter-ply macro voids with areas of $10\,000\,\mu\mathrm{m}^2$ or greater. As

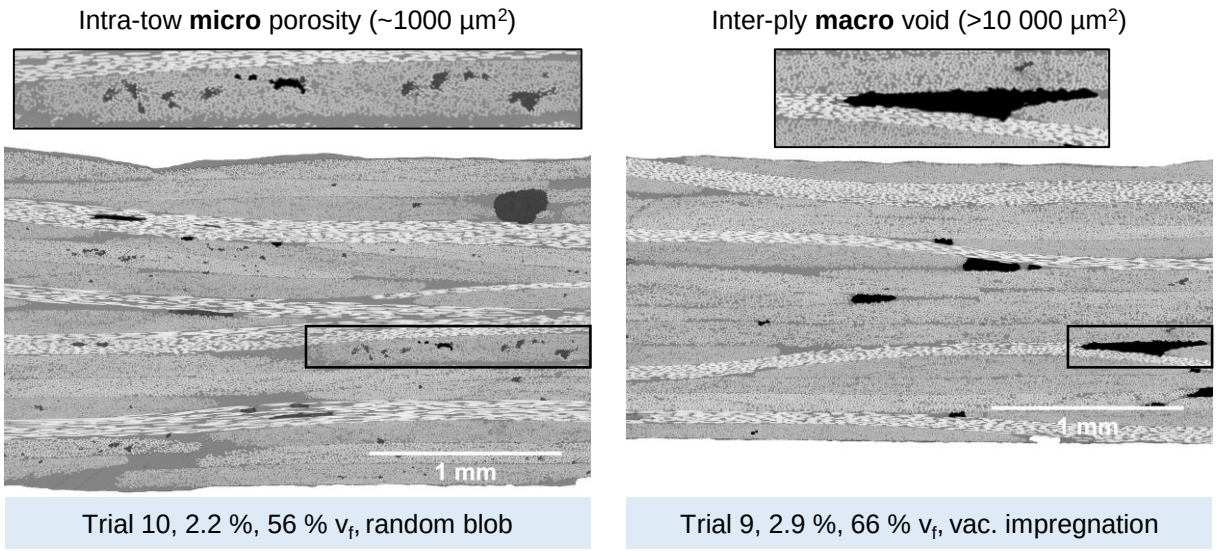

FIGURE 2.13: Micrographs comparing the void morphology for the random blob and vacuum impregnation techniques, for two trials with 8 plies.

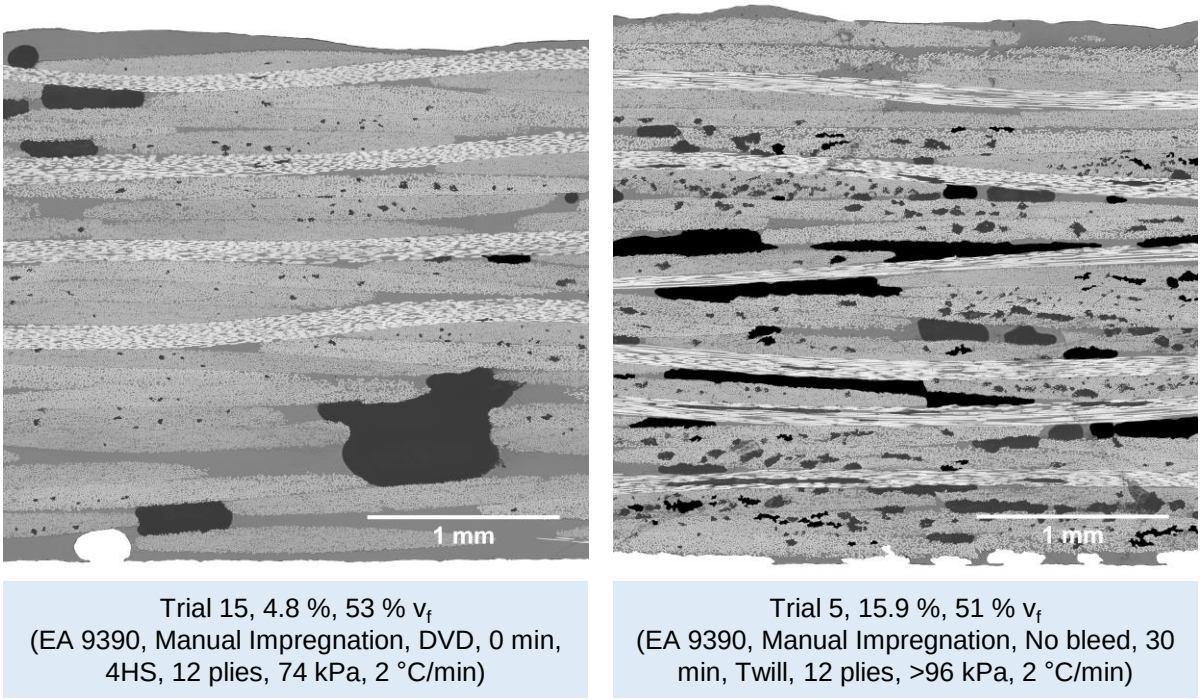

FIGURE 2.14: Micrographs of the lowest and highest void content manual impregnation patches.

noted from observing the micrographs of Figure 2.13, the void morphology seems to be related to the resin impregnation technique. Using 10 000 μm^2 as the cut-off between intra-tow micro and inter-ply macro voids, the average void content for each trial was split into micro and macro components. From these values, the average overall, micro and macro void contents were determined for each impregnation technique and are plotted in Figure 2.15. In agreement with the previous observation, the vacuum impregnation technique had the fewest micro voids, while the random blob impregnation technique had the fewest macro voids. The manual impregnation technique had both the most macro and micro voids. Finally, it is clear why the vacuum impregnation technique led to the optimal process, as it has the lowest average overall void content and standard deviation.

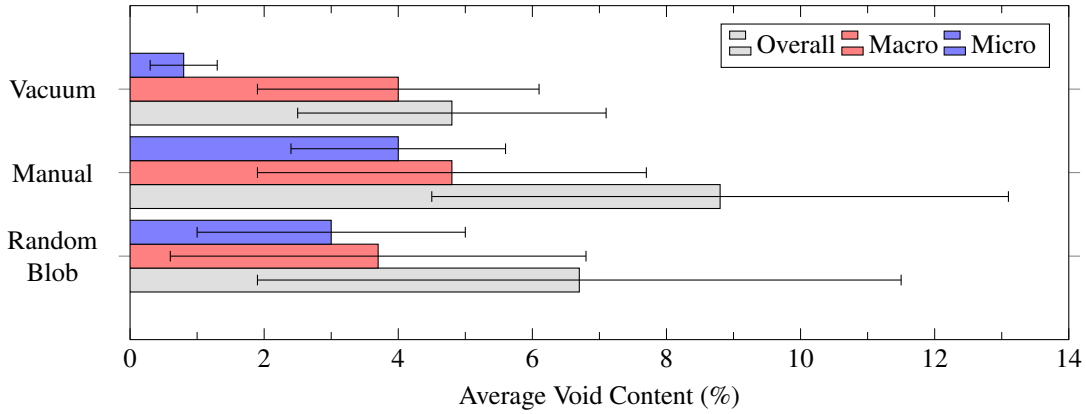

FIGURE 2.15: Average void size distribution by impregnation technique.

2.1.4 Void Content Discussion

Resin Type and Cure Cycle Factors

The resin type proved to be the most influential factor with a 23 % contribution. The slightly different viscosity profiles of the two resins may have contributed to this. However, the resin type also dictated the final cure temperature, which affects the nucleation and growth of voids [77].

A simple analysis of the resin pressure required to suppress void growth can highlight the importance of keeping the temperature at resin gelation to a minimum. To prevent void formation and growth, the hydrostatic resin pressure and surface tension forces must exceed the void pressure [29], [77]. Kardos [77] derived an equation for the resin pressure required to prevent growth

of a pure water void by diffusion. The equation is a function of temperature and the relative humidity at which the resin was equilibrated. As there is a very strong driving force for diffusion of water to pure air voids, it is reasonable to treat voids as pure water [77]. This required resin pressure to suppress void growth is plotted in Figure 2.16. After gelation, no further void growth or dissolution occurs [29]. The EA 9390 patches gelled at temperatures from 100 °C to 121 °C and the Epocast 52 A/B from 79 °C to 93 °C (see discussion on temperature control further below). As can be seen from Figure 2.16, the required resin pressure drops dramatically going from 121 °C to 93 °C. These patches were processed at relative humidities near 20 %, at which the required resin pressure drops from 0.43 atm to 0.17 atm going from 121 °C to 93 °C. Note that the available consolidation pressure cannot exceed 1 atm for a VBO process, and that the resin pressure is likely lower due to the load carried by the fibre bed. Therefore, the effect of final cure temperature may explain why resin type was the most important factor.

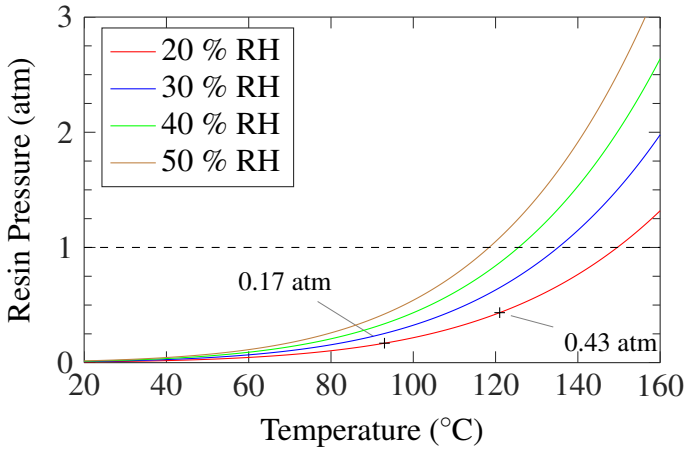

FIGURE 2.16: Resin pressure required to suppress growth of pure water voids.

Temperature Control Problems

Thermocouples placed on top of each bag closely matched the desired cure cycle for the bleed and no bleed bagging arrangements. However, when the DVD chamber was used poor temperature control was observed, characterized by large differences between the oven air temperature and the patch temperature, as well as slower heat up rates. Sample temperature data is provided for DVD patches made with each resin using the two dwell cure cycle in Figure 2.17. When vacuum

was pulled in the DVD chamber, almost all heat transfer would have had to occur by conduction through the tool plate underneath the parent structure. As such, the temperature only reached 30 °C to 40 °C before the DVD chamber was vented at an oven air temperature of 60 °C, with the worst temperature control observed for the 5 °C min^{-1} ramp cure cycle. While the same conditions were maintained for all trials, these temperature lags in the DVD chamber could explain why the cure cycle variable had little effect with only a 2.5 % contribution.

The bagging arrangement contributed 10.0 %, with the DVD method proving best, likely due to its ability to degas the laminate before application of compaction pressure. However, the viscosity evolution calculated from the model in [36] is plotted in Figure 2.17, and demonstrates how the DVD was not used to its full potential. The viscosity only dropped significantly after the DVD chamber was vented, as it this point the temperature rose above ≈ 40 °C. For contrast, the viscosity evolution for the desired temperature profile is also shown in Figure 2.17, and for both resins would have provided viscosities of 10 Pa s or lower to assist with the removal of volatiles during the degasing stage.

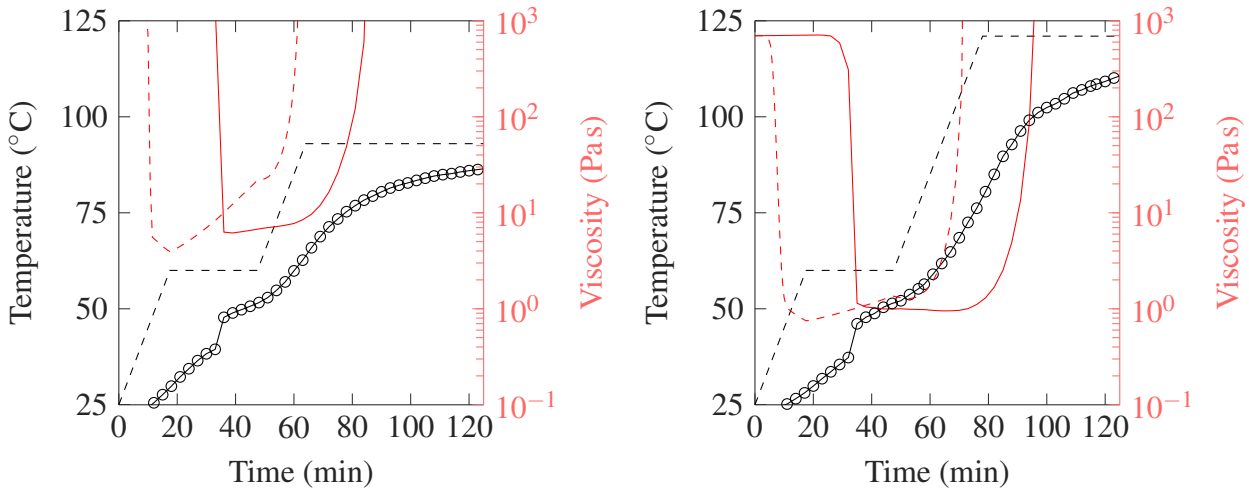

(A) Epocast 52 A/B. (B) EA 9390.

FIGURE 2.17: Desired - - - and experimental —o— temperature along with desired - - - and experimental —— viscosity evolution when the DVD bagging arrangement was used with the two dwell cure cycle.

Impregnation Technique

Voids can form by mechanical entrapment or by nucleation during cure [70]. The mechanical entrapment depends especially on the resin impregnation and lay-up method. So, it is logical that the impregnation and lay-up method was the second most influential factor with a 19.2 % contribution. It is not surprising that the manual impregnation method led to the most porosity: intra-tow air becomes entrapped during impregnation as the resin contains entrapped air and the pressure of a squeegee is the only force to push air out of the ply, while inter-laminar air becomes entrapped during ply collation between the fully impregnated plies. While the vacuum impregnation method can entrap inter-laminar air during ply collation because the plies are fully impregnated, it is effective at removing intra-tow air which resulted in it leading to the lowest overall porosity. The random blob method, which maintains dry regions in the plies after ply collation, provides some air evacuation capability for both intra and inter-laminar air. A glass tool experiment provided further insight.

Glass Tool Experiment To better understand resin flow and gas transport phenomena in random blob impregnated laminates, a simple experimental set-up was devised to visualize the flow of resin once vacuum is applied. The same method was previously used by Préau to visualize void formation in a film adhesive [32], who provides more details on the set-up. In this case, a 10 cm square laminate of 8 plies impregnated by the random blob method with EA 9390 was placed on a transparent glass tool plate. The plies were not compacted during lamination. The laminate's edges were sealed off to air using vacuum bag sealant tape, to mimic the boundary conditions in a scarf repair. Then, the laminate was sealed under a bleed vacuum bag to the glass tool plate, with a heat blanket. A camera placed underneath the glass tool took time lapse images from start of vacuum application.

Full vacuum was gradually applied over a period of 1 min at room temperature as shown by Figure 2.18. The image at 0 s shows the edge of a blob of resin highlighted in blue. As the level of vacuum increased, the resin rapidly flowed, "racetracking" along the tow overlaps where there is less compaction pressure. It can be seen in the image at 20 s how this "racetracking" phenomenon can lead to dry regions at the centre of tows, with several of these dry areas circled in red at the 36 s mark. This may explain why the random blob method often had intra-tow porosity, as air in the tows becomes encircled by resin before it can escape. Secondly, it is clear that the laminate becomes nearly fully impregnated at room temperature very quickly (in 1 min or less) after vacuum is applied. This is unlike the out-of-autoclave prepregs (semi-pregs) that inspired the random blob

method, for which the resin does not flow much at room temperature allowing air evacuation through dry regions [26].

For the same sample, Figure 2.19 shows the evolution of entrapped gas bubbles (humid air) during cure, for a 2 °C min^{-1} ramp to 60 °C and hold for 60 min. From the image at the start of cure, it is clear that all dry areas became fully impregnated after a vacuum hold for several minutes at room temperature. Once the 60 °C dwell temperature was reached, and the resin was near its minimum viscosity, large gas bubbles were visible at nearly every tow crossover, which significantly shrunk or disappeared by the end of the dwell. Little change was visible after the end of the 60 °C dwell as the sample was heated to 93 °C.

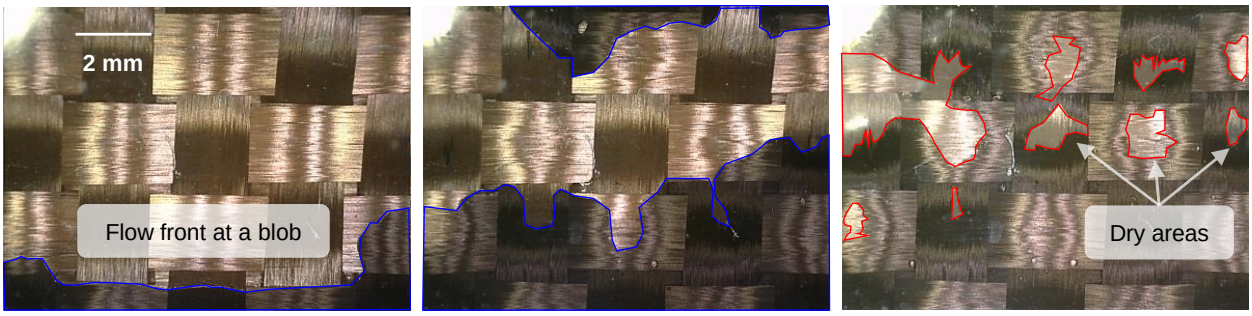

FIGURE 2.18: Resin flow in random blob impregnation. Starting at 00:00:00 (h:min:s), vacuum was gradually applied until full vacuum was reached at a rate of 1000 mbar min^{-1}.

Other Factors

The level of vacuum had almost no contribution, with 74 kPa proving best from the main effects plot. This could be because VBO repairs rely primarily on air extraction for void reduction. Since higher pressures compact the laminate more, they also decrease its permeability to air, perhaps explaining why less vacuum is not detrimental.

The stability of plain weave made it the easiest to work with. However, as demonstrated by the main effects plot, the 2 x 2 twill yielded the lowest porosity followed by the 4HS, perhaps because lower crimp weaves are easier to impregnate [39].

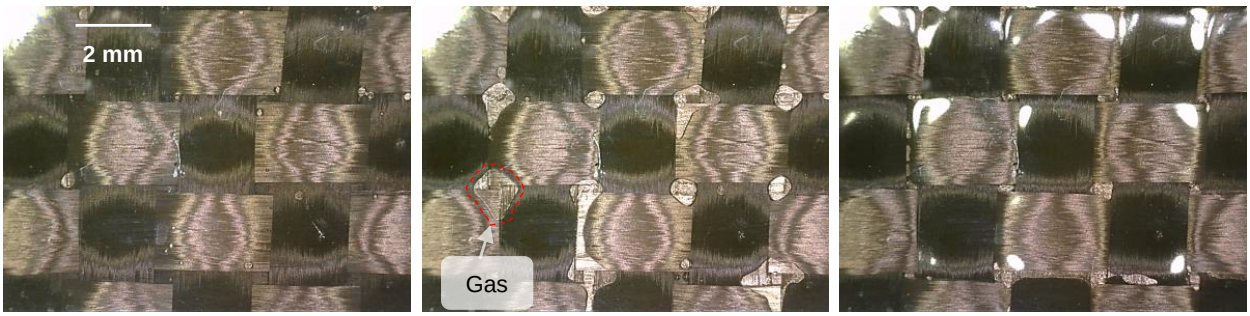

FIGURE 2.19: Evolution of entrapped gas bubbles during cure for random blob impregnation. At 00:11:58 (h:min:s), a 2 °C min^{-1} ramp began from 25 °C to 60 °C.

The all other/error factor contributed 20.5 %. It should be noted that this term includes the influence of factors excluded from the experiment as well as uncontrollable factors [75].

Follow-Up Test

Two additional wet layup patches were manufactured using the same parent laminate tool, except this time cured with a heat blanket. The objective was to test if the importance of the resin type factor was due to the final cure temperature. A secondary objective was to test if the DVD would be more effective with proper temperature control.

Therefore, the two patches were processed with the vacuum impregnation technique, DVD bagging arrangement, twill fabric, 12 plies, a 120 min RT debulk and debulked/cured under full vacuum. Both patches were cured according to the two dwell cure cycle, but with a final hold temperature of 93 °C. The only difference between the two patches: one utilized EA 9390 resin and the other Epocast 52 A/B resin.

The control thermocouple for the heat blanket was placed directly on the patch, isolated by polyester tape, nearly perfectly matching the desired temperature profile with the experimental data shown in Figure 2.20. The viscosity for each resin would have therefore followed the profile shown in Figure 2.20, computed using the model in [36]. Each resin gelled near 93 °C as shown.

Following the same void content measurement procedure by optical microscopy, the measured void contents were:

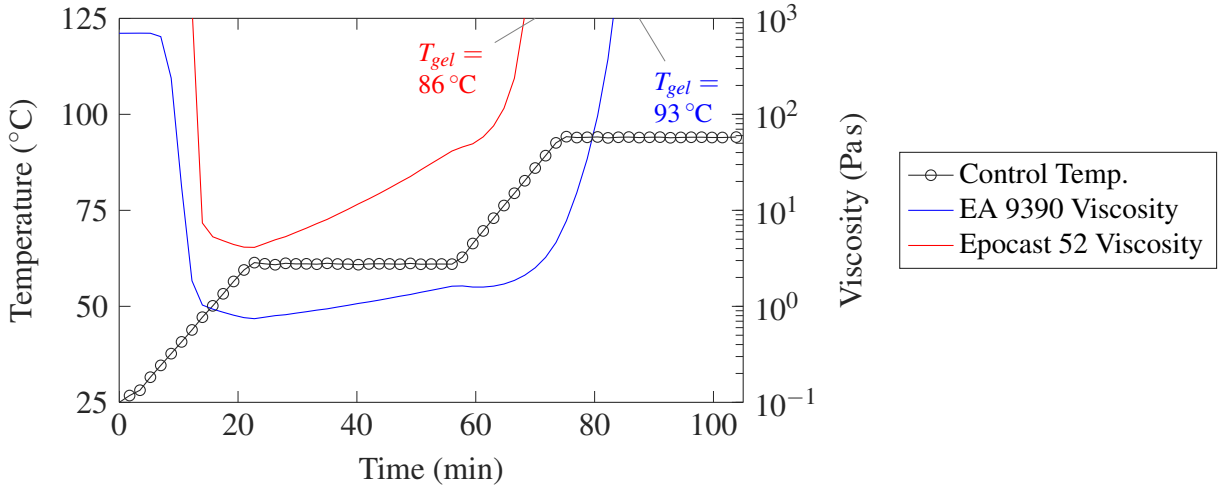

FIGURE 2.20: Temperature and viscosity for two patches cured with a heat blanket.

- 0.68 ± 0.11 % for the EA 9390
- 1.62 ± 0.79 % for the Epocast 52 A/B

The EA 9390, which was the less favourable resin from the DOE study, produced a lower void content than the Epocast 52 A/B this time. This result may suggest that it is really the temperature at gelation, at which voids are locked in the resin [29], that is important as the gelation temperature was reduced here from 121 °C to 93 °C for the EA 9390. Further, the proper temperature control allowed each patch to be degassed properly during the DVD stage, while their viscosities were at a minimum. This may explain why the EA 9390 led to a void content well below the 1.2 % for the optimal process. Further testing would be required to determine whether the cure cycle or the DVD is more important for producing low void content repair patches.

2.1.5 Fibre Volume Fraction Results and Discussion

Results

The fibre volume fraction v_f was computed for each patch, resulting in two values per trial. Values ranged from 40.1 % (Trial 8) to 60.3 % (Trial 10). These results were subjected to the same S/N analysis as the void content, however this time a “nominal is best” criterion was used, with a target

of 65 % v_f. Consequently, the MSD was defined as in Equation 2.23 (based on [71]) where R_i is the v_f for a given patch, while the rest of the analysis was identical.

$$MSD = \frac{1}{2}\sum_{i=1}^{2}(R_i - R_o)^2 = \frac{1}{2}\sum_{i=1}^{2}(R_i - 0.65)^2 \tag{2.23}$$

The main effects and percent contribution of each *significant* (based on F-test) factor are plotted in Figure 2.21. The resin type, RT debulk time, and cure cycle had an insignificant effect on the fibre volume fraction, having F statistics even less than unity. The remaining factors are all significant based on an F-test with a confidence of 85 % or greater.

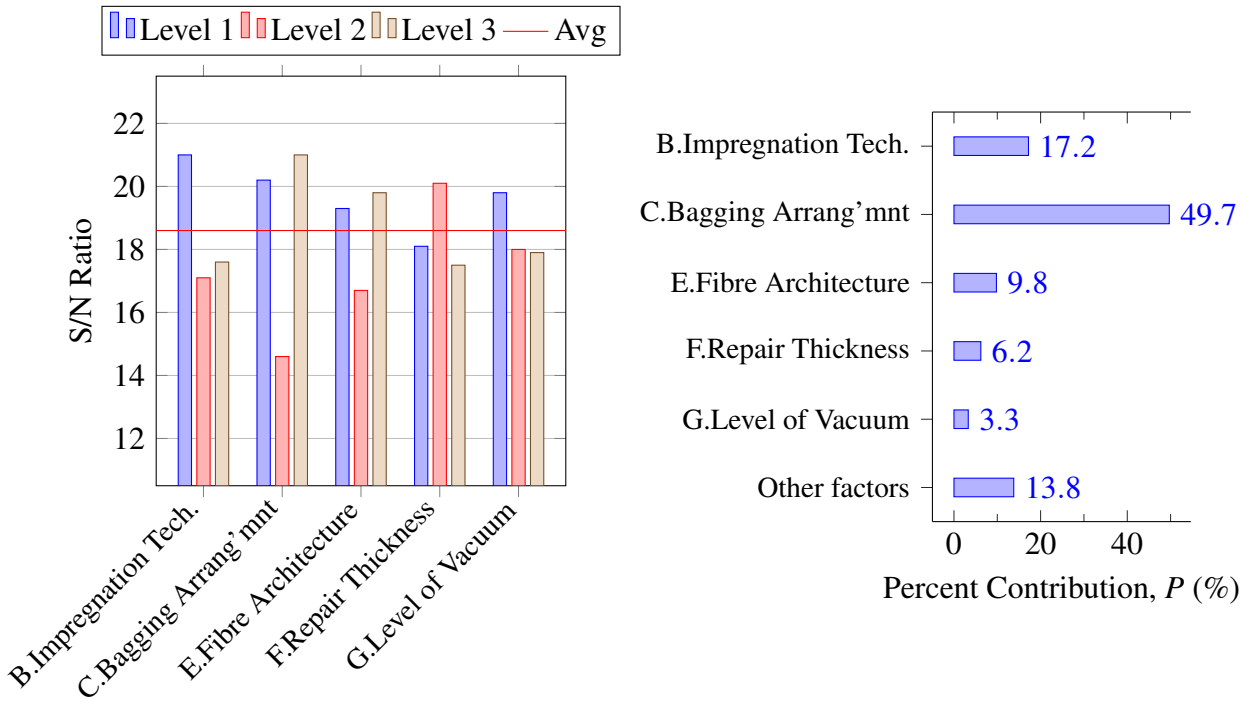

FIGURE 2.21: Main effects plot and percent contribution for fibre volume fraction.

Predicted Optimum

From the main effects plot of Figure 2.21, the highest v_f is expected from a patch made with random blob impregnation, DVD, twill, 8 plies and full vacuum, with the other factors having

TABLE 2.6: Comparison of Optimal Configurations for Porosity and Fibre Volume Fraction

Optimal Configuration for...	**Void Content** (%)	v_f (%)
Minimum Void Content	1.2	52
Nominal v_f (65 %)	1.7	65

insignificant effects. This would yield the target fibre volume fraction (65 %) with a standard deviation of 4.3 %. Note that the linear model of Equations 2.17 to 2.21, used previously to estimate the void content for the optimum condition, can be used in the same way either to predict void content or v_f for any combination of levels. This model was used to predict void content and v_f for Table 2.6, which compares the optimal cases for each. For the optimal v_f case, factors insignificant to v_f were set to their optimal levels for void content, and the converse was done for the optimal void content case.

Discussion

The vacuum bagging arrangement was the most significant factor by far, contributing 50 % to the final v_f. The no bleed arrangement produced the most resin rich laminates, as to ensure full wet out of the fabric, the impregnation techniques used excess resin. Since the DVD method had an inner bag identical to the vertical bleed method, both methods led to a high v_f, with the DVD method being just slightly better from the main effects plot.

Each resin impregnation technique used different amounts of resin, with the least deposited by the random blob method. However, since much excess resin can be bled during cure, this factor contributes 17 % percent to the final v_f, much less than the bagging arrangement.

It's surprising that the twill yielded the best v_f, and not the lower crimp 4HS. Also, while contributing only 6 %, repair thickness is surprising in that the 8 ply thickness led to the highest v_f, followed by the 4 and then 12 ply configurations. This result could be due to the fact the repair patches are tapered and the v_f computed was an average for the whole patch. Additionally, the bleeder may have become saturated for thicker patches. It is interesting to note that the level of vacuum contributes only 3 %, with full vacuum being ideal, and lesser values (74 kPa, 50 kPa) being almost identical.

2.2 Effect of Void Content on Short Beam Shear Strength

While the optimised process from the DOE study (Table 2.4) should yield wet layup repairs of significantly reduced void content, ultimately this reduction was sought to yield improved mechanical properties. Voids are detrimental to matrix dominated mechanical properties, because they reduce (cross-sectional) area and act as crack initiation sites [78], [79]. The magnitude of the reduction in mechanical properties due to voids depends on the property measured and the fibre/matrix materials used [79].

To provide an example of the improvement in mechanical properties that can be achieved from an optimized wet layup repair process, short beam shear tests were performed. Short beam shear was chosen as (1) voids have a pronounced reduction on short beam strength [79], [80] and (2) the small specimen dimensions allow many samples to be cut from a repair patch manufactured using the same methods as the DOE study.

2.2.1 Patch Manufacturing

Three repair patches were processed using the same released parent laminate tool, methods and materials as the DOE study. However, patches were cured with a heat blanket placed on top of the patch, to allow proper temperature control when using the DVD technique. To minimize the through-thickness temperature gradient that arises from such one-sided heating, the underside of the tool was insulated, in the same configuration as used for the inner bag of the DVD chamber in Chapter 3 (see Figure 3.15).

All three patches were made with Epocast 52 A/B resin, 12 plies of $200\,\mathrm{g\,m^{-2}}$ 3k twill fabric in a $[0_{12}]$ sequence, and debulked/cured under full vacuum. This $[0_{12}]$ laminate was chosen to meet short beam strength test requirements.

All patches were cured according to the *two dwells* cure cycle of the DOE study (Figure 2.9), venting the DVD chamber at the same point (15 min into the 60 °C dwell) and with a final hold temperature of 93 °C. The resin impregnation technique, vacuum bagging arrangement and RT debulk time were varied according to Table 2.7 for each sample. The processing levels were chosen so as to include the optimal process (vacuum/DVD patch), a slightly less optimal random blob/DVD patch and a more standard wet layup process (manual impregnation patch).

2.2.2 Procedure

Short Beam Strength

From each patch, twelve short beam strength specimens were cut in the 0° direction on a water cooled diamond saw. After cutting, specimens were placed in an oven for 2 h at 93 °C to guarantee that they were dry and equally cured. Testing was performed in accordance with ASTM D2344 [81]. Specimen thickness was measured to be in the range of $t = 2.274$ mm to 2.970 mm, which meets the standard's requirement that $2.00\,\text{mm} \geq t \geq 6.00\,\text{mm}$. Specimens were cut to provide a width to thickness ratio of 2.0 and an overall length of $6.0t$ in accordance with the standard.

Testing was performed at a rate of $1\,\text{mm}\,\text{min}^{-1}$ and a span of $4.0t$ with a Wyoming Test Fixtures short beam shear fixture in an Insight 5 kN uniaxial electromechanical load frame (MTS Systems Corporation). In accordance with the standard, the fixture's supports and loading nose were 3.0 mm and 6.0 mm in diameter respectively. The test setup is shown in Figure 2.22b.

For each specimen short beam strength F^{sbs} was calculated as per ASTM D2344 [81] from the maximum load P_{max} according to Equation 2.24. Note that this is the equation for the maximum transverse shear stress in a classical beam, which occurs at the mid-plane and is constant along the span. Since the beam is short, the actual transverse shear stress distribution deviates significantly from that of a classical beam [82], and further failure modes aside from interlaminar shear, such as flexure can occur. Consequently, in general F^{sbs} is not recommended for use as design data (e.g. interlaminar shear strength), but rather is preferred for quality control purposes, comparing specimens of the same dimensions [83].

$$F^{sbs} = \frac{3P_{max}}{4bt} \tag{2.24}$$

where:

F^{sbs} is the short beam strength (MPa), P_{max} is the maximum load observed (N)

b is the measured specimen width (mm), t is the measured specimen thickness (mm)

Void Content

Three 25 mm long microscopy specimens were cut at 0° from within the boundary of the patch's smallest ply. The same optical microscopy and image analysis procedure as the DOE study (section 2.1.1) was then used to determine void content.

2.2.3 Results

The expected void content for each patch was calculated from the linear model of Equations 2.17 to 2.21, and is tabulated alongside the measured value in Table 2.7.

The vacuum/DVD patch only differs from the optimal process (Table 2.4) in number of plies (12 vs 4). Consequently, its predicted void content is slightly higher than the optimal case, at 1.7 % vs 1.2 %. This prediction is close to the measured value of 1.6 %. Surprisingly, the random blob/DVD patch had the lowest measured void content at 0.9 %, lower than the intermediate value of 2.5 % predicted. As expected, the manual patch had the highest void content, but at 3.7 % it was lower than the 4.9 % predicted. Since only one patch was manufactured for each of these processes, it is hard to say whether the measured values agree with the predictions, as they could be within the expected variability as indicated by the standard deviations in Table 2.4.

All short beam strength samples appeared to fail in flexural compression. F^{sbs} is plotted against the measured void content for all three patches in Figure 2.22a. While there are only three data points, there is a very strong linear correlation between F^{sbs} and void content for these samples, with a sample Pearson correlation coefficient $r = -0.91$. For each data point, the error bars represent the sample standard deviation.

A one-way ANOVA on the F^{sbs} data established that there are *significant* differences in the mean F^{sbs} values between the 3 patches, with a p-value of near zero ($2.16 \cdot 10^{-11}$ %). This does not however answer which pairs of F^{sbs} values are significantly different. To this end, a multiple comparison procedure using the Bonferroni method was followed using MATLAB [73]. With 95 % confidence, none of the simultaneous confidence intervals overlap, indicating that each pair of average F^{sbs} values are significantly different.

Its also interesting to compare the F^{sbs} values with the value provided in the datasheet [49]. While no processing or test details are mentioned in the datasheet, it is stated that for room temperature dry conditions $F^{sbs} = 53.1$ MPa, for a 36 % resin content T300 3k plain weave laminate cured at 93 °C. As this datasheet F^{sbs} is near that for the manual patch, the datasheet laminate likely has a void content near 3.7 %. Thanks to the significant reduction in void content provided by the vacuum/DVD and random blob/DVD processes, they offer a significant improvement in F^{sbs} relative to the datasheet. In particular the random blob/DVD patch offers a 32 % improvement in F^{sbs}.

TABLE 2.7: Void Content and Short Beam Strength for $[0_{12}]$ Wet Layup Patches

Sample Name	Processing Factors Varied			Void Content (%)		
	B. Impreg. Tech.	C. Bagging Arrang'mnt	D. RT Debulk Time (min)	Measured	Predicted	F^{sbs} (MPa)
Rand. Blob/DVD	Rand. Blob	DVD	0	0.9 ± 0.6	2.5 ± 1.7	70.2 ± 4.9
Vacuum/DVD	Vacuum	DVD	120	1.6 ± 0.8	1.7 ± 1.2	66.1 ± 3.6
Manual	Manual	Bleed	0	3.7 ± 0.4	4.9 ± 3.3	51.3 ± 2.7

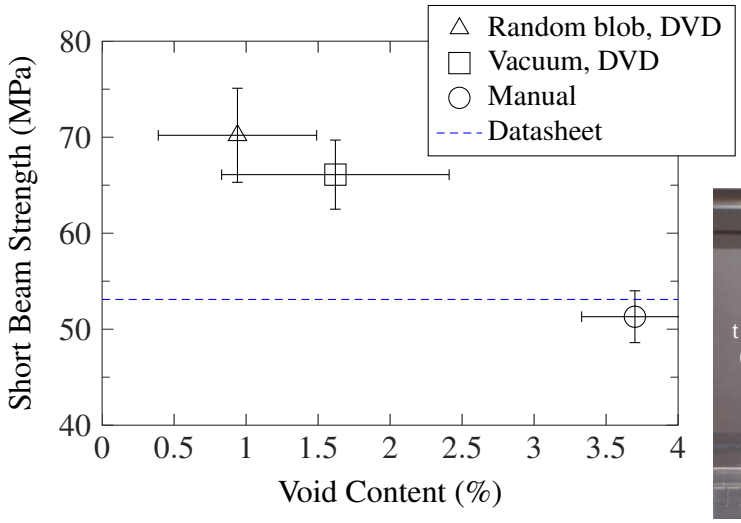

(A) Short beam strength vs void content.

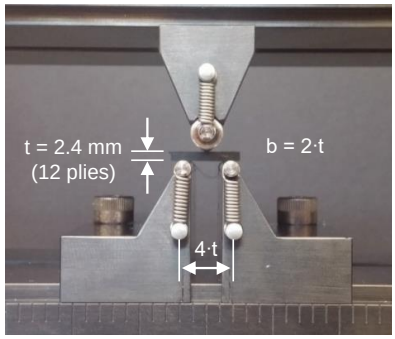

(B) Short beam strength test setup.

FIGURE 2.22: Short beam shear testing of Epocast 52 A/B repair patches with 3k carbon twill in a $[0_{12}]$ sequence.

2.3 Summary

The effect of several processing factors on VBO wet layup repair patch void content and fibre volume fraction was determined experimentally using Taguchi design of experiment techniques. The main findings were:

With VBO processing, the void content within wet layup repair patches can be very high. This was demonstrated by the average void content of 6.3 % for the 18 different wet layup patches

considered.

While resin type was predicted to be the most important factor for porosity with a 22 % contribution, this variable also determined the final cure temperature, with the lower temperature curing Epocast 52 A/B proving better than the EA 9390. Consequently, cure cycle dependent effects on the resin viscosity and volatile pressure contributed to the importance of this factor. To test this hypothesis, one patch was manufactured for each resin with the same process except at the lower temperature, 93 °C cure cycle. This time the EA 9390 led to the lowest void content, at only 0.68 %, indicating the importance of minimizing the temperature at resin gelation.

The resin impregnation technique was almost as significant as the resin type, with the vacuum impregnation method leading to the lowest porosity. While the random blob method had more intra-tow porosity, it did yield below 3 % porosity for two of the tested configurations.

The vacuum bagging arrangement, repair thickness and fibre architecture all had an equal effect on porosity, contributing 10 % each. The DVD bagging arrangement proved best overall for patch quality, though it would present a challenge for curved parts. This was despite the patch temperature lagging the oven air temperature significantly prior to venting the DVD chamber, causing high resin viscosity during the debulk stage. This insulating effect of the DVD chamber may have also caused the cure cycle to seem less important, as this variable contributed only 2.5 %. Subsequent patches that were manufactured using the DVD technique and a heat blanket yielded void contents as low as 0.68 %, demonstrating that this temperature control problem may have caused the importance of the DVD to be underestimated.

Surprisingly, vacuum as low as 50 kPa did not result in higher porosity, and also had relatively little effect (3 %) on fibre volume fraction. By far the most important factor for fibre volume fraction was the vacuum bagging arrangement with a 50 % contribution, with bleed arrangements providing the highest fibre volume fractions. With a 17 % contribution the resin impregnation technique was also important to this end, with random blob proving best as it accurately controls the resin to fibre ratio.

Analysis of the S/N ratios demonstrated that the ideal configuration of Table 2.4 would yield a 1.2 % void content, and this was achieved for one confirmation repair patch. The importance of reducing patch void content was highlighted by the drastic improvement in short beam strength: when void content was reduced from 3.7 % to 0.9 % for an optimized process, short beam strength improved by 32 %.

Chapter 3

Repair of An Aircraft Demonstrator

Temperature, pressure and moisture related process deviations arise when repairing a real structure. Therefore, in this chapter, composite repairs are performed on an actual, decommissioned aircraft part. The main objective is to validate improvements in repair quality seen at the lab scale for wet layup repairs in the previous chapter, and as a secondary objective to test improved semipreg repair techniques with embossed film adhesive [32]. Note the purpose is not to compare the two methods; in practice the choice to use wet layup or prepreg is driven by logistical needs.

3.1 Decommissioned A320 Elevator

A decommissioned composite left hand elevator from an Airbus A320 was generously donated for this research by Delta Airlines. An elevator is a control surface found on the horizontal stabilizer which controls the aircraft's pitch. The donated part had been in service for 14 years, and was likely decommissioned due to unrepairable impact damage as will be explained in the next sections. The part has a thin-skinned CFRP sandwich construction, making it suitable as the aircraft demonstrator part for this project. While no records could be obtained on the part's history, visual and destructive inspection provided adequate information about the part.

3.1.1 Elevator Structural Arrangement

A top view of the elevator in Figure 3.1 shows that the elevator measures approximately 5.2 m by 0.9 m. As received, the upper skin plate already had many bonded repairs. Also visible are five bonding straps, which are strips of aluminum for lightning strike protection. There are no bonding straps on the lower skin plate.

As shown in Figure 3.1, the elevator was cut into two pieces, one half reserved for prepreg repairs and the other for wet layup repairs. In addition to facilitating transport, cutting revealed the elevator's internal construction, as shown in Figure 3.2. The upper and lower skin plates consist of sandwich panels with fiberglass honeycomb core and CFRP skins. The spar and two chord-wise ribs are monolithic CFRP, and these are fastened to monolithic regions of the upper and lower skin plates by Hi-Lok® bolts in a single-lap joint.

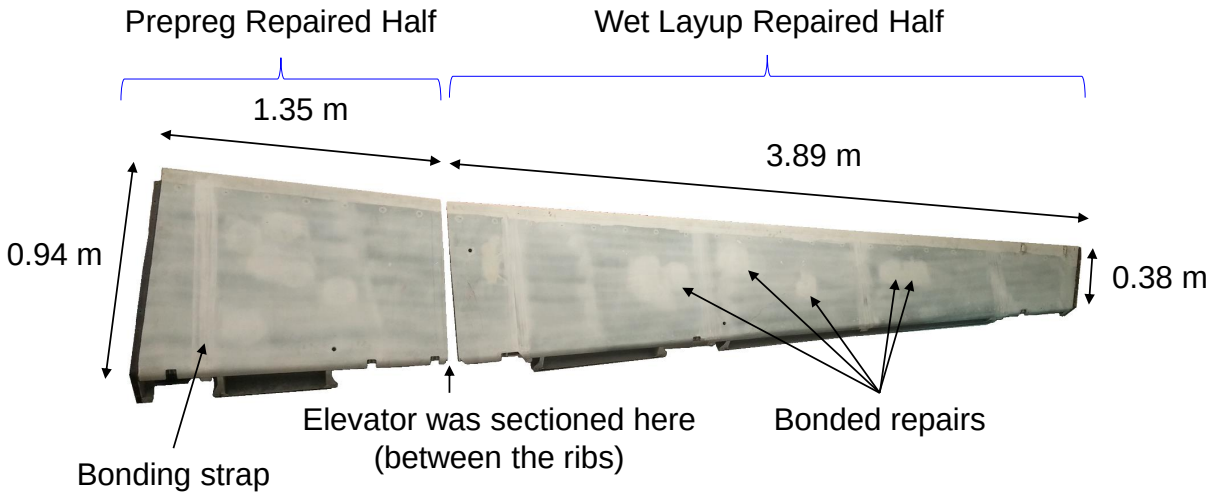

FIGURE 3.1: Top view of the elevator, showing the upper skin plate.

3.1.2 Lower Skin Plate

The lower skin plate was chosen for all repairs performed later in this chapter since it was free of repairs, bonding straps and was mostly undamaged. The only damage found was likely due to impact and occurred over a rectangular area of 1.0 m by 0.3 m as shown in Figure 3.3a. All paint was removed from the external face of the lower skin plate prior to reception except on these damaged regions. When panels were later cut out of the elevator, cracks in the core parallel to the skins were found in these damaged areas as revealed in Figure 3.3b. This damage was probably not repairable because limits are set for repair size and damage spacing: for example these were 250 mm diameter and 150 mm edge to edge for a Boeing SRM section for a similar part [11].

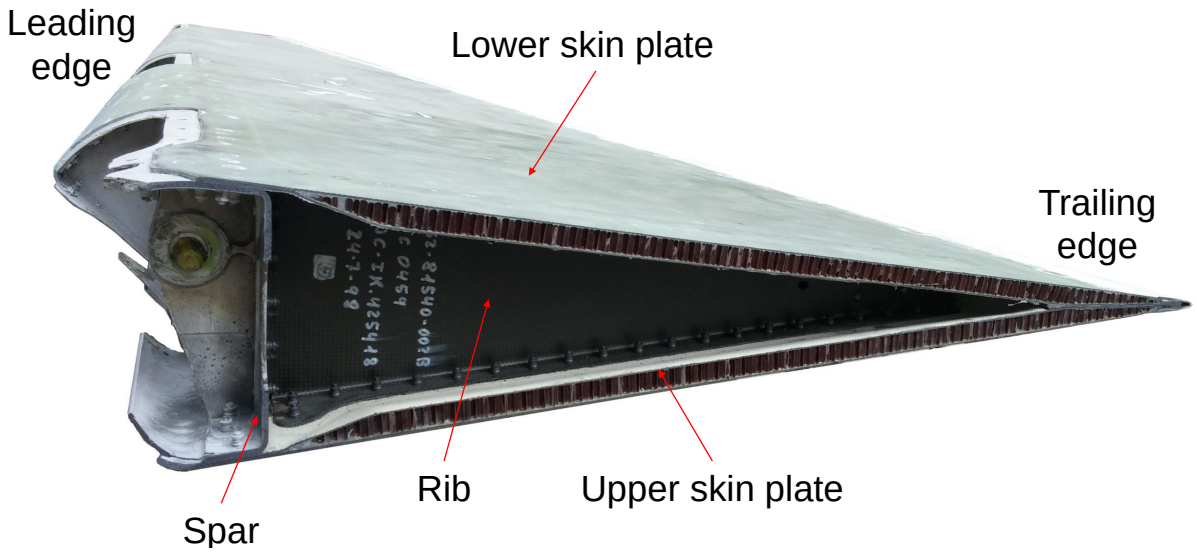

FIGURE 3.2: Cross-section of the elevator showing main structural components and terminology.

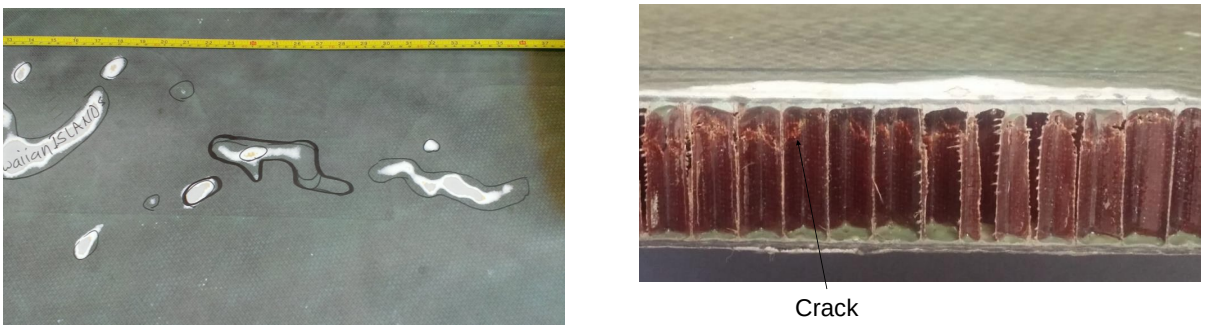

(A) Top view, damage is circled.

(B) Cross-section of damage.

FIGURE 3.3: Impact damage in the as-received lower skin plate.

Materials and Stacking Sequence

From visual inspection and the optical microscopy, it was possible to determine the materials and stacking sequence used in the lower skin plate. The stacking sequence is illustrated in Figure 3.4. All CFRP plies, at least over the core regions, consist of an approximately 195 g/m^2 3k plain weave fabric with thermoset 177 °C (350°F) curing epoxy resin, manufactured in an autoclave prepreg process. The cured ply thickness is 0.18 mm. The ply orientations shown are for the

fabric's warp direction, with the 0° direction being parallel to the spar. On the external face is a ply of adhesive film, which gives the lower skin plate its green appearance. The internal face has a layer of Tedlar®, a PVF film manufactured by DuPont™. These layers are to prevent moisture ingress [84]. Most of the lower skin plate has only two plies per facesheet, in a $[+45°/-45°]$ sequence. The core is a $64\,kg/m^3$ (4.0 pcf), 15 mm thick, 4.8 mm (3/16 in) cell size honeycomb made with glass fabric reinforced phenolic resin sheets. At the locations where the skin plate joins other pieces such as the spar and ribs, the core tapers off to a monolithic skin. As Figure 3.4 shows, near these core chamfers additional plies are added, with 20 mm steps between each additional ply.

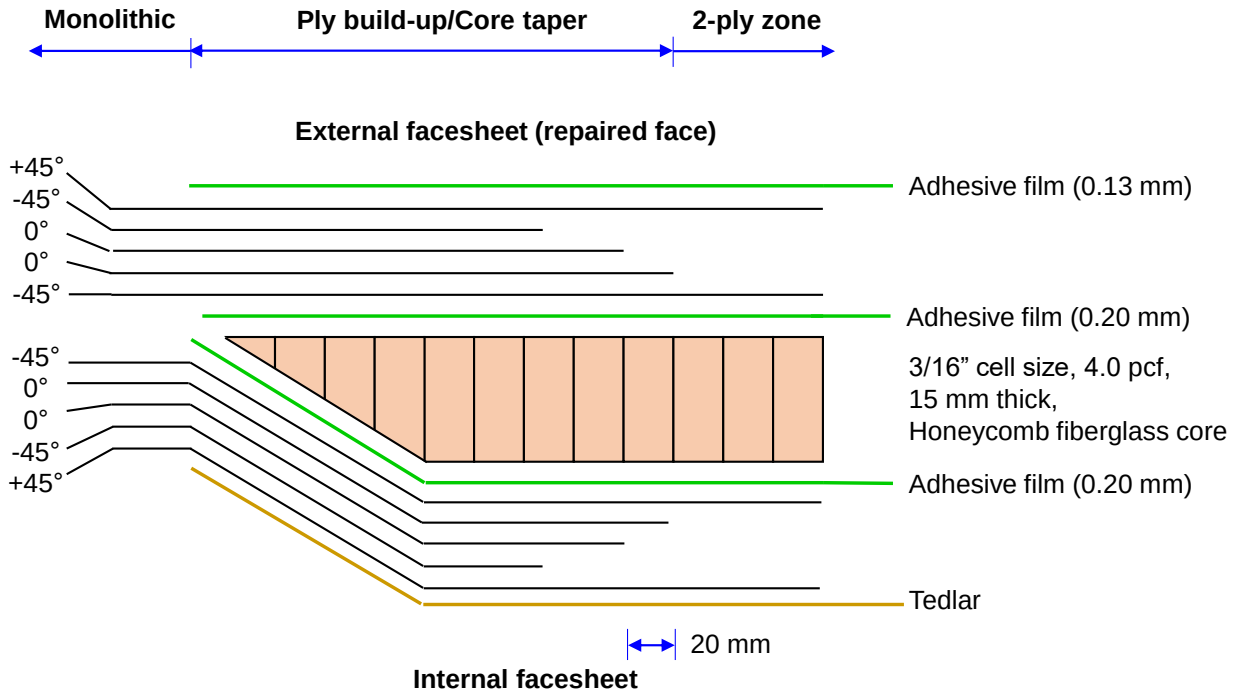

FIGURE 3.4: Typical ply configuration in the lower skin plate.

Glass Transition Temperature

When curing repairs on the lower skin plate, it would be important to stay below the T_g of the part's film adhesive and resin. As an epoxy resin is heated past its T_g, it transitions from an elastic to a viscoelastic material with greatly reduced stiffness and strength [85]. The coefficient of thermal expansion and specific heat capacity increases above the T_g as well [85]. As a result of these

effects, and coupled with the thermal gradients in heat blanket cures, locally heating above the part's T_g could cause residual stresses in the facesheets or lead to disbond between skin and core when air entrapped in the core pressurizes due to the applied heat.

Samples were taken from both the external and internal facesheet of the lower skin plate, as shown in Table 3.1. The T_g was assessed by DMA using the same procedure as applied to the repairs later in this chapter, described in section 3.2.3, with the exception of heating rates of $1\,^{\circ}\mathrm{C\,min^{-1}}$ to $5\,^{\circ}\mathrm{C\,min^{-1}}$ as shown in Table 3.1.

Using an angle grinder with a diamond grit blade, samples were cut in a full core thickness, 5 ply region at mid chord between the two internal ribs . Then, specimens were precisely cut on a water-cooled saw (Rubi Diamant DX-350) with a diamond grit blade, ensuring that edges were parallel. Final specimen dimensions were 60.00 mm long and 7.95 to 8.24 mm wide. The core was cut off using a knife, as close to the facesheets as possible. Using a water-cooled grinder, as much of the remaining core and adhesive as possible were removed and sanded flat, taking care not to damage the laminates. The stacking sequence for each sample is given in Table 3.1. The angles indicate the fabric's warp direction relative to the span of the sample, with the first (left most) ply being directly on the roller supports. The (internal) face of each sample that had been bonded to the core was always placed on the roller supports. Sample 1, from the internal facesheet, also had a thin 0.02 mm layer of Tedlar®, a thermoplastic PVF film. In analyzing the results, a nominal thickness of 1.000 mm was used for all 3 samples as they had the same number of plies. Their actual thickness measurements deviated slightly from this value due to the additional amount of adhesive film present. While in this case the stacking sequence could not be changed, it should be noted that the fibre orientations can have an effect on the T_g value [85], and the aforementioned ASTM standard prescribes that one of the major fibre directions be aligned with span [86].

The specimen mass was recorded before (W_i) and after (W_f) DMA testing, and the weight loss percentage WL calculated according to Equation 3.1. All 3 samples lost 0.586-0.799 % mass as indicated in Table 3.1, likely representing moisture as the test end temperature of 225 °C should be well below the resin's degradation temperature. Further, sample 3 was subjected to a 2 hour drying cycle at 120 °C prior to testing, losing 0.811 % mass. This drying cycle matched the drying cycle used in all subsequent repairs in this chapter. From Table 3.1 we can see that sample 3 was however not fully dry prior to testing, as it still lost an additional 0.639 % mass. It is also questionable how representative this is of the actual drying cycle, as due to its free edges, the DMA sample would have more surface area for moisture loss.

$$WL,\% = \frac{W_i - W_f}{W_i} \times 100,\ where\ \mathrm{i} - \mathrm{initial}, \mathrm{f} - \mathrm{final} \tag{3.1}$$

The T_g was determined from the onset in storage modulus drop as shown for sample 3 in Figure 3.5, and explained further in section 3.2.3. The peak of the $\tan\delta$ curve, T_t, was also recorded. The test results are in Table 3.2. Despite the drying of sample 3, all samples yielded nearly identical T_g values of 122 °C to 123 °C. While samples 2 and 3 yielded similar T_t values, the inner facesheet sample 1 yielded a far higher value of 171 °C compared to 154-159 °C. This could be due to the higher ramp rate used for sample 1, or perhaps an effect of the Tedlar® film.

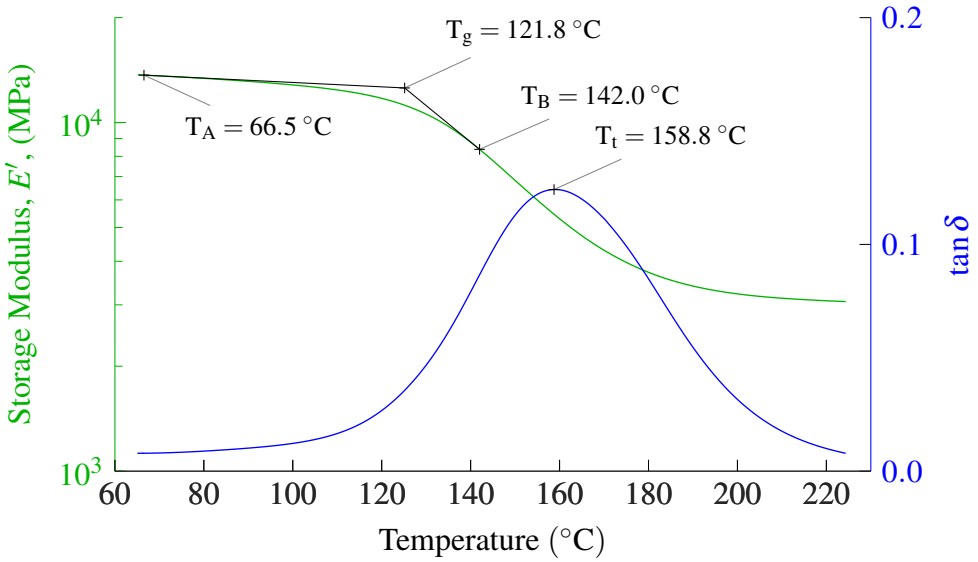

FIGURE 3.5: DMA curves for sample 3 excised from the lower skin plate's external facesheet.

3.2 Experimental Methodology

Since the lower skin plate was free of existing repairs, mostly intact (no pre-existing damage) and free of obstructions (such as bonding straps), it was decided to perform 8 bonded scarf repairs on its external face. To validate the previous work in this thesis, 4 of these repairs were performed using wet layup procedures and materials. The other 4 repairs were performed using prepreg, to validate new procedures developed [32]. Intact regions on the lower skin plate were chosen for the

TABLE 3.1: DMA Test Setup for Lower Skin Plate

No.	Facesheet	Heating Rate (°C/min)	Stacking Sequence	WL post-drying (%)	WL post-DMA (%)
1	Internal	5	$[+45/90_2/+45/-45/\text{tedlar}]$	N/A	0.586
2	External	1	$[+45/90_2/+45/-45]$	N/A	0.799
3	External	1	$[+45/90_2/+45/-45]$	0.811	0.639

TABLE 3.2: DMA Results for Lower Skin Plate (°C)

No.	T_A	T_B	T_g	T_t
1	66	168	122	171
2	77	148	123	154
3	67	142	122	159

repairs, rather than attempting to repair actual damage, to allow the same geometry to be used for all repairs and to avoid introducing uncontrolled factors in this experiment.

3.2.1 Repair Design

The chosen repair patch geometry is shown in Figure 3.6. It consists of a rectangular repair patch on the external facesheet, with a 2° scarf angle. The core is exposed over an area of 75 mm by 100 mm, which would represent the extent of damage in a real repair as shown in Figure 3.6b. In the case of the wet layup repairs, the facesheet was removed up until the core, but the existing core was left intact. For the prepreg repairs, the core was replaced. The next sections explain this choice of repair geometry.

Repair Depth

Repair to the core and external facesheet is considered the most common type of repair for honeycomb sandwich panels [11]. Such repairs are often needed for foreign object damage, for instance

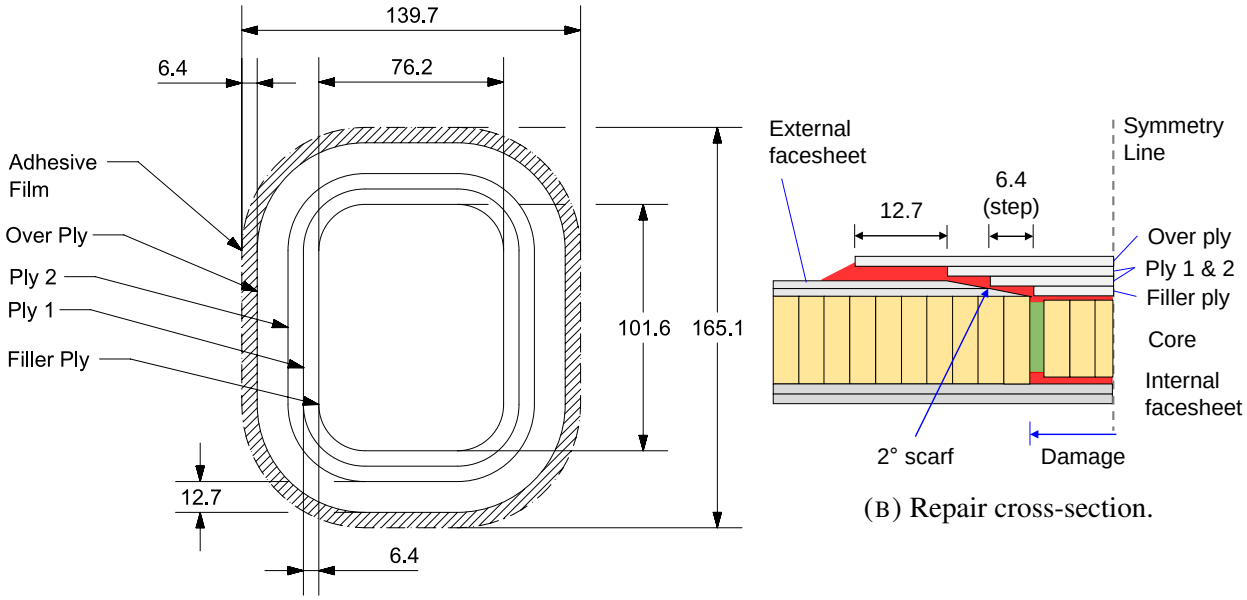

(A) Repair patch dimensions.

(B) Repair cross-section.

FIGURE 3.6: Bonded scarf repair geometry for a prepreg repair, dimensions in mm. Wet layup repair geometry differs in only two respects: the existing core in the elevator was maintained and no film adhesive was used.

due to hailstorm, runway debris or ground vehicles [87]. The existing damage found on this elevator, core fracture, Figure 3.3b, is an example. With much of the elevator's facesheets having only two plain weave plies for a total thickness of 0.4 mm, the core can easily be damaged.

It was thus decided to replace the core and patch the external facesheet for the prepreg repairs. This would also provide the exact same scenario to the repairs studied by Préau [32], [42]. In a wet layup repair, the core has to be closed-out with potting compound to prevent resin from dripping into the cells and leading to a resin starved patch or adding excess weight. Since the cells are closed-out, core replacement was expected to have little influence on the resulting patch quality. So, it was decided only to close-out, but not replace, the core for the wet layup repairs.

Damage Size, Shape and Orientation

The repair geometry of Figure 3.6 has complete removal of the external facesheet over a rectangular area of 75 mm by 100 mm, and removal of the core in this area for the prepreg repairs. This was deemed large enough for the destructive testing plan below, and representative of actual in-service

repairs. For comparison, other composite repair studies have used circular damage diameters of 51 mm [42], 90 mm [41] and 100 mm [69].

In practice, the shape of the repair would either match the damage, or be a simplified shape such as a circle to facilitate the repair process. The rectangular shape here was chosen in order to create a simple geometry for subsequent 4-point bending tests. The rectangular damage was also oriented so as to allow the maximum number of patches and bending test specimens to be fit on the elevator, resulting in the patch orientation of Figure 3.9 with regards to the elevator's warp clock.

Scarf Angle

The best strength recovery with minimal pristine material removal is obtained when the limiting strength of the adherends matches the strength of the scarf joint [17]. The optimal scarf angle is therefore dependent on the materials, stacking sequences and loading conditions. Fortunately, extensive testing has been performed in the literature using some of the prepreg materials used in this chapter; Cytec's CYCOM® 5320 with T650-35 carbon 3k plain weave and Cytec FM® 300-2M film adhesive. Tensile tests on monolithic scarf repair coupons using these materials demonstrated <3.2° scarf angles led to net section failure in the adherends, provided porosity in the bondline was low, while porous bondlines led to adherend failure for smaller 2.6° scarf angles only [18]. A scarf angle of 2° was chosen for the repairs in this chapter, which should therefore yield good strength recovery.

Repair Ply Stacking Sequence

The stacking sequence for the repair patches matched the lower skin plate's local stacking sequence in orientation and number of plies, with an additional internal 45° ply and an additional external 45° ply. The additional internal ply was termed a *filler ply*, and was cut to the same dimensions as the exposed core. The additional external ply is referred to as an *over ply* and was cut to extend 12.7 mm beyond the end of the scarf as shown in Figure 3.6a.

The filler ply is non-structural as it forms a butt joint with the scarfed facesheet. Such plies are frequently used in co-bonded scarf or step repairs to composite sandwich panels, such as those specified by the Boeing 757 SRM (section 51-70-03) [11]. The purpose of the filler ply is to reduce the waviness in stepped, co-cured patches where they are bonded to scarfed or stepped parent laminates. In reality the repair patches implemented here are "stepped" patches (see Figure 3.6b)

so it was chosen to include such a filler ply. Filler plies can also compensate for core plugs that are not thick enough. Over-plies have been shown to significantly reduce the peak in shear and peel stresses that normally develop at the edge of a scarf joint [88]. They are often seen in SRM specifications [11], and for these reasons were included.

3.2.2 Repair Processing Test Matrix

Prepreg Repair Test Matrix

Materials The prepreg repair materials used were described in detail in the introduction. To summarize, two different plain weave carbon prepregs from Cytec Engineered Materials (now Cytec Solvay Group) were used: Cycom®5320 semipreg [43] and Cycom®977-2 autoclave prepreg [46]. The film adhesive used was FM®300-2M, with 293 $\mathrm{g\,m^{-2}}$ weight, 0.25 mm nominal thickness and a non-woven polyester carrier [48].

To splice the vertical sides of the core plug to the elevator's core, FM®410-1 foaming adhesive with 2.5 mm nominal thickness was employed [89]. This foaming adhesive can be cured at 121 °C and expands to 1.7–3.5 times its original thickness during cure.

It should be noted that all the prepreg materials used except the 977-2 had exceeded their manufacturer recommended shelf-life (storage time at $-18\,^{\circ}\mathrm{C}$). The FM300-2M used expired June 2013, 3 years before these experiments. To assess the effect of this aging, two FM300-2M specimens were analyzed by ramping at $2\,^{\circ}\mathrm{C\,min^{-1}}$ in a DSC, and the results compared to the same tests performed on fresh material in [34]. The initial, uncured glass transition temperature (onset T_f) had advanced from $-14.2\,^{\circ}\mathrm{C}$ to $-0.7\,^{\circ}\mathrm{C}$, while a comparison of the total heat of reaction suggested the degree of cure had advanced 4.3 % relative to fresh material. When the aged DSC heat flow curves were overlayed with the fresh heat flow curves, it was clear the onset of the exothermic reaction had shifted $\approx 7\,^{\circ}\mathrm{C}$ lower. These observations are nearly identical to the behaviour of FM300-2M that has reached its maximum (20 day) room temperature out-time [32].

Since the same core material as originally used in the elevator was not available, a $96\,\mathrm{kg\,m^{-3}}$, 3.175 mm cell size, 19 mm thick Nomex core was used instead for the core plug. This Nomex core provided similar stiffness and equivalent strength, but had to be manually sanded down to the 15 mm thickness required.

TABLE 3.3: Prepreg Repair Test Matrix

Carbon Prepreg	Adhesive Perforation & Embossing	RT Debulk	Elevator Skin	Patch
977-2	No	20 min first/last ply	$[+45/-45]$	$[-45/+45/-45/+45]$
	Yes			
5320	No	< 10 min last ply		
	Yes			$[-45/+45/-45/+45_2]$

Test Matrix The prepreg repair test matrix is presented in Table 3.3. As shown, two repairs were performed with either the 5320 semipreg or 977-2 autoclave prepreg, and one of each of these repairs utilized the embossed/perforated film adhesive. Prepreg repairs without the embossed/perforated adhesive used an unmodified, or "baseline" adhesive. A room temperature, pre-cure vacuum debulk was performed as indicated. Normally an extended pre-cure vacuum hold is performed with semipregs, however this step was forgotten in the first of the 5320 repairs performed and so was omitted for consistency. For the 5320 repairs approximately 10 min or less passed between pulling vacuum on the bag and start of cure. The elevator skin being repaired had a two ply stacking sequence as shown at all prepreg repair locations. However, the elevator's stacking sequence was misinterpreted for the 5320/baseline repair, resulting in a fifth ply exclusively for this patch as shown.

Process Controls Following a practice used by industry, one process control laminate was cured alongside the 977-2 repairs, and another alongside the 5320/baseline repair. Each process control was cured under the same heat blanket and vacuum bag as the corresponding repair, on a piece of release film on a flat section of the elevator. These laminates measured 150 mm by 150 mm, with a 10-ply $[0/90]_5$ stacking sequence using the same material as the corresponding repair. The stacking sequence permitted short beam shear tests to be performed in accordance with ASTM D2344 [81]. The process controls were also subjected to the same destructive evaluation as the repairs for comparison, as clearly in practice only the process controls can be destructively evaluated.

TABLE 3.4: Wet Layup Repair Test Matrix

Impregnation Technique	DVD	RT Debulk	Elevator Skin	Patch
Vacuum	No	1 h	$[+45/-45]$	$[-45/+45/-45/+45]$
	Yes	No		
Random Blob	No	1 h	$[+45/0/0/-45]$	$[-45/+45/0/0/-45/+45]$
	Yes	No		

Wet Layup Repair Test Matrix

Materials Only one two-part resin system, the Henkel EA 9390 Aero studied in the previous chapter, was used for the wet layup repairs [50]. This resin served to both impregnate the repair plies and to bond the patch to the lower skin plate. For the reinforcement, $\approx 200\,\mathrm{g\,m^{-2}}$ dry carbon 3k plain weave fabric from Lincoln Fabrics was used. After scarfing, the lower skin plate's remaining adhesive film generally fully closed off the cells of the exposed core. The occasional open cell was closed out with Magnolia Magnobond 77-4 A/B two-part epoxy syntactic potting compound.

Test Matrix A total of four wet layup repairs with different processing variables were implemented as shown by Table 3.4. The vacuum and random blob impregnation techniques were used for two repairs each. One vacuum impregnation and one random blob impregnation patch was debulked in a double vacuum debulk (DVD) chamber as indicated. For repairs that were not subject to DVD, after the patch was applied to the lower skin plate and vacuum bagged, a 1 h room temperature debulk under full vacuum was performed ("RT Debulk" column). Table 3.4 also shows the stacking sequence of elevator and patch for each repair. Only the random blob/DVD repair is in a thicker, 4-ply region of the lower skin plate.

Cure Cycles

All heating cycles used are presented in Table 3.5. The heating cycles selected for a given repair depended on the materials involved (9390, 5320, 977-2, FM300-2M), and the processing step. Each repair area was first dried; all repairs used the *Dry-2* cycle, except those using 977-2 prepreg for which the *Dry-1* cycle was used. The CACRC standard for pre-repair drying [19] suggests to

dry at the intended cure temperature for the duration of the cure when no OEM or SRM guidelines are available, and so this was the motivation for drying at 121 °C. However, heating above 100 °C leads to a risk of skin-core disbond due to moist air in the honeycomb core pressurizing, for this reason industrial partners on this project suggested the *Dry-1* cycle. Both drying cycles were limited to 2 hours due to time limitations when performing the repairs.

For all prepreg repairs, manufacturer recommended cure cycles were used [43], [46], [48], [89]. For prepreg repairs in which the core was replaced, the *core cure* cycle was performed to cure the film and foaming adhesives prior to application of the patch. A single cure at 177 °C was then performed for the 977-2 repairs as per the datasheet [46]. The 5320 repairs were cured slightly above the datasheet recommendation at 125 °C (vs 121 °C), for 3 hours instead of 2 hours, to ensure the entire patch will at least reach gelation (107 °C for 3 hours is the minimum required to exceeded the 48 % degree of cure at gelation based on the model in [35]). After this cycle the degree of cure is only 72 %, so this was followed by a post cure at 177 °C.

Based on the work in Chapter 2, the wet layup repairs were cured in a 3 hold cycle. If the DVD process was specified, a first hold at 60 °C was performed in the DVD chamber, venting the chamber 45 min into the 60 °C hold. The de-bulked patch was then removed from the DVD chamber and cured on the elevator following the *9390 cure* cycle. For non-DVD repairs the *9390 DVD* and *9390 cure* cycles were performed consecutively without returning to room temperature in between.

In association with the heating cycles of Table 3.5, Table 3.6 presents the corresponding flow and thermo-chemical behaviour for each resin system. Models and experimental data from the literature for cure kinetics, viscosity and glass transition temperature were used with the heating cycles to produce Table 3.6. The cure kinetics and viscosity models for each material were obtained from the references in Table 3.8, while the T_g models were from [34], [35], [90] as well as the author's previous DSC testing of the 9390. Table 3.6 highlights the main differences between the resin systems. The minimum viscosity is indicated by μ_{min}, final degree of cure by α_f and final glass transition temperature by T_{gf}.

The 9390 cure cycle is plotted in Figure 3.7. As shown, the viscosity is kept near a minimum for the entire 60 °C hold, to promote removal of air and volatiles during the DVD. Gelation was also designed to occur in the intermediate dwell at 93 °C, staying below 100 °C to mitigate void nucleation and growth. The final hold at 121 °C ensures a complete degree of cure while minimizing total cycle time–at 232 min, the combined *9390 DVD*/*9390 cure* is shorter than the cycles used

TABLE 3.5: Heating Cycle by Material and Processing Step

Cycle	Ramp/Hold 1			Ramp/Hold 2			Ramp/Hold 3		Cycle Time
	(°C/min)	(°C)	(min)	(°C/min)	(°C)	(min)	(°C/min)	(°C)	(min)
Drying Cycle									
Dry-1	2.78	82.2	120	2.78	25	0	–	–	161.2
Dry-2	2.00	121	120	3.00	25	0	–	–	200.0
Core Plug Cure									
Core cure	2.78	121	120	2.78	25	0	–	–	189.2
Patch Cure									
9390 DVD	2.78	60	60	5.00	25	0	–	–	79.6
9390 Cure	2.00	93	25	1.67	121	45	3.00	25	152.8
5320 Cure	2.00	125	180	3.00	25	0	–	–	263.3
5320 Post	2.00	177	120	3.00	25	0	–	–	246.7
977-2 Cure	2.78	177	180	2.78	25	0	–	–	289.4

for 977-2 (289 min) and 5320 (510 min).

The 977-2 cure cycle is also plotted in Figure 3.8, showing the degree of cure evolution for both the 977-2 and the FM300-2M adhesive. The FM300-2M cures very quickly as it is designed to cure at lower temperatures, reaching almost full cure at the start of the dwell. As shown in Table 3.6, the 977-2 is a relatively high flow system, exhibing a much higher flow number than the 5320 (1.42 vs 0.364), and gelling 31 minutes into the dwell. Further, it is interesting to note that both the 977-2 and FM300-2M only vitrify during the cool down after the dwell, as their T_{gf} are both below 177 °C.

3.2.3 Repair Quality Assessment

Non-Destructive Inspection

Non-destructive inspection (NDT) was performed by the Centre Technologique en Aérospatiale (Saint-Hubert, Quebec) on the completed repairs. The purpose was to detect any major defects in

TABLE 3.6: Flow and Thermo-Chemical Behaviour by Material and Cycle

Cycle	Resin	Gel Point		Flow Num.	μ_{min}	α_f	T_{gf}
		t (min)	T (°C)	(min/P)	(Pa s)		(°C)
9390 DVD	EA 9390	–	–	5.575	0.7	0.21	-15.4
9390 Cure	EA 9390	44	93	0.524	3.9	0.95	145.2
5320 Cure	5320	113	125	0.364	5.5	0.72	130.6
	FM300-2M	61	125	0.018	139.0	0.92	137.9
5320 Post	5320	–	–	–	–	0.95	195.7
	FM300-2M	–	–	–	–	1.00	152.9
977-2 Cure	977-2	86	177	$\approx$ 1.42 [46]	$\approx$ 2.0 [46]	0.92	169.4
	FM300-2M	43	144	0.014	135.4	1.00	152.9
Core cure	FM300-2M	54	121	0.016	135.4	0.89	131.9

the repairs such delaminations or disbonds. Three NDT techniques were used that require only one-sided access:

- Manual pulse-echo ultrasound (MUT): A single transducer from a portable ultrasonic system is manually moved over the inspection area, which is sprayed with water to act as a couplant. The inspector observes the A-scan (amplitude vs time) to spot defect echos and manually draw the boundaries of defects on the part.

- Automated phased array ultrasound (AUT): The repaired elevator sections were placed in a water immersion tank, and scanned by an automated phased array probe. The results are plotted as amplitude C-scans at different times, corresponding to different depths in the repair.

- Flash infrared thermography (iRT): Two symmetrically placed flash lamps were used to rapidly deliver a 6 kJ pulse of thermal energy to a repaired area over a time scale of milliseconds, after which the surface temperature was recorded with a Telops MW1000 infrared camera. To enhance the appearance of defects, infrared images were post processed with software. The time derivative of the surface temperature was plotted at different times to view defects at different depths.

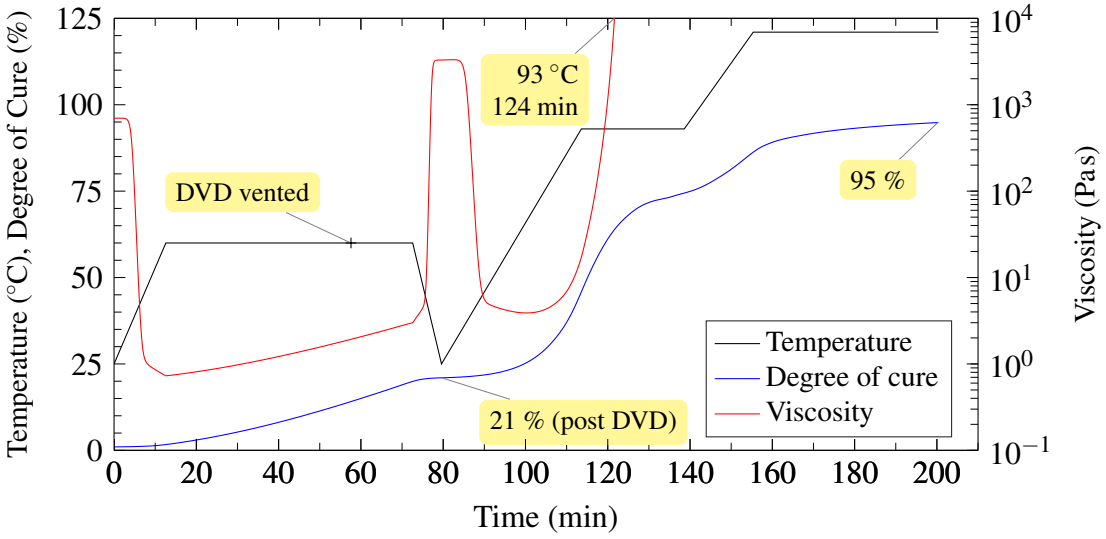

FIGURE 3.7: Cure cycle for all demonstrator wet layup repairs. Degree of cure and viscosity are shown for the EA9390 resin using the model from [36]. When the DVD was specified, the patch was removed from the DVD chamber after the 60 °C dwell near 25 °C. When the DVD was not used, the cure cycle ramped directly from 60 °C to 93 °C. Viscosity and degree of cure evolution were computed using the model in [36].

Reference standards are required for interpreting the NDT results. To this end artificial defects were placed in the 5320/baseline repair and the random blob/DVD repair. Defect locations are presented alongside the results.

Destructive Test Matrix

The destructive tests carried out on the cured repairs are listed in Table 3.7, while the location of each specimen on the repair patch is shown in Figure 3.9. All specimens were cut on a water-cooled diamond saw.

The next sections provide further detail about each test method. Note that some tests were applied only to certain repairs. The random blob/DVD and 5320/baseline repairs served as reference standards for NDT and contained multiple artificial defects, so they were not tested in bending. Since the core was not replaced for the wet layup repairs, and no adhesive film was used, there was no interest in examining the adhesive fillet or bondline quality.

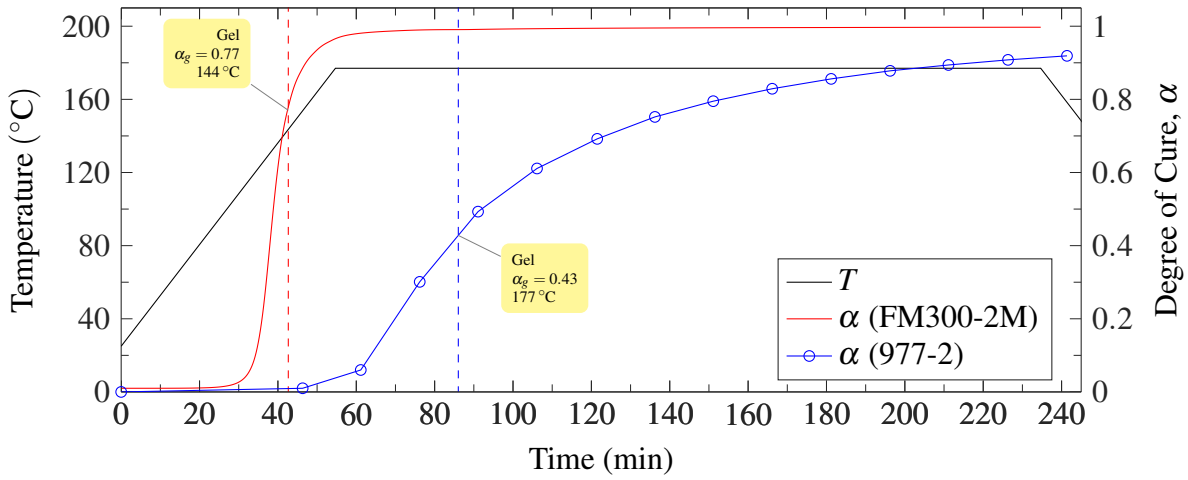

FIGURE 3.8: Cure cycle used for the 977-2 repairs, with degree of cure evolution for both the 977-2 and the FM300-2M adhesive. Gelation point for each system is also indicated by the dashed line. Note the 977-2 degree of cure is based on experimental data [91], while the FM300-2M degree of cure is based on a model [34].

Bending Test

Purpose Four-point bending tests were performed on 50 mm sections cut through each repair as shown in Figure 3.9, as well as on three pristine samples to compare failure load and mode. Due to time limitations, neither strain gauges nor transducers to measure displacement (LVDTs) were employed. Thus only an approximate measure of stiffness was available using the crosshead displacement data. Four-point bending tests were chosen as (1) the test setup can be adjusted to promote failure in the repaired facesheet, (2) the fixture is simple and inexpensive to fabricate and (3) only a section of the repair is needed, allowing other destructive test samples or sensors to be placed in the repair as shown in Figure 3.9.

The rectangular shape for the patch was selected to provide a simple 1D scarf geometry for the bending test sample, a test configuration used in other scarf repair and joint studies to facilitate interpretation of the test results [18], [92]–[95].

Specimen Orientation The span of the bending test sample matches the elevator's 0° direction. Only this orientation could allow the placement of multiple test samples due to the elevator's high aspect ratio and the need for long/slender specimens to promote facesheet failure. The true facesheet thickness and stacking sequence were discovered only after scarfing: all tested repairs were to facesheets with only two plain weave plies in a $[+45/-45]$ sequence with a core ribbon

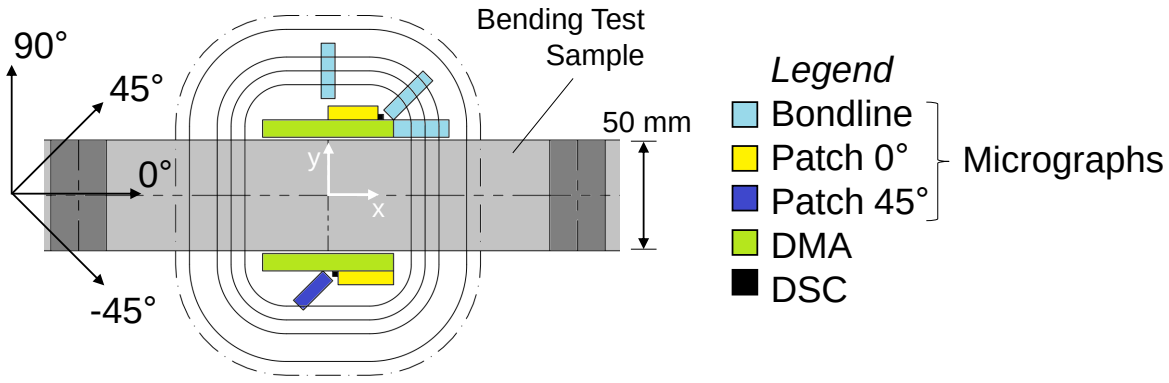

FIGURE 3.9: Location of destructive test specimens in the repair patch.

direction of 100°. For such a laminate a bending test in the 0° direction would place relatively small tensile/compressive stresses on the fibres and relatively large shear stresses on the matrix (in relation to the relative strength of fibre and matrix). The undesirable result is that these bending tests are more of shear test of the matrix, and further these tests will create only small bondline shear stresses. For instance, $\pm 45°$ laminates are tested in tension to determine matrix shear properties (ASTM D3518 [96]). Had the stacking sequence been known prior to scarfing, picture frame shear testing would have been selected and a circular repair patch employed instead. This would load the repaired panels in the manner the lower skin plate was designed for. Four point bending tests were still performed as described next, acknowledging that *useful results may not be obtained*.

Test Fixture A schematic of the four point bending test setup is shown in Figure 3.10. The test fixture was custom built for this purpose in accordance with ASTM D7249-12 [97]. Flat aluminum loading pads, coloured cyan in Figure 3.10, were used with width $L_{pad} = 25$ mm. The loading pads can pivot on precision ground, case hardened 1566 carbon steel shafts. A 3.175 mm thick, 50 mm wide piece of silicon rubber was placed between the loading pad and sample to further distribute the load and prevent any stress concentration at the edge of the load applicator.

The test dimensions are shown in Figure 3.10: support span S, loading span L as well as panel width b, for which it was previously mentioned that $b = 50$ mm was chosen. The standard dimensions of ASTM D7249-12 [97] were deviated from to promote failure in the repaired facesheet, and to place the repair patch between the two load application points (points B and C) on the compression side facesheet. The repair patch was placed on the compression side as the external (repaired)

TABLE 3.7: Demonstrator Destructive Test Matrix

Test	Quantity Measured	Number of Samples	Orientation (°)	Repairs Tested	Sample Size (mm)
DMA	T_g, T_t	2	0	All	60×8
DSC	T_g, H_{res}	1	N/A		2×2
Microscopy	Patch Void Content	2	0	All	25×5
	Bondline Void Content	3	0, 45, 90	Prepreg only	
	Adhesive Fillet Height	3	0, 0, 45		
Bending Test	Force, Crosshead displacement	1	0	All except NDT stds.	660×50

facesheet was stronger than the internal facesheet in compression, as the external facesheet was on the tool side when the elevator was processed.

Support and Loading Span Linear sizing calculations were first performed to determine S and L for failure in the repaired facesheet at a load small enough not to fail the core by shear or crushing. However due to the very compliant $[+45/-45]$ facesheets, this linear analysis revealed that large deflections and rotations would occur, well outside the limitations of a linear analysis. Geometrically non-linear static finite element analysis with contact conditions at supports/load applicators would be the suitable method for estimating failure loads and deflections [98]. Given the uncertainty in material properties, the possibility that progressive damage/material plasticity are significant, and considering the possibility there may not be a span for which skin failure can be achieved, it was decided not to perform such a time consuming analysis. Instead, additional pristine specimens were tested to experimentally determine S and L, leading to the selection of $S = 430\,\text{mm}/L = 185\,\text{mm}$ as will be shown in the results section.

Microscopy

Void content and morphology both within the patch and in the adhesive along the scarf bondline were assessed by optical microscopy. Specimens 25 mm in length were cut from multiple locations as shown in Figure 3.9. Then, samples were cast in epoxy resin and polished up to 0.3 μm with a Forcipol variable speed grinder/polisher equipped with a Forcimat automatic head. Images

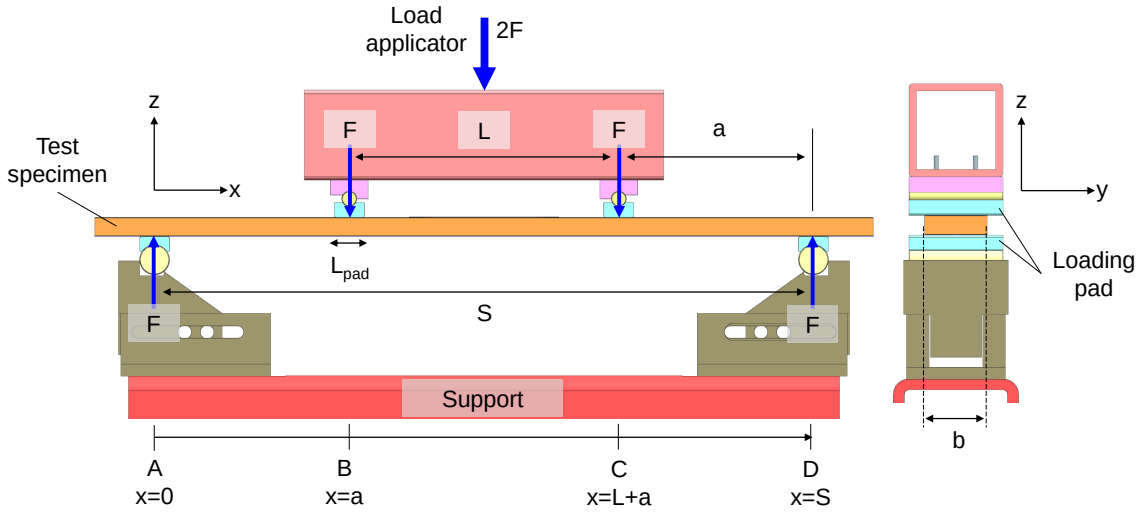

FIGURE 3.10: Demonstrator bending test geometry. Final test dimensions were $b =$ 50 mm, $S = 430$ mm, $L = 185$ mm.

were captured at 10x magnification using an upright Nikon Eclipse L150 microscope with a 100 $\times$ 100 mm Märzhäuser motorized stage along with a Sentech STC-MBS231U3V digital camera (0.58 μm/pixel at 10x magnification) and DCI Capture Software.

Patch Internal Quality Patch internal quality was assessed by cutting two 0° specimens from near the middle of the patch as shown in yellow in Figure 3.9. Note that for such a cut most of the fibres are at $\pm 45°$ due to the stacking sequence. Void content was computed by comparing area of voids, A_{void}, to specimen cross-sectional area, $A_{cross-section}$ (the image was cropped to include only the patch plies and none of the adhesive at the patch/core interface) as per Equation 3.2. This task was accomplished by thresholding with the image analysis software ImageJ thanks to the high contrast between voids, fibres and resin.

$$Patch\ Void\ Content\ (\%) = (100\%)\frac{A_{void}}{A_{cross-section}} \tag{3.2}$$

Bondline Void Content Bondline void content was assessed in the adhesive along the scarf between the patch and the lower skin plate facesheet; therefore this was not measured for the wet layup repairs as they did not use a film adhesive. A total of three specimens, at 0°, 45° and 90° were cut for each repair as shown in cyan in Figure 3.9. Figure 3.11 shows how the image was cropped to include only the adhesive along the scarf. For the lower image of Figure 3.11, $A_{bondline}$ is the

area of all adhesive and voids (the entire area that is not white), and A_{void} consists of just of the area of voids which appear darker than the adhesive. These areas were computed by thresholding in ImageJ, then bondline void content was calculated by Equation 3.3. As shown the bondline was considered to be the area between the lower skin plate's scarfed facesheet and the fibres of the most internal repair ply. It was possible to distinguish between the lower skin plate's resin and the adhesive as the scarf was fairly straight, the resin didn't polish as smoothly and thanks to the presence of the non woven polyester scrim in the adhesive. However, this definition would include some of the resin from the repair plies, especially at resin rich ply terminations.

$$Bondline\ Void\ Content\ (\%) = (100\%)\frac{A_{void}}{A_{bondline}} \tag{3.3}$$

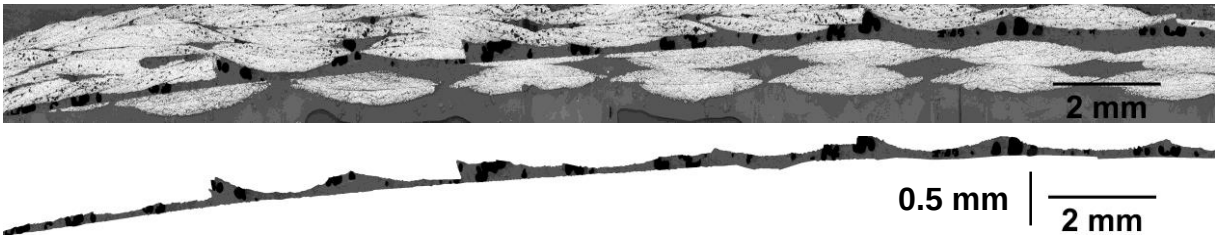

FIGURE 3.11: Scarf region for a prepreg repair (top), with repair patch on top and scarfed external facesheet on bottom. The bondline was isolated as shown in the lower image, for determination of bondline void content. Image was scaled to 50 % in the horizontal direction as shown by the different horizontal/vertical scale bars to better fit on the page.

As can be seen in Figure 3.11, in a cross-section view the bondline only accounts for about 15 % of the image. Thus a large number of cross-sections are necessary to obtain an accurate void content estimate. A more accurate estimation of void content, distribution and morphology in the adhesive can be obtained through single X-ray images, which allow an in-plane view of the adhesive and its voids thanks to the fluorescence of the FM300-2 adhesive as presented in [18].

Adhesive Fillet Quality Adhesive fillet quality between patch and core plug was assessed from three samples cut within the boundary of the core plug, two at 0° and one at 45°, shown yellow and dark blue in Figure 3.9. The two 0° samples were the same ones used for patch void content. Since film adhesive was not used and the core was not replaced for the wet layup repairs, the quality of

patch/core adhesion was only assessed for the prepreg repairs. Additionally, one 0° micrograph of the internal facesheet and core plug provided a rough assessment of internal adhesive fillet quality.

Cell walls provide a small area for bonding, so good fillet formation is critical for mechanical properties dependent on the integrity of the core to facesheet bond such as interlaminar shear or flatwise tension. Skin/core delamination could be a risk under pressure/temperature variations that occur due to a flight cycle, as well as due to moisture present in the cells which can expand upon freezing or heating above 100 °C. An example is the ground-air-ground effect, wherein core pressure remains high (near 1 atmosphere) while the ambient pressure drops due to the aircraft reaching high altitude, which causes disbond growth in Mode I tension [99].

It is well documented that larger adhesive fillets lead to improved skin/core adhesion dependent mechanical properties such as flatwise tensile strength [100] and delamination resistance in the climbing drum peel test [101], [102]. In addition to adhesive fillet size, quality is also important: high porosity has been shown to decrease flatwise tensile strength [103] and peel strength [101]. As well, voids in the fillet act as crack initiation sites [102]. While large fillets with minimal porosity yield the best mechanical properties, ultimately these fillets need only be as strong as the cell walls which they join to the facesheets.

Therefore the micrographs were analysed both qualitatively for fillet regularity and porosity, as well as well as quantitatively in terms of meniscus height. To quantify fillet size from micrographs, authors have examined fillet area [100], fillet throat thickness [100] and height [32], [103], [104]. Only menisci height was chosen for the quantitative analysis here as it was shown to provide a useful metric of delamination resistance [103], especially combined with knowledge of the core pressure during processing, which can be estimated from the menisci height thanks to data available for the same film adhesive in [32]. A minimum of 20 menisci were measured per repair, with individual measurements for the fillet on either side of the cell wall, from the start of the cell wall to the end of the fillet as shown in Figure 3.12.

DMA

Two 60 mm long by ≈8 mm wide specimens were cut from the repair patch as shown in Figure 3.9 for DMA testing. Referring to Figure 3.9, one sample was cut above the bending test sample (if a y-axis were aligned with the 90° axis, this would be where $y > 0$), and one below, these will be referred to as the *upper* and *lower* samples further on. Samples were spaced in this way to look for correlations with in-plane temperature gradients observed during cure of the repairs.

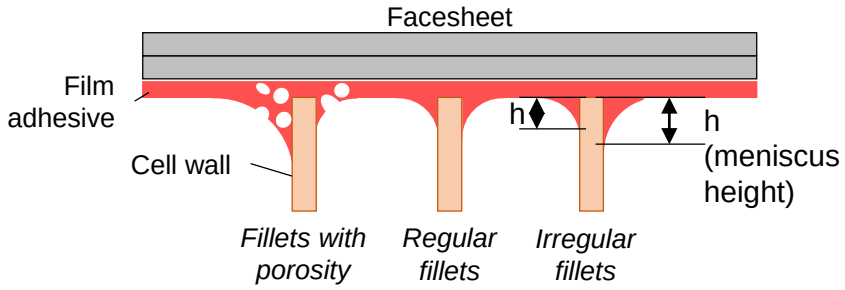

FIGURE 3.12: Example of skin/core adhesive fillets, showing qualitative factors (porosity, regularity) and measurement of meniscus height.

Two specimens of the same dimensions were also cut at 0° from the process control laminates. Since only the repair patch was tested, the core was cut off each sample as close as possible to the repair using a knife. Core that remained was then lightly sanded until flat on a water cooled polisher, leaving most of the adhesive film, so as to induce minimal heating of the specimen and hence alteration of the degree of cure. Samples were allowed to dry at ambient conditions for at least 24 h prior to testing.

On a TA Instruments Q800 DMA, in accordance with ASTM D7028 [86], samples were subjected to 0.1 % strain amplitude sinusoidal displacements at a rate of 1 Hz in 3-point bending with a 50.00 mm span, while the cell was heated at a rate of 5 °C min^{-1} from 30 °C to 240 °C and then again from 30 °C to 240 °C. During the first ramp from 30 °C to 240 °C, the T_g of the repair patch was obtained, while reheating from 30 °C to 240 °C served to determine a fully cured, final T_{gf} for the specimen.

As per ASTM D7028 [86], T_g was identified as the onset of the storage modulus drop on a plot of logarithm of storage modulus against linear temperature. Two tangent lines were intersected to determine the T_g; one at a temperature before the transition, T_A, and another between the midpoint and inflection point of the storage modulus drop, T_B. The temperature at which $\tan\delta$ was a maximum, T_t, was also recorded for comparison.

DSC

Two samples approximately 2 mm by 2 mm were cut from the repair patch as shown in Figure 3.9 for DSC testing. Due to time constraints only one of these two samples was tested, and its location

(above or below the bending test sample relative to Figure 3.9) was unfortunately not recorded. The core was cut off using a knife, leaving only the repair patch with some cured adhesive film remaining.

Dynamic tests were performed on a TA Instruments Q100 DSC in modulated mode (MDSC), ramping at a rate of $2\,^{\circ}\mathrm{C\,min^{-1}}$ from $40\,^{\circ}\mathrm{C}$ to $250\,^{\circ}\mathrm{C}$ while modulating at $+/-\ 1.272\,^{\circ}\mathrm{C\,min^{-1}}$ every 60 s. These test parameters were chosen based on guidelines for hard to detect glass transitions [105]. This linear heating ramp also best matches the cure kinetics models available in the literature for each material used.

The modulation permits the total heat flow signal, dQ/dt, to be deconvoluted into reversing and nonreversing components, $\dot{Q}_{rev}$ and $\dot{Q}_{nonrev}$. In Equation 3.4, C_p is the heat capacity of the specimen, dT/dt the heating rate (with constant and sinusoidal parts) and $f(T,t)$ the heat flow due to kinetic processes [106]. The linear heating ramp provides information to determine dQ/dt, while the modulated temperature variation provides information to compute the reversing (heat capacity) component $\dot{Q}_{rev}$. The kinetic or nonreversing component of heat flow, $\dot{Q}_{nonrev}$, is obtained from the difference of the total and reversing heat flow. In practice these heat flows were computed from TA Instruments Universal Analysis software, which deconvolutes the raw heat flow signal using discrete Fourier transforms [107], [108].

$$\frac{dQ}{dt} = C_p \frac{dT}{dt} + f(T,t) = \dot{Q}_{rev} + \dot{Q}_{nonrev} \tag{3.4}$$

Glass transitions are expressed by an increase in heat capacity, and hence appear in the reversing heat flow signal. An effect not corrected for here is that glass transitions are frequency dependent, with shorter modulation periods leading to higher glass transition temperatures [105]. This effect does not appear for glass transitions (if visible) in the total heat flow signal [105]. Exotherms due to cure appear in the nonreversing heat flow signal. Enthalpic relaxations, which depend on the thermal history of the specimen, also appear in the nonreversing heat flow [106], and can make it difficult to accurately integrate the residual exotherm. These relaxations frequently occur after glass transitions, due to increased molecular mobility above the glass transition temperature. Consequently, MDSC provided numerous advantages over standard DSC, for which glass transitions would likely have been obscured in the total heat flow signal by residual exotherms or enthalpic relaxations [106]. Further, MDSC provides a more accurate assessment of residual exotherms, for which the residual heat can be reduced in part by heat capacity effects in the total heat flow signal [106].

Glass Transition Therefore, for each repair/process control specimen, glass transition temperatures were assessed from the reversing heat flow. The standard method for glass transition temperature assignment by DSC, ASTM E1356 [109], was followed. The standard constructs three tangent lines; one before the transition, a second at the inflection point and a third at a point after the transition. The intersection of the first and second tangents is termed the onset temperature, T_f, while the intersection of second and third tangents termed end temperature, T_e. The half-height temperature, T_m, is a point on the second tangent with a heat flow that is the average of those at T_f and T_e. The glass transition temperature is defined as T_m as it is said to correlate best with that measured by other techniques.

Residual Heat of Reaction The residual heat of reaction, H_{res}, was computed from the nonreversing heat flow by integrating any apparent residual exotherms using a linear baseline . However, this value had to be corrected as the samples consisted of both inert carbon fibres and one or two resins. All repair specimens contained both the patch resin and adhesive film. As the FM300-2M adhesive cures at much lower temperatures than the 977-2 and 5320, for the prepreg repairs H_{res} was assumed to be entirely due to the 977-2 or 5320. Similarly, the existing adhesive film in the lower skin plate was assumed to be fully cured and so H_{res} was assumed to be due only to 9390 for the wet layup repairs.

The nonreversing heat flow signal provided by the software, $\dot{q}_{nonrev}$, was already normalized by the sample mass m_s, so it had to be normalized by the patch resin mass, m_r, as per Equation 3.5. Accurately determining m_r would have been a challenge as the samples contained varying amounts of (fully reacted) adhesive, and no tests were performed to assess fibre volume fraction. One method to assess the fibre volume fraction would be to stop the MDSC test before any resin degradation, and to recover the sample and burn off the resin(s) in a thermogravimetric analyser (TGA). For a rough estimate, m_r was computed using the fibre and patch resin densities, ρ_f and ρ_r, assuming a 55% fibre volume fraction, v_f, as per Equation 3.6.

$$H_{res} = \int_{t_1}^{t_2} \dot{q}_{nonrev} dt \cdot \frac{m_s}{m_r} \tag{3.5}$$

$$m_r = m_s \frac{1 - \rho_f v_f}{\rho_f v_f + \rho_r (1 - v_f)} \tag{3.6}$$

Degree of Cure The degree of cure, α, can easily be calculated from H_{res} by Equation 3.7, where H_T is the total heat of reaction for a given resin system [106]. Values for H_T were found from

TABLE 3.8: Models for Material Cure Kinetics and Total Heat of Reaction

Material	**Ref.**	**Total Heat of Reaction H_T**			
		H_T (J/g)	$\pm$ (J/g)	**No. Tests**	**DSC Ramp Rate** (°C/min)
977-2	[90]	441.0	3.1	5	1
5320	[35]	529.9	4.0	4	2
9390	[36]	486.5	14.6	3	10/5/2
FM300-2M	[34]	311.7	3.4	2	2

the literature for each resin system, and are provided in Table 3.8 for reference. All H_T values in Table 3.8 are based on dynamic DSC ramps, and the references cited for 5320, 9390 and FM300-2M also provide cure kinetics models which were used elsewhere in this chapter.

$$\alpha = \frac{H_T - H_{res}}{H_T} \tag{3.7}$$

3.2.4 Repair Processing

Scarfing, Core Removal and Bondline Preparation

Scarfing was performed by professionals at CFP des Moulins (Terrebonne, Quebec), a school which offers training in composite repair. A GMI Aero Leslie scarfing kit was used for this task, pictured in Figure 3.13. The Leslie consists of a die grinder, which is held in a tool holder that threads into a guide. The tool holder was connected to a vacuum for dust extraction. The Leslie system also requires a scarfing jig to be adhered to the part being scarfed. Custom acrylic scarfing templates, as shown in Figure 3.14a, were lasercut to give the desired repair geometry. The Leslie's guide rests on these templates, and a circular lip on the guide contacts the vertical walls of the jig to control the in-plane position of the cutter. The threads in the tool holder and guide provide precise depth control. A 2° cone shaped diamond grinding bit created the desired scarf angle. The grinder is moved around the perimeter of the jig to create the scarf, with parts of the jig removed in steps until the entire thickness is scarfed. A cylindrical grinding bit was used in the center of the repair where the entire external facesheet was fully removed, along with the core for the prepreg repairs. This system thus allows for accurate, manual scarfing, yielding identical scarf geometry

for all 8 repairs. An example of the core removal for a prepreg repair is shown in Figure 3.14a, while a completed scarf for a wet layup repair is shown in Figure 3.14b. As Figure 3.14b shows, enough of the lower skin plate's film adhesive remained to keep the core closed-out for the wet layup repairs, thanks in part to the precision of the scarfing.

FIGURE 3.13: GMI Leslie scarfing equipment.

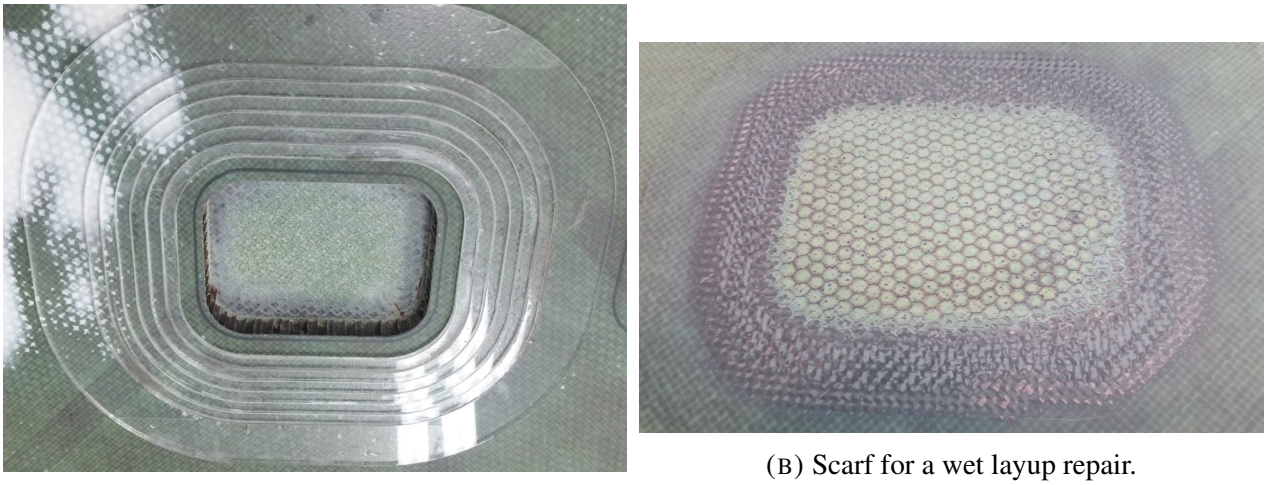

(A) Scarfing templates.

(B) Scarf for a wet layup repair.

FIGURE 3.14: Scarfing of the lower skin plate.

Bondline Surface Preparation Immediately prior to the drying step for each repair, the bond area (scarf, internal facesheet under core plug) was first cleaned with isopropyl alcohol, making sure

TABLE 3.9: Vacuum Bagging Arrangements for Demonstrator Repairs

Bleed bag	**No bleed bag**
Nylon vacuum bagging film 4 plies of breather (thick, non-woven polyester, 10 oz/yd^2, N10) Heat blanket Scoured nylon peel ply FEP non-perforated release film Bleeder/breather (thin, non-woven polyester 2-4 oz/yd^2)	
FEP perforated release film (0.38 mm dia., 12.7 mm pitch)	FEP non-perforated release film
Scoured nylon peel ply	Peel ply impregnated with 977-2 resin
(*Elevator/repair surface*)	

to wipe away the solvent before it evaporated with lint and silicone free RympleCloth®. Light manual dry sanding with 180 grit sandpaper followed, making sure to remove any gloss for good adhesion. A dry wipe with RympleCloth® was performed until all carbon dust was removed.

Drying

To remove as much pre-bond moisture in the lower skin plate as possible, each repair area was dried immediately prior to either the core replacement (prepreg repairs) or patch lamination (wet layup repairs). Using the same positions as the subsequent repair steps, thermocouples were placed in several locations around the repair. The area was then vacuum bagged using the *bleed bag* arrangement of Table 3.9 to allow moisture to escape. The bag was kept under full vacuum while the heat blanket went through the drying cycle specified (see Cure Cycles). Details on thermocouple placement, the heat blanket and controller are in the Temperature and Pressure Deviations section. After the drying cycle was complete, the bag was kept under vacuum until the core replacement step was ready to begin.

Core Replacement

For the prepreg repairs, the core was replaced in a rectangular area measuring 75 mm by 100 mm (3 by 4 in) as shown previously in Figure 3.6. For each prepreg repair a Nomex core plug was cut to size, sanded to 15 mm thick, dried for 2 h in an oven at 120 °C and placed in sealed bag until immediately before insertion in the repair. All consumables and adhesives were cut to size prior to opening the drying cycle vacuum bag. Then, the drying cycle vacuum bag opened: all consumables aside from the vacuum bag/sealant tape were re-used for this step. A piece of FM300-2M adhesive film was first placed in the core cavity. FM410-1 foaming adhesive was wrapped around the perimeter of the core plug, then the core plug was inserted into the cavity. The bleed (see Table 3.9) vacuum bag was then re-sealed with new sealant tape and nylon vacuum bagging film. Vacuum was then pulled and the area was heated through the core cure cycle specified (see Cure Cycles).

Prepreg Repair Patch Application

Prior to opening the vacuum bag from the core replacement step, once again all consumables and prepreg materials were cut first. According to the test matrix (Table 3.3) and the required stacking sequence (Table 3.3), plies of either 977-2 or 5320 prepreg were cut. Either embossed or unmodified FM300-2M adhesive film was cut to size according to the test matrix (Table 3.3). Adhesive film was embossed using the procedure described in [32]: it was sandwiched between two layers of non-perforated FEP release film, placed over a piece of aluminum honeycomb core, and pulled into the cells under vacuum while being heated to 90 °C for 5 min. If embossed adhesive was required, it was cut 6.4 mm larger than the over-ply, so that an air pathway could be created with the breather. For unmodified adhesive, the adhesive was also cut to 6.4 mm larger than the over-ply if 5320 prepreg was used, or 6.4 mm larger than the filler ply if 977-2 prepreg was used at the urging of industrial partners.

Immediately after opening the core replacement bag, the adhesive film was placed. For the 977-2 prepreg, the first ply was then laminated, and the repair was sealed in a bleed bag (see Table 3.9) and debulked under vacuum for 20 min. The remaining repair plies were then laminated. If 5320 prepreg was used, the repair was sealed in a bleed bag (see Table 3.9).

Since the 977-2 repairs were performed simultaneously, they were sealed under the same vacuum bag, along with a process control laminate. Peel ply impregnated with 977-2 resin (instead of “dry” peel ply) was placed over each of these patches. The impregnated peel ply was extended

beyond the over-ply for the 977-2/baseline repair, while it was cut to within the border of the over ply for the 977-2/embossed repair so as not to block the air evacuation channels. Non-perforated release film was used over the process control and 977-2/baseline repair, while perforated release film was used over the 977-2/embossed repair so as to connect the embossed adhesive to vacuum.

After the vacuum bag was sealed, the 977-2 repairs debulked under vacuum at room temperature for 20 min, prior to beginning the cure cycle required (see Cure Cycles). Repairs with 5320 prepreg were not debulked and proceeded to the cure cycle, and subsequently a post cure cycle (see Cure Cycles).

Wet Layup Repair Patch Application

Resin Impregnation Dry carbon plain weave fabric was first impregnated and plies cut according to the method specified by the test matrix of Table 3.4. These impregnation methods are outlined in the previous chapter.

Double Vacuum Debulk If DVD was specified by the test matrix (Table 3.4), the patch was laminated onto a piece of FEP release film over a composite tool plate, in a purpose built DVD chamber. The DVD chamber is shown schematically in Figure 3.15. Over the patch was a perforated release film, a thin ($4\text{oz}/\text{yd}^2$) breather, non perforated release film, peel ply, a heat blanket and the inner vacuum bag. A thermocouple placed adjacent to the patch was used to control the heat blanket through the specified heating cycle (see Cure Cycles). Vacuum was pulled in both the inner vacuum bag and the rigid structure, to degas the patch without compaction pressure. The rigid chamber was vented to atmosphere 15 min prior to ending the 60 °C dwell to consolidate the patch.

Patch Lamination The 9390 laminating resin was brushed onto the repair area, applying the minimum amount to fully wet the surface. Then, either the patch was removed from the DVD chamber and carefully placed on the scarf, or the individual plies were collated onto the scarf. The patch was then sealed in a bleed vacuum bag (see Table 3.9). If specified by the test matrix (Table 3.4), the patch was debulked at room temperature under full vacuum. Then, the repair was heated through the cure cycle specified (see Cure Cycles).

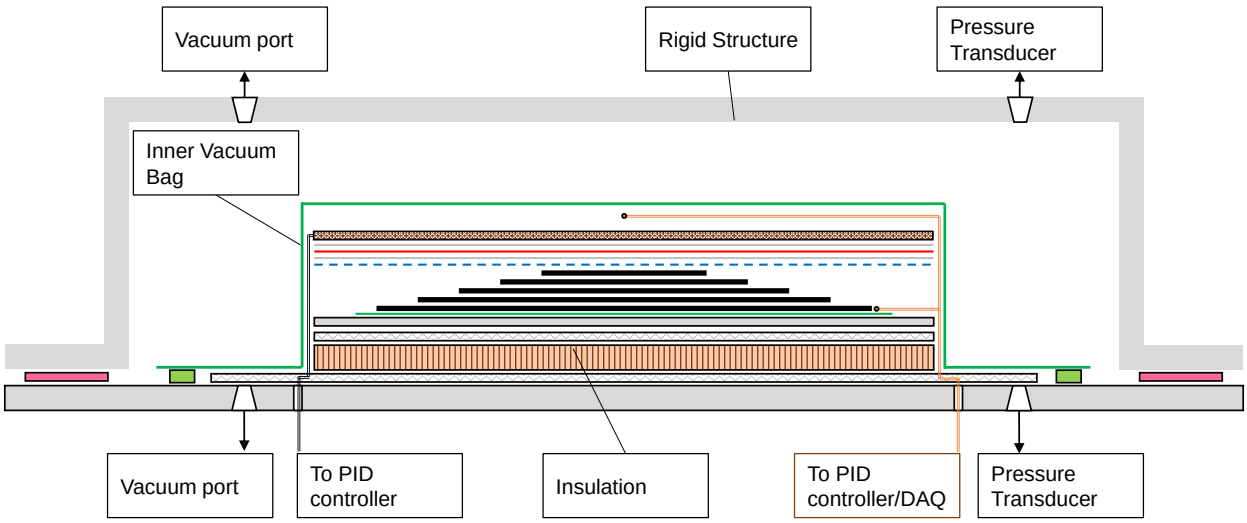

FIGURE 3.15: DVD fixture, showing patch underneath a heat blanket inside the inner vacuum bag.

3.3 Results and Discussion

3.3.1 Repair Processing Data

Ambient Conditions

The prepreg repairs were performed at three different workspaces, two of which did not have air conditioning (Bombardier and CFP des Moulins), so the variation in ambient conditions for these repairs is substantial as shown by Table 3.10. Its also worth noting that the (uncured) adhesive film absorbs ambient moisture, an effect dependent only on the relative humidity. An empirical model for the fully saturated moisture content in FM300-2M film adhesive as a function of relative humidity is available in [32], with values provided in Table 3.10 to give an upper bound on the pre-bond water content in the adhesive. For reference, Préau estimated the as received moisture content in this film adhesive to be 0.10 wt %, and the fully saturated value to be 0.90 wt % [32]. The nomex core plug also absorbs ambient moisture, and while it was dried and kept in a sealed bag prior to installation in the repair, it could've absorbed moisture at these high humidity levels in the interim between opening of the vacuum bag after the core cure and encapsulation under the adhesive film and repair plies.

TABLE 3.10: Environmental Conditions for the Prepreg Repairs

Repair	**Location**	**Ambient Conditions**			**Adhesive Sat. Water Content**
		T (°C)	RH (%)	P (mbar)	(wt %)
977-2 Baseline & 977-2 Embossed	BA	24	40	1010	0.18
5320 Baseline	McGill	21	43	1014	0.20
5320 Embossed	CFP	28	36	1010	0.14

Contrary to the prepreg repairs, all wet layup repairs were performed at McGill in the same air conditioned room, at 24 °C and 40-43 % relative humidity. However the resin was mixed in a separate room at 26-30 °C and 45-54 % relative humidity, a process which entraps a significant amount of air in the resin.

Temperature and Pressure Deviations

Temperatures during drying, core replacement, cure and post cure were monitored by 3-5 thermocouples for each repair. Figure 3.16 shows the in-plane locations of all thermocouples used in the vicinity of the patch superimposed. In Figure 3.16 each thermocouple location is represented by a circle. Most repairs had thermocouples placed at 3 of the 4 locations labelled *right*, *upper*, *left* and *lower*. These locations were 25 mm from the edge of the over-ply because in a real repair scenario thermocouples cannot be placed on the patch as they would leave an imprint. Thermocouples at these locations were used to control the heat blanket. As indicated, these thermocouples were placed directly on top of the external facesheet. For only two wet layup repairs and one prepreg repair 1 or 2 thermocouples were placed to monitor temperatures directly on or inside the repair.

An obvious consideration for minimizing temperature deviations is the control system and the heat blanket used. The prepreg repairs performed at Bombardier and CFP des Moulins (Table 3.10) were cured with a GMI Aero Anita EZ09, which used the average of three thermocouples per repair to control the power supplied to the heat blanket. GMI Aero heat blankets were used for these repairs; a 305 mm square one for the 5320/embossed repair and a 610 mm square one for both 977-2 repairs and process control which were cured simultaneously.

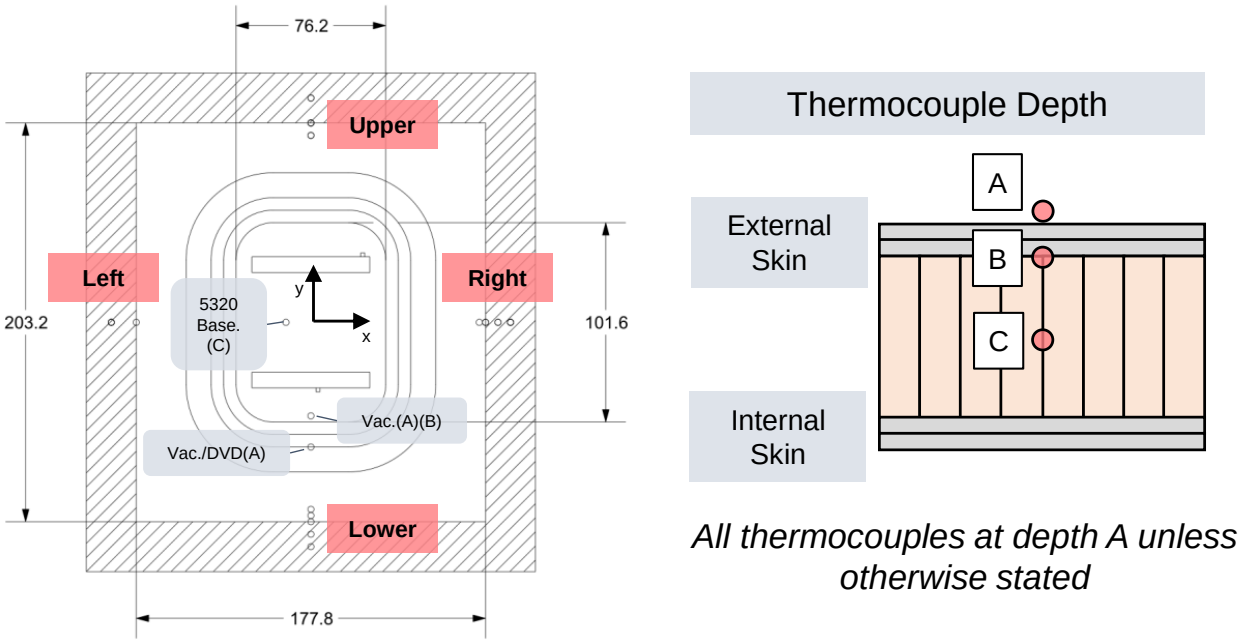

FIGURE 3.16: The small circles in the image at left represent the in-plane location of a thermocouple. The locations of thermocouples used during *all* repairs are superimposed in this image; 2-4 thermocouples were used per repair. Thermocouples were placed in or on the patch for only three of the repairs at the depth indicated by the letter code.

For the 5320 baseline prepreg repair and all wet layup repairs, a system assembled using an Omega CN7800 controller [33] that relied on a single control thermocouple was used, along with a 305 mm by 610 mm heat blanket from Heatcon. The Omega CN7800 had to be tuned prior to drying each repair, so that the optimal PID values were used for each heating cycle. This tuning was performed following manufacturer recommendations at the cure temperature, and led to control that accurately matched the desired profile without overshoot.

The quality of the temperature control was assessed by comparing the data from each thermocouple to the desired cure cycles. Borrowing terminology from [110], for each heat-up ramp and dwell three quantities were computed: the average heating rate R_L, steady state dwell temperature T_{ss} and Δt_{ss}, the time to reach T_{ss} after the desired dwell had started. The point (t_{ss}, T_{ss}) was defined to be where the rate of temperature change, dT/dt, was *steadily* less than $\pm 0.1\,^{\circ}\mathrm{C\,min}^{-1}$. All thermocouples at depth A or B (Figure 3.16) had a ramp rate close to the desired rate, and $\Delta t_{ss} \leq 3$ min. Many thermocouples overshot both the desired temperature and/or T_{ss} at the end of

TABLE 3.11: Pressure and Temperature Deviations During Patch Cure

Repair	**Vac. Leak Check** (mbar/min)	$P_{bag,avg}$ (mbar)	$\min(\Delta T_{ss})$ (°C)	$\max(\Delta T_{ss})$ (°C)
977-2 Baseline	34	194	-1.3	1.4
977-2 Embossed			-0.9	1.8
5320 Baseline	91	35	-6.6	5.7
5320 Embossed	9	134	-3.3	3.1
Vacuum	No Data	45	-2.2	13.0
Vacuum/DVD	64	126	-14.9	9.6
Rand. Blob	71	48	-79.1	20.2
Rand. Blob/DVD	66	52	-20.3	12.2

the heating ramp, in which case $\Delta t_{ss} = 0$ as there is no lag.

Therefore the main temperature deviation was between T_{ss} and the desired dwell temperature, T_d. The maximum and minimum of the difference $\Delta T_{ss} = T_d - T_{ss}$ are reported in Table 3.11 for all thermocouples from each repair (excluding the in core thermocouple), at the highest T_d of the associated "patch cure" cycle of Table 3.5. Both underheating, $\min(\Delta T_{ss})$, and overheating, $\max(\Delta T_{ss})$, are reported as both can be problematic, either leading to incomplete conversion or voids respectively.

As nearly all thermocouples were placed on top of the external facesheet (depth *A* of Figure 3.16), ΔT_{ss} is a measure of the in-plane temperature gradient. For the prepreg repairs, all repairs cured using the GMI Aero system had temperature deviations $|\Delta T_{ss}| \leq 3.3$ °C, which is not surprising as the control was based on the average of all thermocouples in use for this system and the heat blankets allowed large overlap. For the 5320/baseline repair, the minimum and maximum deviations ΔT_{ss} are about twice that of the other prepreg repairs, due to the single-thermocouple control, and also because this repair was closer to the trailing edge, which acted as a heat sink.

The wet layup repairs all show larger in-plane temperature gradients than the prepreg repairs, and analysis of the data, control thermocouple placement, heat blanket position and repair location on the elevator suggested the following causes:

1. A single thermocouple was used for temperature control rather than the average of several thermocouples.

2. The heat blanket was not large enough: While it provided > 75 mm overlap from the edge of the repair, often 50 mm or less overlap was provided for the *upper* or *lower* thermocouples.

3. The single control thermocouple was sometimes placed on heat sinks (ply buildups, too close to leading or trailing edge...) or too close to the heat blanket edge (*upper* or *lower* thermocouples).

To elaborate on cause (2), near the edge of the heat blanket a large in-plane temperature gradient would be expected as the adjacent unheated area causes a large in-plane heat flux [33]. An overlap of 75 mm has been recommended to account for this gradient for thin sandwich structures [11]. For cause (3), the wet layup repairs were on a section of the elevator with much smaller chord, so the repairs were both much closer to heat sinks and the heat blanket's shorter dimension had to be oriented in the chord wise direction.

Pressure deviations were also caused by differing vacuum bag qualities. A leak check was performed on each bag as per the CACRC's ARP 5143 [20], by disconnecting the vacuum line and recording the drop in vacuum over a 5 minute period. The associated leak rate for each repair (for the patch cure) is shown in Table 3.11. CACRC guidelines suggest a maximum leak rate of $34\,\mathrm{mbar\,min^{-1}}$ (5 inHg in 5 min). As shown many repairs exceeded this leak rate; these all had bags that included the trailing edge fasteners, a potential leak source. Another factor is the differing level of vacuum available from the vacuum pump system, since repairs were performed at different facilities. The effect of both leaks and the vacuum pump is visible in the average bag pressure during patch cure, $P_{bag,avg}$, reported in Table 3.11. A lower level of vacuum was available at Bombardier and CFP des Moulins, which explains why these repairs have higher bag pressure.

Not discussed yet is the through thickness temperature gradient due to one sided heating. For the wet layup/vacuum repair this gradient was measured by two thermocouples: one placed on the external face of the patch, T_{ext}, and another between patch and core, T_{int}. These thermocouples were placed at $(x,y) = (0, -47.6\,\mathrm{mm})$ with regards to Figure 3.16, which is within the boundary of the exposed elevator core. The repair patch stacking sequence was $[45_4]$, which is approximately 0.8 mm thick. These temperatures are plotted in Figure 3.17, along with the desired cure cycle T_{des} and evolution of viscosity and T_g for both T_{int} and T_{ext}. To calculate T_g, viscosity and degree of cure evolution this experimental temperature data was fed into the models from [34], [35], [90] and

Table 3.8. Exceptionally for all repairs, inexperience with the controller for this wet layup/vacuum repair led to the final dwell at 121 °C being held for 3 h 51 min instead of the 45 min as desired, which is why T_{des} is not matched during cool down. The effect of holding this dwell excessively long is discussed with the degree of cure results in section 3.3.5.

During the final 121 °C dwell, the through thickness temperature gradient was $T_{ext} - T_{int} \approx 11.5\,°C$. The cure gradients that result from such temperature gradients are a concern for (1) reaching complete cure, (2) in terms of residual stress build-up and (3) for the effect on the flow-compaction phenomena. In this case, both T_{int} and T_{ext} exceeded the desired cure temperature, so both reached the desired degree of cure. Residual stresses can lead to delamination, matrix cracking or disbond if the magnitude is high enough [111]. Residual stress build-up begins after gelation, as at this point the resin modulus begins to increase considerably culminating in an elastic solid at vitrification [111]. After gelation, the resin also begins to shrink considerably due to polymerization [111]. Since the external face of the patch gels 11 min sooner than the internal face, significant shrinkage and modulus development will begin sooner in the external region than the internal region, which can cause residual stresses to develop and/or warpage [111].

Also note that gelation and vitrification occur at temperatures about 30 °C apart for the 9390 with this thermal history. Ideally gelation and vitrification should occur at the same temperature: any thermal expansion in the adherent between gelation and vitrification will result in residual stress development, in a way analogous to tool-part interaction [112]. In terms of point (3), even for the hotter external face the chosen cure cycle still leads to a long flow time so there should be adequate time for impregnation of any dry areas and for the laminate to be consolidated. Also it is important to note that the the hot side gels above 100 °C, and this overheating could lead to increased porosity.

Core Pressure

Pressure in the honeycomb core plug was monitored for the 5320/baseline repair, during cure and post cure of the patch. A procedure for *in-situ* measurement of honeycomb core pressure previously used by Kratz [113]–[115] and patented by The Boeing Company [116] was followed. Core pressure was measured by a piezoresistive silicon micromachined pressure sensor from Measurement Specialties (MS5407-AM). This sensor offers high sensitivity, 0.2 % linearity from 0 bar to 7 bar and maximum operating temperature of 125 °C, with a small 6.4 mm square base and 2.9 mm height as shown in Figure 3.18. This sensor was embedded at the bottom of the core plug, near the

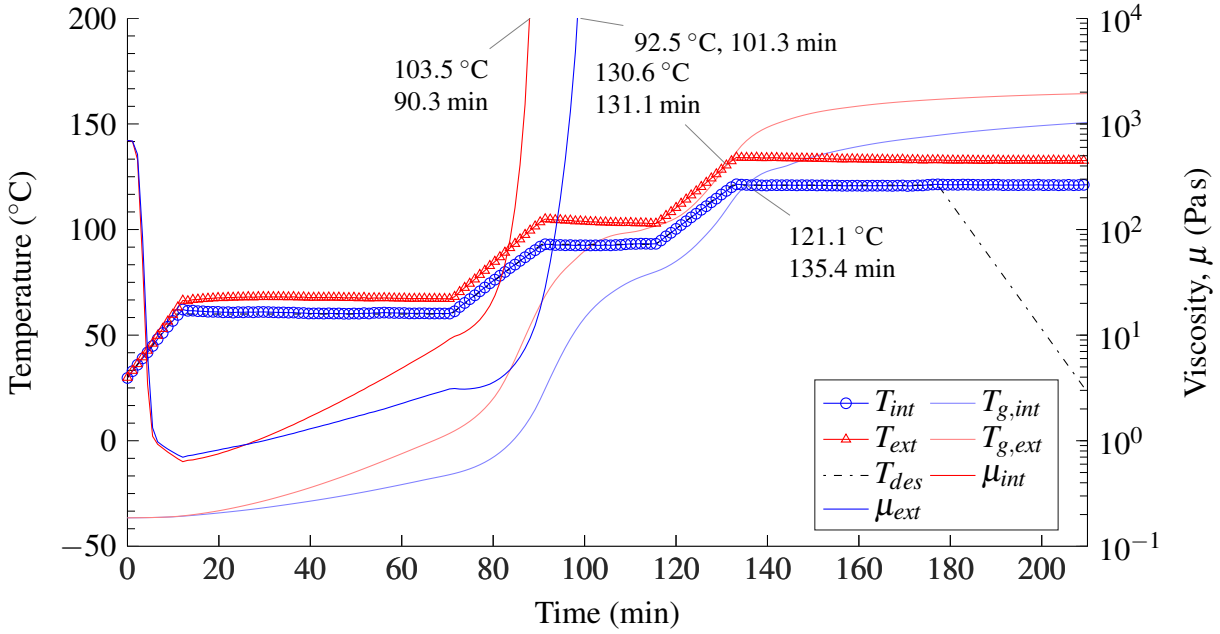

FIGURE 3.17: Through thickness temperature gradient for the wet layup/vacuum impregnation repair, with a $[45_4]$ laminate ≈ 0.8 mm thick. Two thermocouples were placed near the center of the patch. One directly on the core (T_{int}), the other between the most external ply and the release film (T_{ext}). T_g and viscosity μ were computed from T_{int}/T_{ext} using the models of [36]. Gelation and vitrification points are highlighted.

middle of the patch as shown schematically in Figure 3.18. Four 28 gauge enamel coated copper magnet wires were soldered to the sensor, for a wheatstone bridge type connection with the DAQ. To protect the sensor and avoid any electrical shorts, the soldered terminals were also covered in RTV silicone. Temperature compensation was provided by placing a K-type thermcouple adjacent to the sensor as shown in Figure 3.18. To avoid introducing leaks in the repair or the vacuum bag, all wires were encapsulated on both sides in either film adhesive or foaming adhesive up to the edge of the repair. Prior to use in the repair, a four point calibration procedure was performed at two temperatures (22 °C and 115 °C) and two pressures (16 mbar and 1019 mbar).

Core pressure results for the patch cure are presented in Figure 3.19. The temperature of the control thermocouple T_{ctrl} (placed in the *upper* location of Figure 3.16) is plotted, along with the viscosity of the 5320 and FM300-2M for this thermal profile using the models of [35] and [34] respectively. At the start of cure the core pressure is around 800 mbar. As the temperature rises,

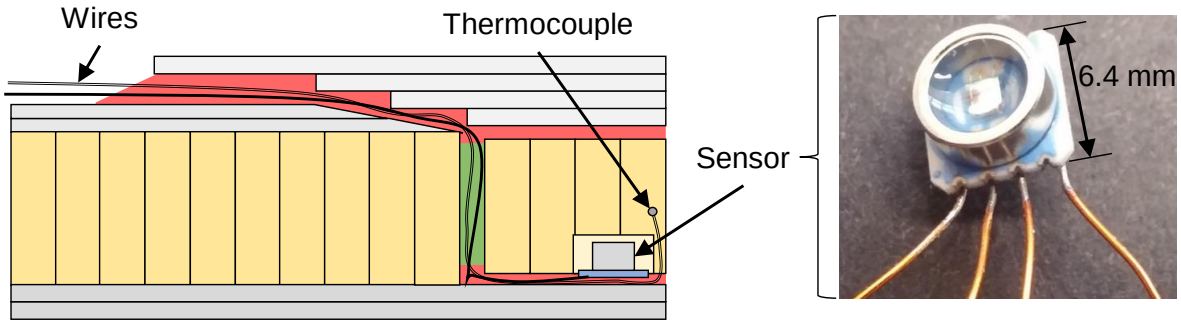

FIGURE 3.18: Cross-section schematic of the miniature pressure transducer in the 5320/baseline repair at left, with image of the transducer at right.

there is a corresponding rise in core pressure, peaking at 970 mbar when T_{ctrl} reaches 85 °C. At this point, the viscosity of the 5320 prepreg drops considerably, and the core pressure begins to drop, reaching a minimum of 647 mbar. Transverse air permeability of semi-pregs is known to increase at higher temperatures as lower viscosities permit through thickness air flow, explaining this drop in core pressure [42], [117]. When the adhesive gels at the end of the temperature ramp, the core pressure begins to rise again as air flow is restricted. Also note at adhesive gelation/end of the ramp in T_{ctrl}, T_{core} is still rising, explaining why core pressure keeps rising. Core pressure keeps rising to 750 mbar when T_{core} levels off. Once T_{core} enters the dwell, core pressure then gradually decays, even after gelation of the 5320 prepreg. Such a drop in core pressure after prepreg gelation was seen for similar materials and conditions [32], perhaps as a result of air passing through interconnected pores in the patch.

The temperature measured adjacent to the pressure transducer, T_{core} is also plotted in Figure 3.19 to give an idea of the temperature at the base of the core plug. T_{core} is ≈ 21 °C lower than T_{ctrl}, which is similar to the temperature gradients predicted by FEA with similar boundary conditions [32]. This relatively large temperature gradient could make it difficult to cure the film adhesive, as near 105 °C the maximum degree of cure achievable for FM300-2M is about 75 % [34]. Since a post cure at 177 °C was performed for this repair, full cure occured as T_{core} reached 147 °C.

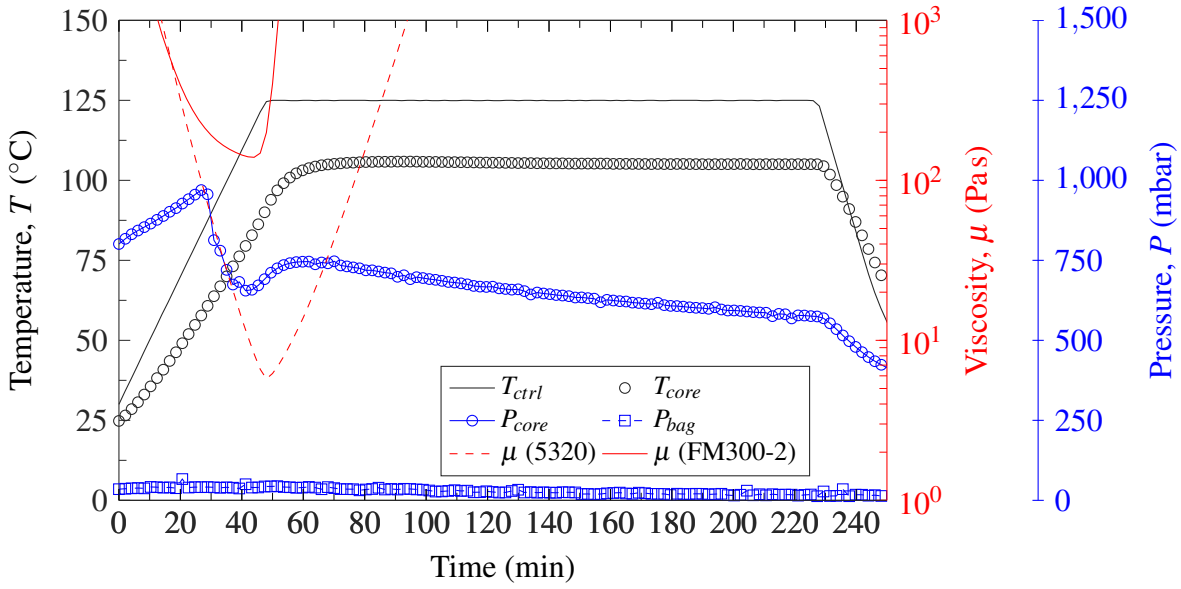

FIGURE 3.19: Measured core pressure evolution during cure of the 5320/baseline repair.

3.3.2 Non-Destructive Inspection

Interpretation of these NDT results requires reference standards with artificial defects placed at known locations. Artificial defects (non perforated FEP release film) of different shape and size were cut and placed at different depths in one wet layup repair and one prepreg repair: random blob/DVD and 5320/baseline. A schematic of the defect placement in the 5320/baseline patch is shown in Figure 3.20. The defect placement in the wet layup repair was identical with two exceptions: (1) defects C and D were smaller (19 mm diameter) but placed at the depth of A & B respectively, and (2) since no adhesive film was used defects E-G were placed either directly on the dry scarf or after resin was brushed onto the scarf.

NDT results for the prepreg reference standard are shown in Figure 3.21. Observing the reference standard results permitted the detection capabilities, in terms of depth and defect size, to be estimated for each method, which are summarized for the prepreg and wet layup repairs in Tables 3.12 and 3.13 respectively. The numbers in these tables refer to the repair plies, for example 1/2 refers to the interface between plies 1 and 2. The plies are numbered starting from 1 going from most external to most internal ply. The smallest detectable defect was considered to be a 6.4 mm circle as this was the size of the smallest artificial defect (A and B). For the wet layup

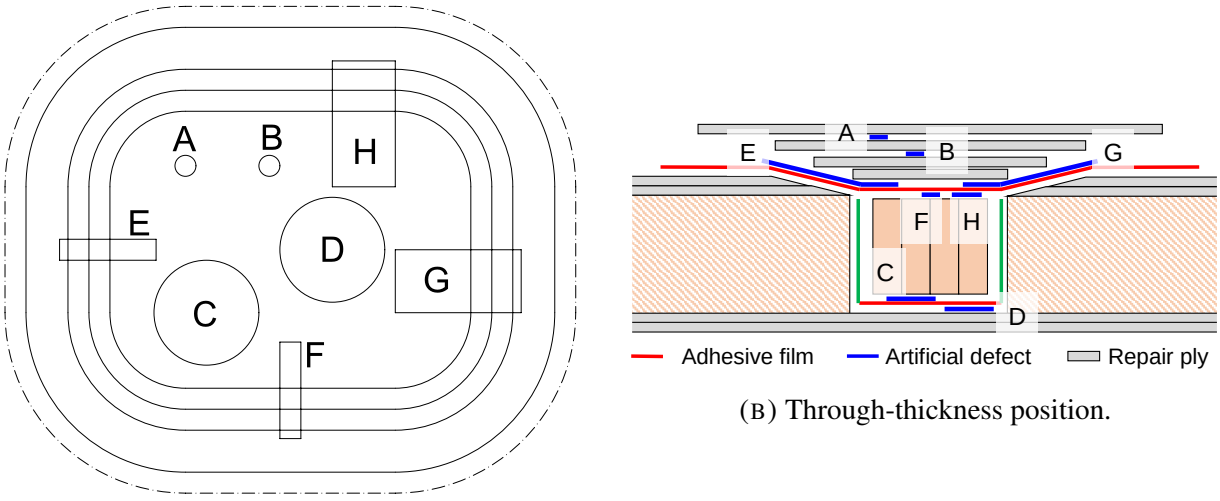

(A) In-plane position.

(B) Through-thickness position.

FIGURE 3.20: Location of artificial defects A-H in the 5320/baseline repair.

repair, "adhesive" refers to 9390 resin that was brushed onto the bondline.

For the prepreg, Table 3.12 shows that MUT and AUT are limited in depth to the ply 4/adhesive interface. Defects F and H, which extended to the adhesive/core plug interface, correspondingly disappear in (Figure 3.21). While the iRT led to very clear images, it was generally limited in depth to the ply 3/ply 4 interface. This is due to the anisotropic thermal conductivity of CFRP materials, which is about 9 times higher in-plane than through the thickness [118]. It was however the quickest method, and in the field a repair could be inspected in a few minutes, which is significantly faster than a portable MUT system, for which it could take 30 min to scan a repair.

Porosity attenuates ultrasound signals and for high void contents leads to noisy signals inhibiting detection [118]–[120]. Both the prepreg and wet layup reference standards had significantly lower void contents in the patch and bondline then the other repairs (see Prepreg Repair Microscopy). So, the detection capabilities obtained with the reference standards may not be achievable for all repairs tested. For Préau, levels of patch and bondline porosity similar to the 977-2 repairs here prevented the visualization of any bondline defects by laser UT [32]. Other prepreg repairs had foaming in the adhesive fillets (Figure 3.27), which is also known to prevent visualizing defects at the core-skin interface by laser UT [32].

In several repairs dark regions were observed in the iRT images at the ply dropoffs. As an example a vacuum/DVD repair iRT image is shown in Figure 3.22. Such dark regions indicate an

TABLE 3.12: NDT Smallest Detectable Defect Diameter for Prepreg Repairs

Technique	**Ply Interface**				
	1/2	2/3	3/4	4/Adhesive	Adhesive/Core
MUT	6.4 mm				–
AUT	6.4 mm				–
iRT	6.4 mm			–	–

TABLE 3.13: NDT Smallest Detectable Defect Diameter for Wet Layup Repairs

Technique	**Ply Interface**						
	1/2	2/3	3/4	4/5	5/6	6/Adhesive	Adhesive/Core
MUT	6.4 mm						
AUT	6.4 mm						
iRT	6.4 mm			–	–	–	–

inhomogeneity, such as an air pocket or a resin rich area. The micrograph of Figure 3.22 revealed this dark region to be entrapped air at a ply termination. Similarly, the perimeter around the core plug where the foaming adhesive was used appears dark in the iRT scans, as it has significantly different heat transfer properties than the composite plies. This made it difficult to observe defects in the core splice, as a splice with excessive gaps (entrapped air) appeared the same as good core splices (filled with foaming adhesive). For both 977-2 repairs, the core plug was undersized, and the foaming adhesive did not expand enough to fill the gap with the elevator's core. The visual appearance is shown in Figure 3.23 for the 977-2/embossed repair. In the cured patch, a resin starved indent was visible around the perimeter of the core plug. This defect is however not so clear in the iRT image of Figure 3.23.

Aside from the core splice issue, no major defects were detected in any of the repairs by iRT, MUT or AUT. It is however interesting to note that a large skin-core disbond occured near the random blob/DVD repair. This area had accidentally been overheated to near 200 °C during the drying stage. This disbond was only noticed after the repair was cut form the elevator, exposing the disbonded skin. An indication of this disbond was however clearly visible in the AUT scan. The MUT and iRT scans were however limited to the repair areas, which raises an important point:

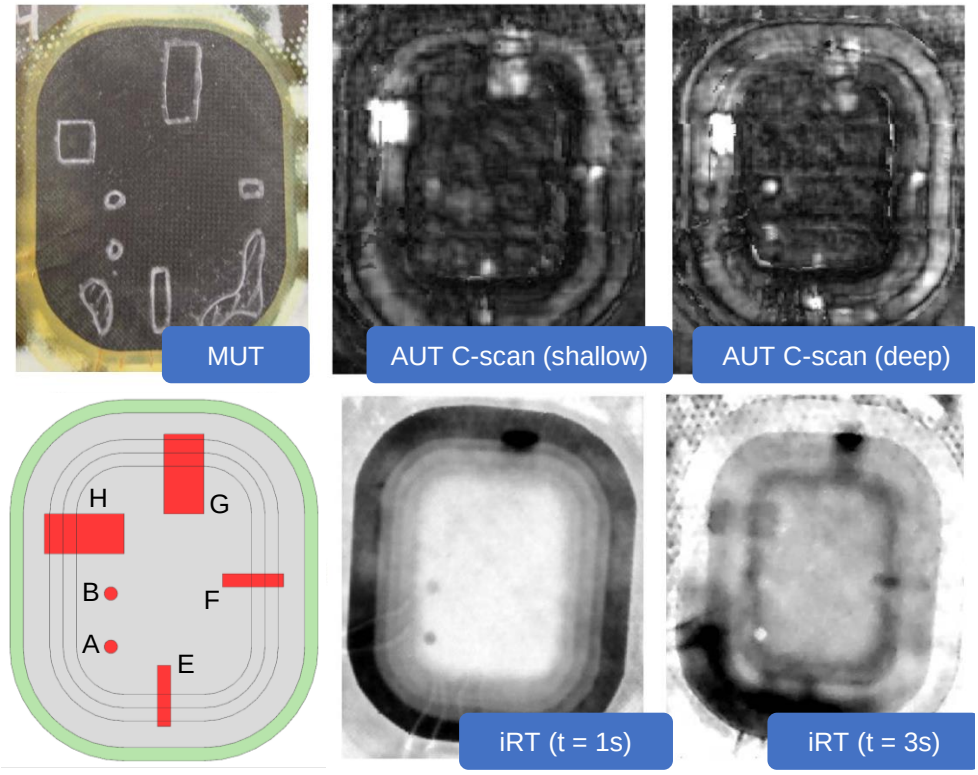

FIGURE 3.21: Prepreg (5320/baseline) reference standard NDT results.

NDT should be performed on the entire area heated during a repair, not just the repair patch itself.

3.3.3 Microscopy

Prepreg Repair Microscopy

Bondline Void Content Figure 3.24 presents the void content measured in the patch and bondline for each of the prepreg repairs. With the 5320 prepreg, the embossed/perforated film adhesive yielded a nearly void free bondline (0.7 %), while the baseline adhesive still maintained a small, 4.6 % bondline void content.

Surprisingly, the engineered adhesive film didn't reduce the bondline void content for the 977-2 repairs, as they had 23.5-27.4 % bondline void content. A number of factors could be responsible, and it is difficult to make any conclusions without further testing:

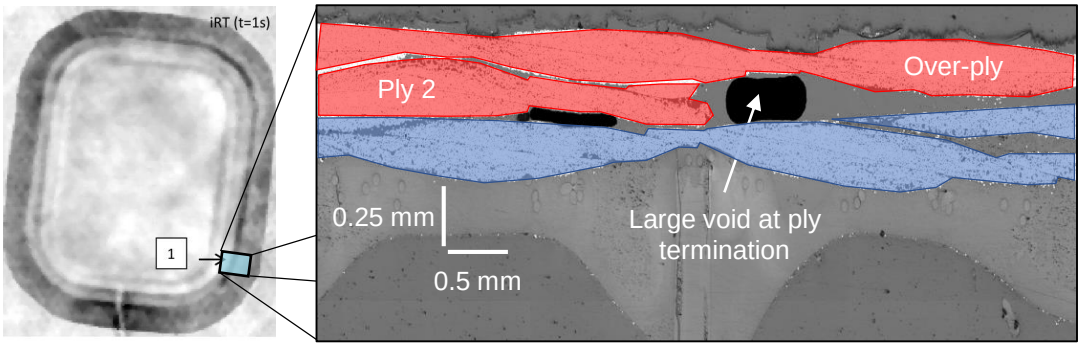

FIGURE 3.22: The dark indication (1) in the iRT image proved to be a large void by comparison with a micrograph cut at the same location. Note the micrograph is scaled to 50 % in the horizontal dimension relative to the vertical.

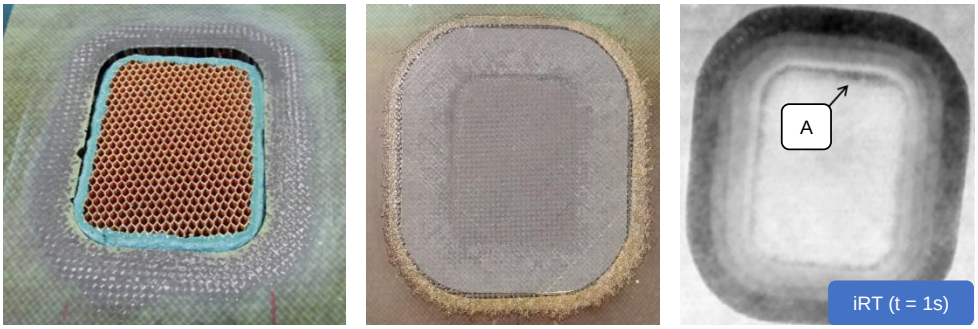

FIGURE 3.23: The core plug for the 977-2/embossed repair was cut too small, resulting in a gap with the parent core. The dark region labelled *A* is the appearance of this gap in the iRT image.

1. **Intermediate debulks** A room temperature vacuum hold was performed for 20 min after the first (filler) ply was collated. This could have prematurely closed the air evacuation channels in the embossed adhesive, as such intermediate debulks were not previously used with the embossed adhesive. The reduced compaction pressure (Table 3.11), $\Delta P = P_{atm} - P_{bag} = 1000 - 200 = 800$ mbar, and high ambient temperature of 24 °C for this repair would have had competing effects on the channel closure time, and no data is available for this combination in [32].

2. **Gelation temperature** When used with the 977-2 cure cycle, the adhesive film gelled at a temperature of 144 °C instead of 120 °C as when paired with the 5320. Based on Préau's [32]

process envelopes, a gelation temperature of 144 °C leads to moisture induced porosity for these processing conditions (see Tables 3.10 and 3.11), while gelation at 120 °C is within the safe zone for no void growth.

3. **Reduced level of vacuum** The adhesive pre-cure moisture content was at least 0.18 wt % due to the relative humidity (Table 3.10) and additional moisture could have diffused into the adhesive from the lower skin plate or core plug. For a 140 °C cure and the similar conditions of $P_{adh} = \approx 0.8\Delta P = 600\,\text{mbar}$ and 0.27 wt % moisture, Préau's model and experiments predict a 23 % void content in the adhesive [32], which is close to the 23.5-27.4 % bondline void content observed.

4. **Cold flow of 977-2** Semipregs such as 5320 are designed to have little or no flow during room temperature vacuum holds [35], which can extend to 16 h or more. This keeps dry regions in the semipreg open. The resin flow behaviour of the 977-2 resin at room temperature is unknown here, so it is possible that it could have flowed into the embossed adhesive and blocked off air pathways before all of the air could be evacuated.

5. **Off-gassing** While semipregs such as 5320 release few volatiles during cure, reportedly below 1 wt % [40], the amount of volatiles released by the 977-2 could not be found in the literature.

The sample bondline micrographs of Figure 3.25 show that the 5320/embossed bondline is void free, while the 5320/baseline has a few well spaced voids. The 977-2 bondlines both appear similar with many closely spaced voids.

Patch Void Content The void content within the patch was close to ≈ 6 % for both 977-2 repairs, while it was on the order of 3 % for each 5320 repair. The embossed and perforated adhesive didn't reduce average void content in the patch for either material; in fact in both cases the void contents were $\approx 1\%$ higher for the embossed and perforated combination. Since the unmodified adhesive has a very low transverse permeability to air [121], less air flows through the thickness from the core into the patch in the baseline adhesive case, perhaps explaining why the embossed/perforated case had higher patch void content.

Void morphology within the patch can be assessed qualitatively from the micrographs in Figure 3.29. In the case of both 977-2 repairs, significant amounts of inter-laminar and intra-tow

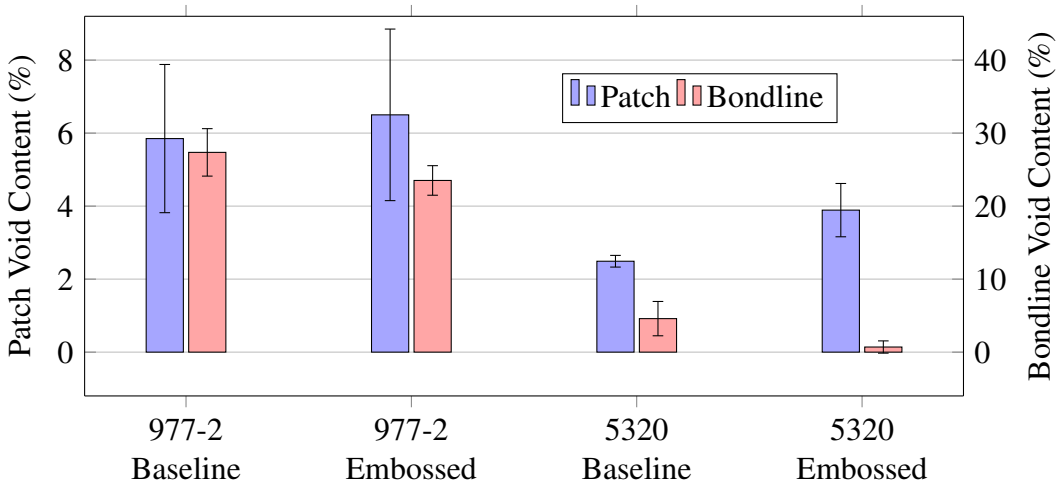

FIGURE 3.24: Void content in the patch and bondline for the prepreg repairs. For patch void content, error bars represent the minimum and maximum values measured (there were two micrographs per repair), while error bars represent the standard deviation for bondline void content.

porosity are present. For the 5320 repairs, the baseline adhesive repair had relatively little intra-tow porosity in comparison to the 977-2 repairs, while the 5320 repair with the engineered adhesive had virtually no intra-tow porosity. However, both 5320 repairs had inter-laminar voids, and these appear slightly larger in the engineered adhesive case. Similarly, Préau [32] observed with the same 5320 material that intra-tow porosity disappeared in the embossed/perforated adhesive case, but inter-laminar voids remained, consistent with the lack of surface openings in the un-cured prepreg (Figure 1.3a).

The pressure difference that consolidates the patch can be expressed by Equation 3.8 [115], where the ambient pressure is $P_{ext} \approx 1$ bar, the vacuum level in the bag is $P_{bag} = 35$ to 194 mbar and the pressure in the core is P_{core}. From the patch micrographs of Figure 3.29 it is visible that the 5320/engineered adhesive patch is wavier than the 5320/baseline patch, indicating a lower core pressure and hence higher compaction pressure. While increased compaction is generally desirable, to suppress voids and improve fibre volume fraction, increased skin waviness in sandwich panels can be detrimental to compressive strength [122].

$$\Delta P = P_{ext} - P_{bag} - P_{core} \tag{3.8}$$

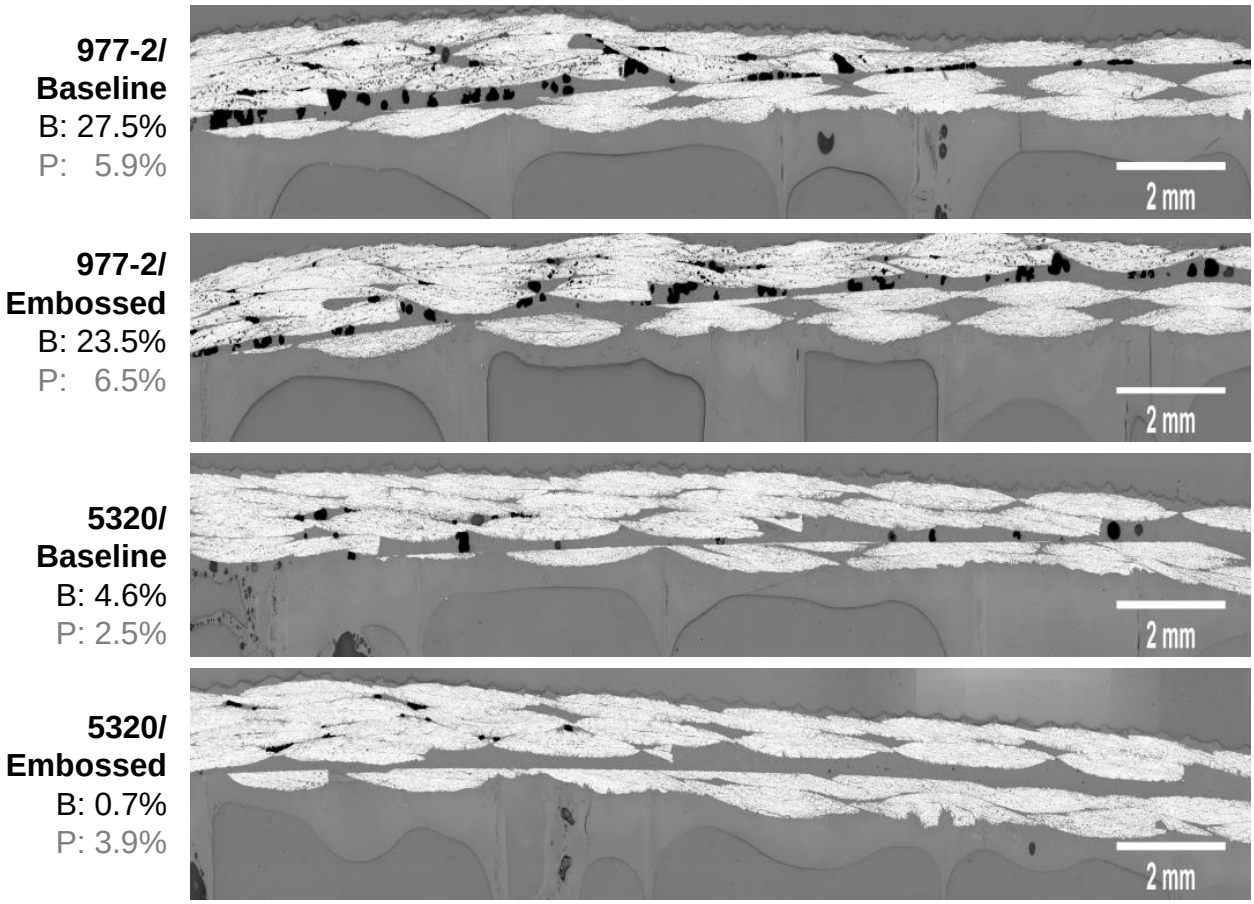

FIGURE 3.25: Micrographs from the scarf bondline at 0° or 90° from the prepreg repairs. The patch is on top. Images are enlarged 2 times in the vertical direction relative to the horizontal direction. Bondline ('B') and patch ('P') void contents are provided at left. Note that the adhesive film only extended to the end of the second ply for the 977-2/Baseline case, whereas it extended beyond the largest ply for all other repairs.

Adhesive Fillet Quality The adhesive fillets between patch and core can be examined qualitatively from the sample micrographs of Figure 3.29, and quantitatively from the menisci height box plot of Figure 3.27. The mean menisci heights for the 977-2/baseline and 977-2/embossed repairs are both $1\,\text{mm} \pm 0.5\,\text{mm}$. The 977-2/baseline fillets are free of foaming, indicating core pressure was high throughout the cure. The 977-2/embossed fillet morphology suggests initially

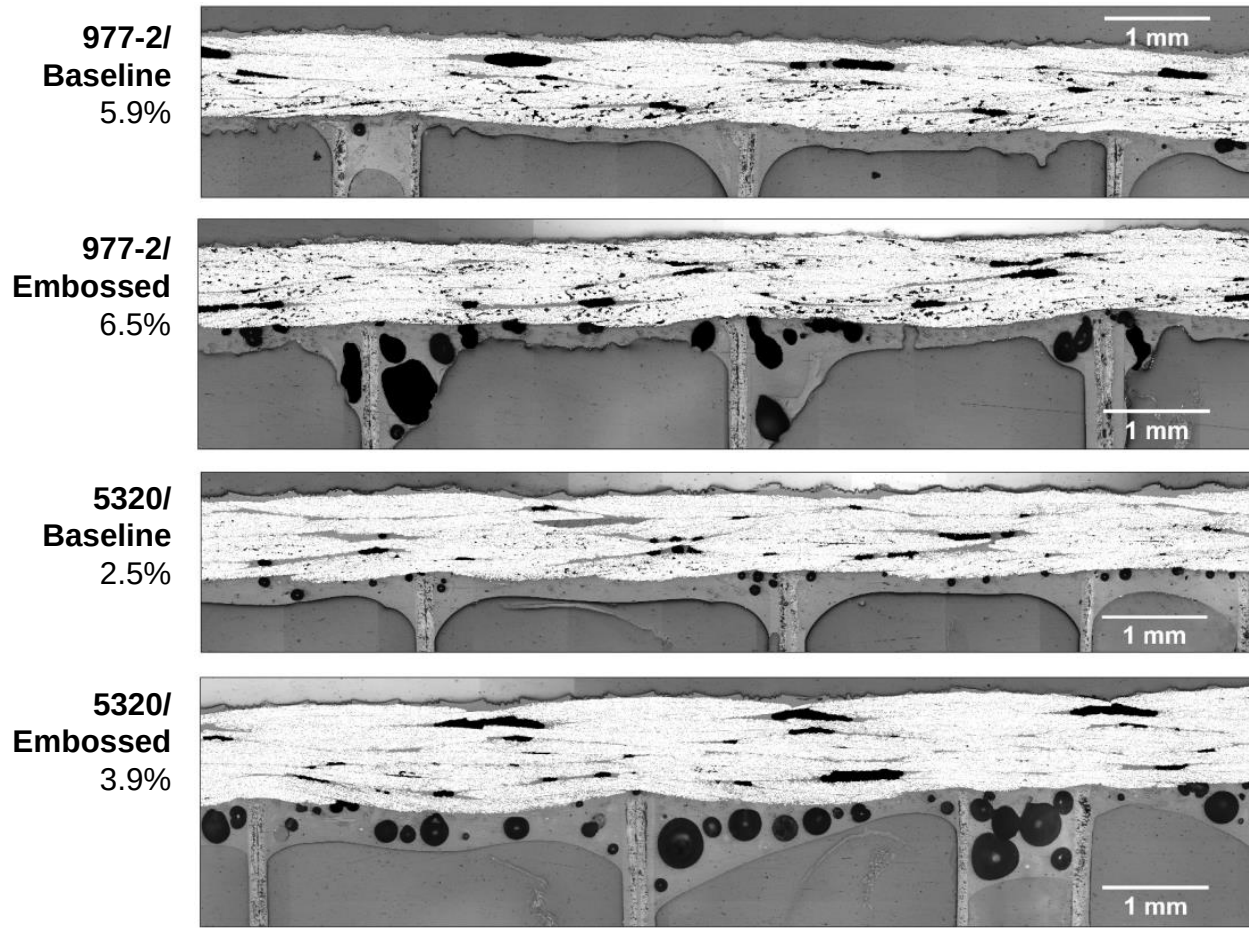

FIGURE 3.26: Sample 0° micrographs showing prepreg repair void morphology (within the patch) as well as adhesive fillet morphology. Patch internal void content on the left.

low core pressure levels led to foaming, while pressurization due to moisture and the high gelation temperature (144 °C) led to increased core pressure and voids that appear to have burst. A high core pressure near the adhesive gelation for the 977-2/embossed repair would also explain why this patch doesn't seem any wavier than the 977-2/baseline patch.

The 5320/baseline repair had a mean menisci height of $0.48\,\text{mm} \pm 0.23\,\text{mm}$, while the 5320/embossed repair had a larger mean menisci height of $0.71\,\text{mm} \pm 0.27\,\text{mm}$. The 5320/embossed fillets exhibited the foaming typical of low core pressures at adhesive gelation [32], on the order of $P_{core} \approx 200\,\text{mbar}$ or less. The core pressure at adhesive gelation for the 5320/baseline repair

was 746 mbar as measured by the miniature pressure transducer (see Core Pressure section). The menisci for the 5320/baseline repair have no foaming, and are very uniform as exhibited by the small standard deviation in menisci relative to the other repairs. The 5320/baseline menisci height and qualitative appearance are very similar to those reported by Préau [32] for the same materials and processes.

The average menisci height for the 977-2 repairs was nearly twice that of the 5320 repairs, despite having higher core pressures. This could be due to there being more resin available to flow from the patch to the fillets due to the bagging arrangements used (impregnated peel ply & non perforated vs perforated release film), as well as the much lower viscosity exhibited by the 977-2 (see Table 3.6). When more resin was available to flow from the patch to the cell walls, Okada [102] also observed larger fillets.

Wet Layup Repair Microscopy

Patch Void Content The patch void content for each wet layup repair is plotted in Figure 3.28. The DVD seems to have been the most important processing variable: the vacuum/DVD and random blob/DVD repairs had patch void contents of 3.2 % and 0.25 % respectively, compared to 8.52 % and 7.49 % for these impregnation methods without DVD. The DOE study of the previous chapter suggested that vacuum impregnation would yield lower porosity than random blob, however the random blob method yielded lower porosity here both with and without DVD. In the DOE study resin impregnation technique had a larger percent contribution than DVD, at 19 % compared to 10 %, however in practice DVD was clearly far more important. It is also interesting that the random blob/DVD repair had a lower void content than the predicted optimum of the DOE study: 0.25 % compared to 1.2 %. This random blob/DVD repair was also the thickest, at 6 plies compared to 4 plies for the other patches, reinforcing the result of the DOE study that thickness has little effect on porosity.

Sample Micrographs The void morphology of each patch shows similar trends to that of the previous chapter, as shown by the sample micrographs of Figure 3.29. The vacuum repair has the largest inter-laminar voids, with very little intra-tow porosity: impregnating the plies under vacuum removes all intra-tow air, but allows air to become entrapped between these fully impregnated plies during lamination. The random blob repair has smaller inter-laminar voids than the vacuum repair, as some of the air entrapped between plies can be removed when vacuum is pulled. However

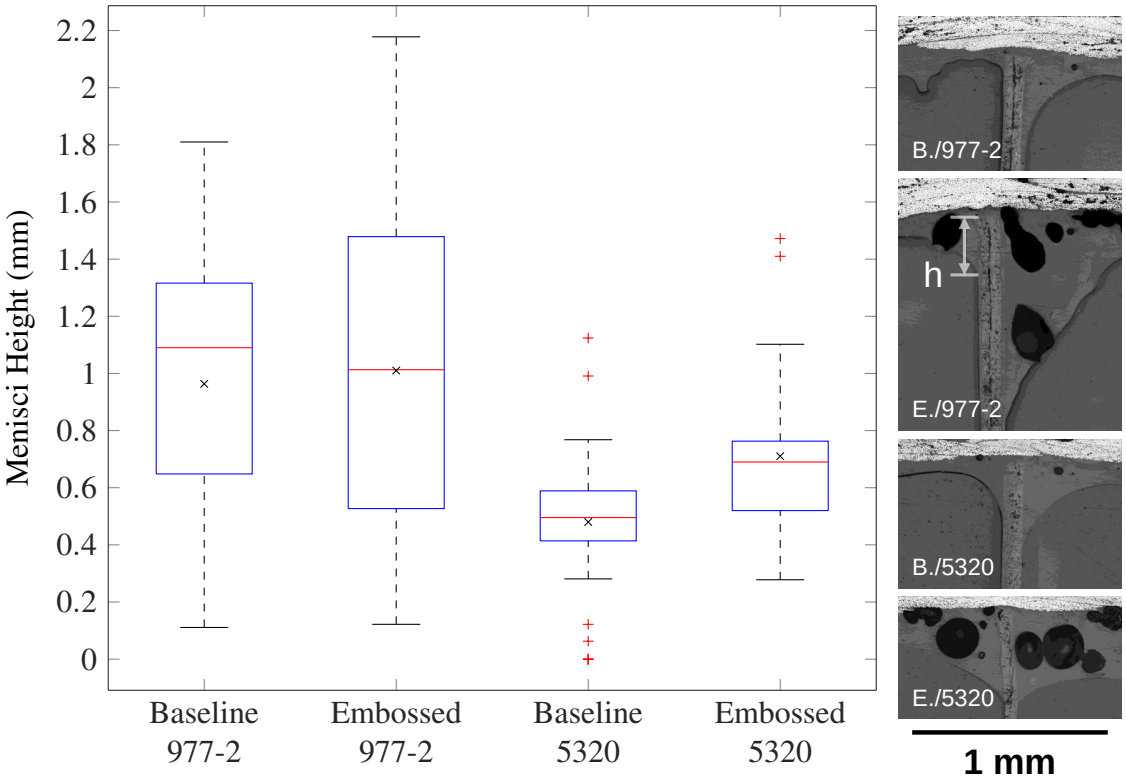

FIGURE 3.27: Menisci heights for each repair, with mean and outliers represented by an 'x' and a '+' respectively. Optical micrographs for each repair show typical adhesive fillets, with foaming evident for the embossed adhesive repairs. Menisci height, *h*, was measured from the top of the cell wall to the end of the fillet as shown in the micrograph.

intra-tow porosity occurs when vacuum is pulled because resin flows and blocks off air evacuation pathways before all the intra-tow air can be removed.

When the DVD patches are laminated onto the bondline, air becomes entrapped between patch and bondline as there is no air evacuation pathway through a fully impregnated patch. Consequently voids are visible between the patch and bondline in both DVD patches. After lamination onto the elevator, the DVD patches were cured in a bleed bagging arrangement. However, there is little need to bleed off resin during this stage, as a bleed bagging arrangement was used during the DVD. Switching to a no bleed arrangement for the cure might be a solution to increase the resin pressure and help mitigate porosity between patch and bondline.

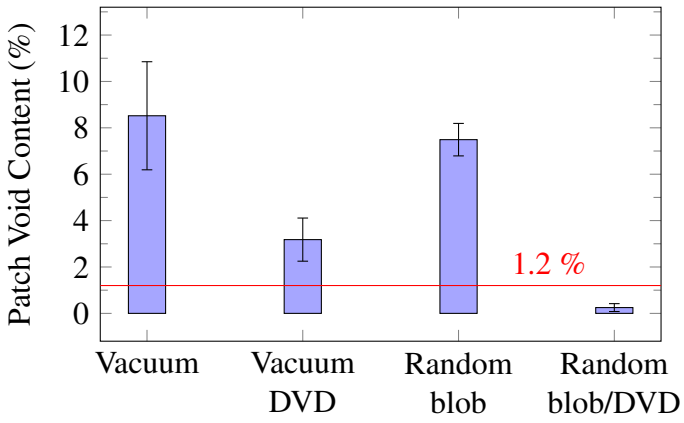

FIGURE 3.28: Void content in the patch for the wet layup repairs.The DOE study of the previous chapter predicted 1.2 % as the void content of the optimally processed patch.

3.3.4 4-Point Bending Tests

All pristine and repaired test specimens were from sections of the lower skin plate with symmetric two ply $[+45/-45]$ facesheets. All tested repairs had $[-45/+45/-45/+45]$ patches, with the exception of the 5320/embossed repair which had an extra ply, $[-45/+45/-45/+45_2]$. In this way the main differences between samples were the repair materials, defects (voids, incomplete cure, ...) and any local variation in lower skin plate properties such as due to aging or damage. Note that the repairs with artificial defects, 5320/baseline and random blob/DVD, were not tested in bending.

A pristine specimen was first tested at support and loading spans of $S = 560\,\text{mm}$ and $L = 230\,\text{mm}$. As a result of the compliant $\pm 45°$ facesheets, the specimen reached the deflection limit of the fixture without failing, and exhibited a non-linear load deflection curve as a result of the large rotations at the supports. Rotations at the supports were so large that at $\approx 75\,\text{mm}$ of crosshead deflection, the load peaked and then began to *decrease* with increased deflection. While no catastrophic failure was observed, this specimen and all subsequent specimens exhibited permanent curvature, perhaps as a result of matrix plasticity and/or progressive damage (matrix cracking). Large strains, material and geometrically non-linear behaviour are also observed for the similar case of tensile testing of $\pm 45°$ CFRP laminates [96], [123].

To achieve skin failure it was thus clear that S and L had to be decreased, at the increased risk of core failure. Two pristine specimens were tested at the reduced spans of $S = 430\,\text{mm}$ and

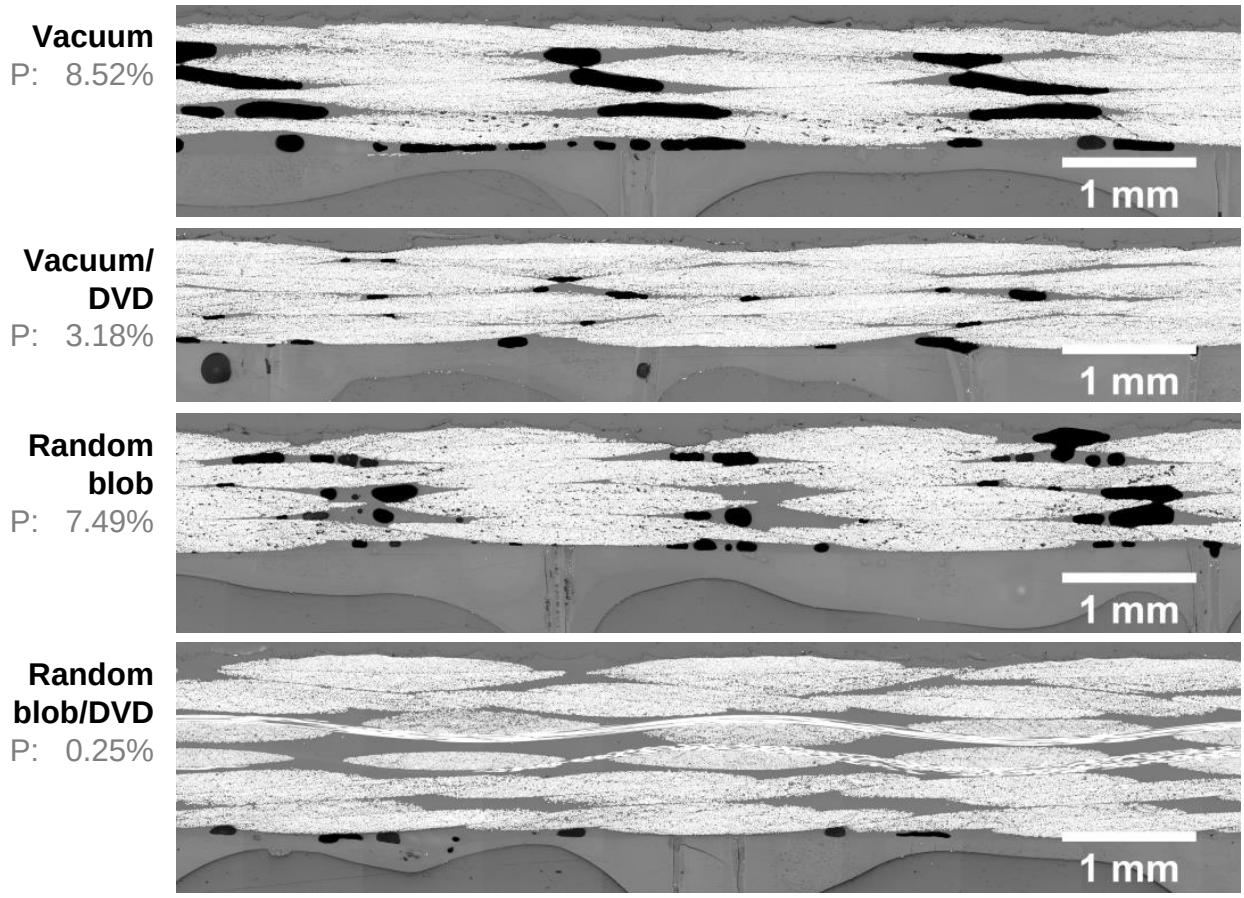

FIGURE 3.29: Sample 0° micrographs showing wet layup repair void morphology (within the patch). Patch internal void content and processing method on the left. Note the lower skin plate's adhesive between facesheet and core was not removed during scarfing and is visible above.

$L = 185\,\text{mm}$: Pristine-T with the internal facesheet on the tension side, and Pristine-C with the internal facesheet on the compression side. In both cases, the internal facesheet failed, either in tension or compression, which is logical as this facesheet is wavier having been on the bag side when the lower skin plate was manufactured. As shown by Figure 3.32, Pristine-T failed in the gauge region while Pristine-C failed at the outer edge of a load applicator. Images of the failure are also shown in Figure 3.31: the clean vertical split in the core for Pristine-T and minimal core damage for Pristine-C suggest that these are both facesheet failures. Since these spans yielded facesheet failures for the Pristine-T and Pristine-C specimens, it was chosen to test the repaired

specimens at the same spans. Since the Pristine-T specimen was stronger, repaired specimens were tested with the internal facesheet on the tension side.

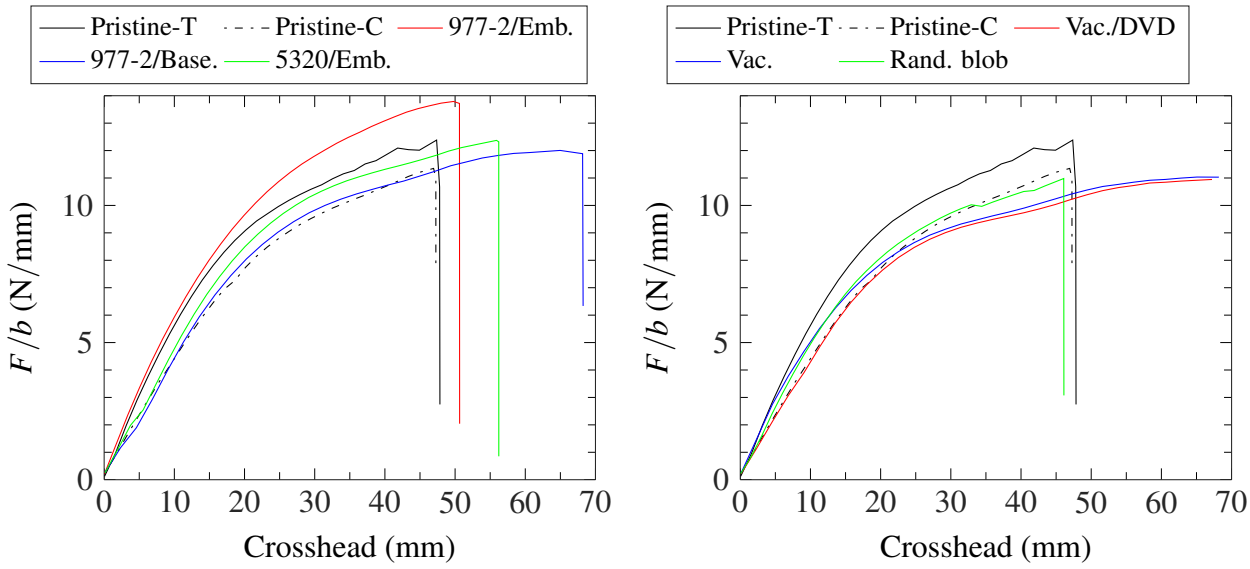

(A) Prepreg. (B) Wet layup.

FIGURE 3.30: Load F normalized by specimen width b against crosshead displacement in 4-point bending. (F is the load at a *single* application or support point.)

The load deflection curves for the prepreg repair specimens are plotted alongside the Pristine-T/Pristine-C curves in Figure 3.30a. The load F at a single load applicator normalized by the specimen width b is plotted against the crosshead position. All prepreg repair specimens failed outside the gage region in core shear, at the locations shown in Figure 3.32. The shear failures were nearly identical in appearance, with that for the 977-2/embossed specimen shown in Figure 3.31. Observing videos of the tests in slow motion showed that core shear failure occurred first, followed by the external facesheet.

The load deflection curves for the wet layup repairs are plotted alongside the Pristine-T/Pristine-C curves in Figure 3.30b. No visible or audible failure occurred in the vacuum/DVD and vacuum wet layup specimens before the deflection limit of the fixture was reached. However, they did exhibit significant permanent deformation after removal from the fixture. The random blob specimen was slightly stiffer, and perhaps for this reason the internal facesheet failed in tension at the location along the span indicated in Figure 3.32. After this tension failure, the core split apart and the repair patch delaminated from the core and one of the scarfs, as shown in Figure 3.31. It was

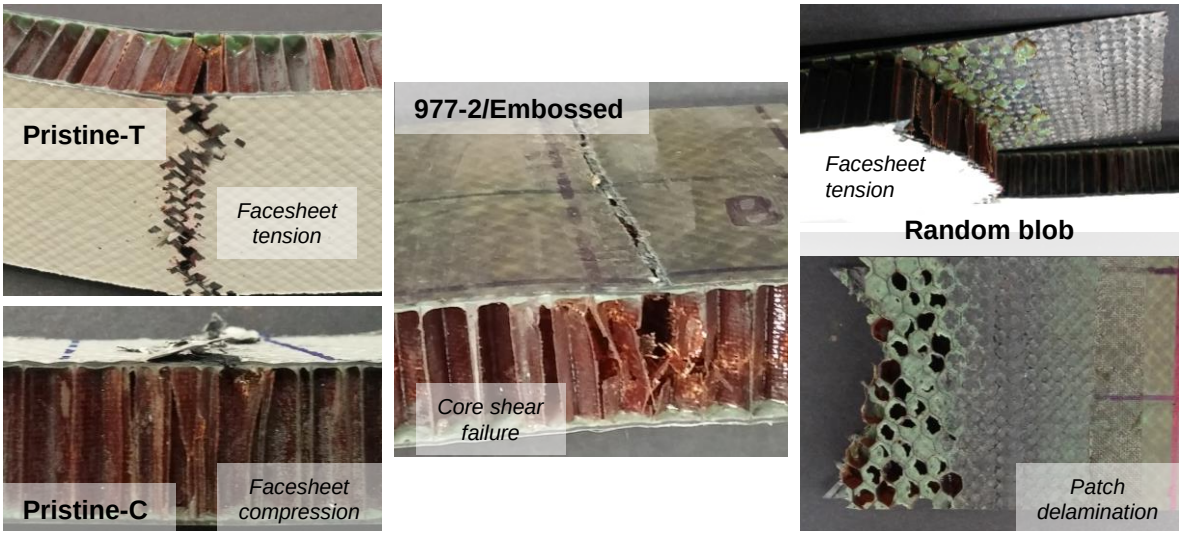

FIGURE 3.31: Representative images of the bending test failure modes.

thought the internal facesheet failed first because the core split and disbonded in a similar manner for the Pristine-T specimen as shown in Figure 3.31.

Since all repaired specimens failed outside the repairs, no correlation can be made between failure strength and repair quality (void content). For repaired panels that did rupture, it can be said that the repairs provided at least an equivalent or greater strength to the corresponding failure mode (core shear or internal facesheet tension).

3.3.5 Degree of Cure and Tg

As described in the methodology section, samples were excised from each repair and process control for MDSC and DMA testing. Degree of cure was computed from the measured MDSC residual heat of reaction (H_{res}), and T_g was measured from both the DMA and MDSC curves. Sample DMA and MDSC curves are presented first, followed by tabulated degree of cure and T_g results.

DMA Test Results

A difficulty encountered when interpreting the DMA results was that all repair specimens contained two resins: the resin of the repair plies (5320, 977-2 or 9390) and the adhesive (FM300-2M

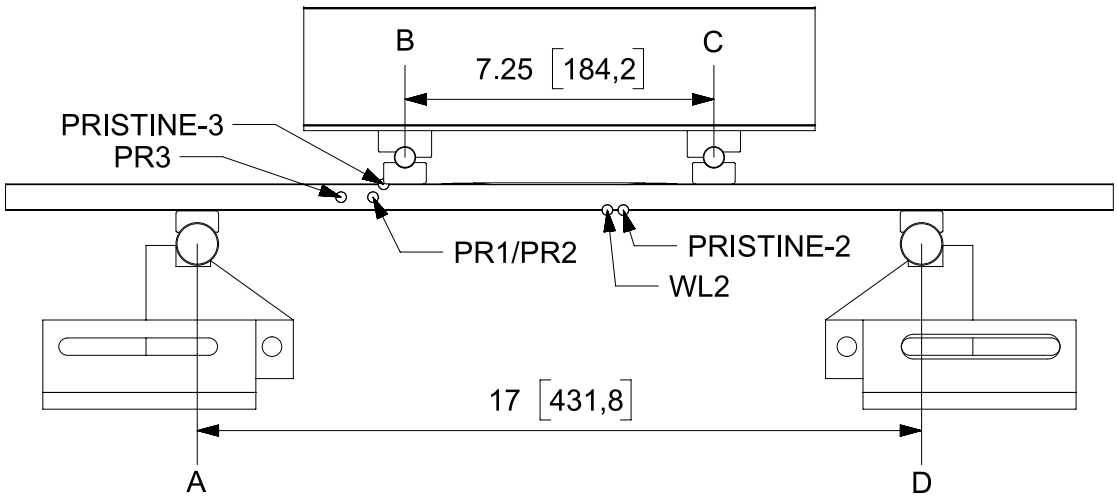

FIGURE 3.32: Bending test failure locations along the span and through the thickness.

or the OEM's adhesive). DMA has enough sensitivity to detect transitions due to multiple resins: for example for RTM samples containing small amounts of a binder, DMA analysis could detect glass transitions due to both the binder system and the RTM epoxy resin [106]. Compare the DMA curves for a 5320 process control, which has only 5320 resin, and the 5320/baseline repair in Figure 3.33. For the process control laminate, the drop in E' is very sudden and the $\tan\delta$ curve has a single, narrow peak. For the 5320/baseline repair, a T_g is visible in the E' curve for both the FM300-2M at a lower temperature and the 5320 at a higher temperature. There is also a shoulder in the $\tan\delta$ curve, suggesting that the $\tan\delta$ curve really has one peak corresponding to each material. Further, the corresponding T_g values agree with the values to be expected for 5320 and FM300-2M as previously shown in Table 3.6. Note also that the 5320/baseline repair had a $[45_4]$ stacking sequence compared to $[0]_{10}$ for the process control, which affects the magnitude and slope of E'.

For the wet layup repairs, two glass transitions were visible only for the two non-DVD repairs. Figure 3.34 shows the E' and $\tan\delta$ curves for one of the non-DVD repair samples (random blob). In the first temperature ramp of Figure 3.34a, the first drop in E' and peak in $\tan\delta$ were thought to be due to the 9390, while the second drop in E' and peak in $\tan\delta$ might be due to the OEM film adhesive. To investigate whether this second peak was due to the film adhesive or additional curing

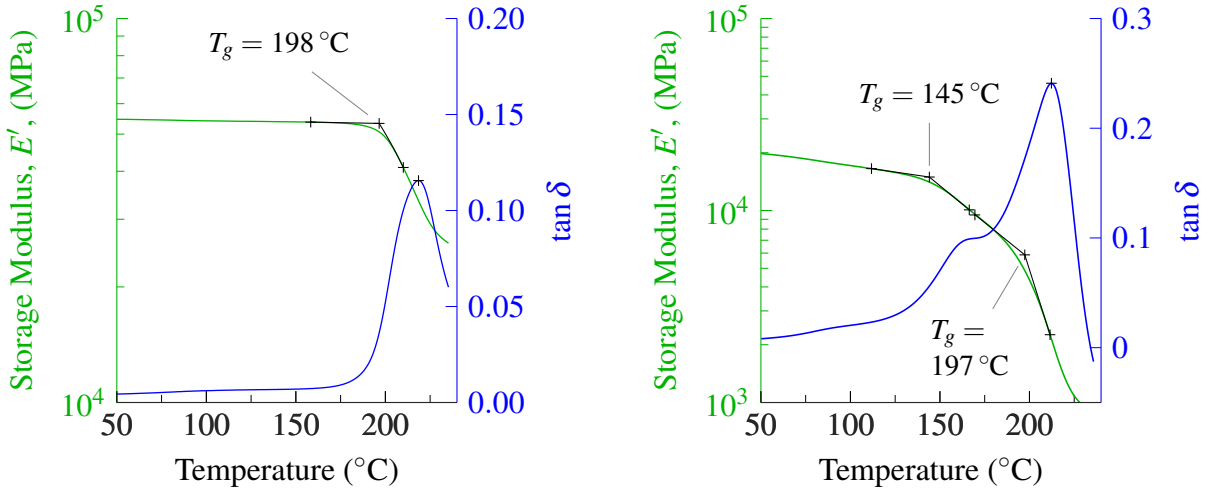

(A) 5320 process control. (B) 5320/baseline repair.

FIGURE 3.33: Sample DMA curves for a prepreg process control and repair.

of the EA 9390, all wet layup samples were subjected to an identical second temperature ramp. As shown in Figure 3.34b, the second temperature ramp only has one glass transition, and this was consistent for all wet layup repair specimens. This could mean that the second glass transition was actually due to additional curing of the 9390.

MDSC Test Results

As described in the DSC methodology section (3.2.3), glass transition temperatures were assigned from the reversing heat flow curves, and residual heats of reaction (H_{res}) were calculated from the nonreversing heat flow curves.

Like the DMA specimens, repair samples contained both the repair patch resin and remnants of adhesive film. Two glass transitions were apparent in almost all prepreg samples; the lower transition corresponding to the FM300-2M film adhesive and the higher one either the 5320 or 977-2 resin. An example MDSC curve for the 977-2/baseline adhesive repair is shown in Figure 3.35, demonstrating the two glass transitions (T_{m1} and T_{m2}). Also clear in Figure 3.35a is the small residual cure exotherm in the first heating, $H_{res} = 2.82\,\mathrm{J\,g^{-1}}$, which disappears completely upon reheating in Figure 3.35b. When normalized by the resin mass following the procedure of section 3.2.3, $H_{res} = 7.48\,\mathrm{J\,g^{-1}}$. Due to the additional curing in the first temperature ramp, there is a corresponding rise in the glass transition temperatures in the second heating. This rise in T_m

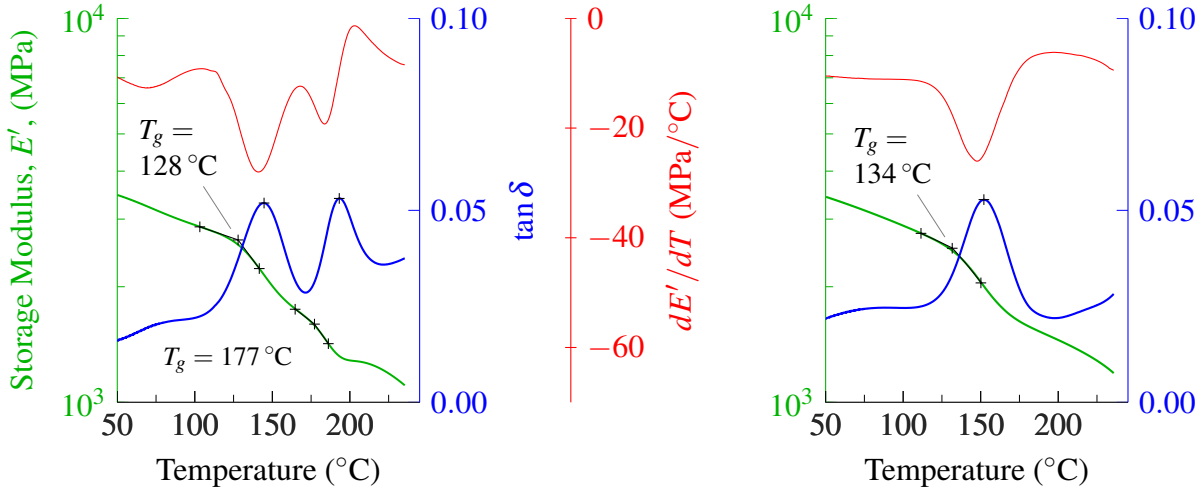

(A) First temperature ramp. (B) Second temperature ramp.

FIGURE 3.34: DMA curves for a specimen from the wet layup, random blob repair. Observing the dE'/dT curve helps to identify hard to detect glass transitions.

occurs most markedly for the 977-2 resin, going from 180 °C to 190 °C, further validating the assumption that H_{res} is due entirely to the repair patch resin (see 3.2.3). In *all* MDSC tests, residual cure exotherms were only visible in the first temperature ramp, indicating complete conversion always occurred in the first temperature ramp.

In all wet layup repair samples, only one T_g was visible with temperatures varying widely from 128 °C to 177 °C. It was therefore not always clear whether this T_g was attributed to the OEM film adhesive or the 9390 resin. It was assumed that if $T_g < 174$ °C, the datasheet T_g for 9390 [50], then the transition was due to the 9390.

In general, glass transitions in the reversing heat flow curves tended to be very subtle. This is partly due to the sample mass which varied from 8.74 mg to 20.79 mg as it was difficult to cut samples that were both small enough to fit in the DSC pan and as large as possible with the equipment available. The samples contained fibres, so the actual amount of resin in the samples varied from approximately 2.1 mg to 10.6 mg. It has also been noted that DMA is about 10 times more sensitive for detecting glass transitions in cured composite samples [106], so the DMA T_g results should be considered more reliable.

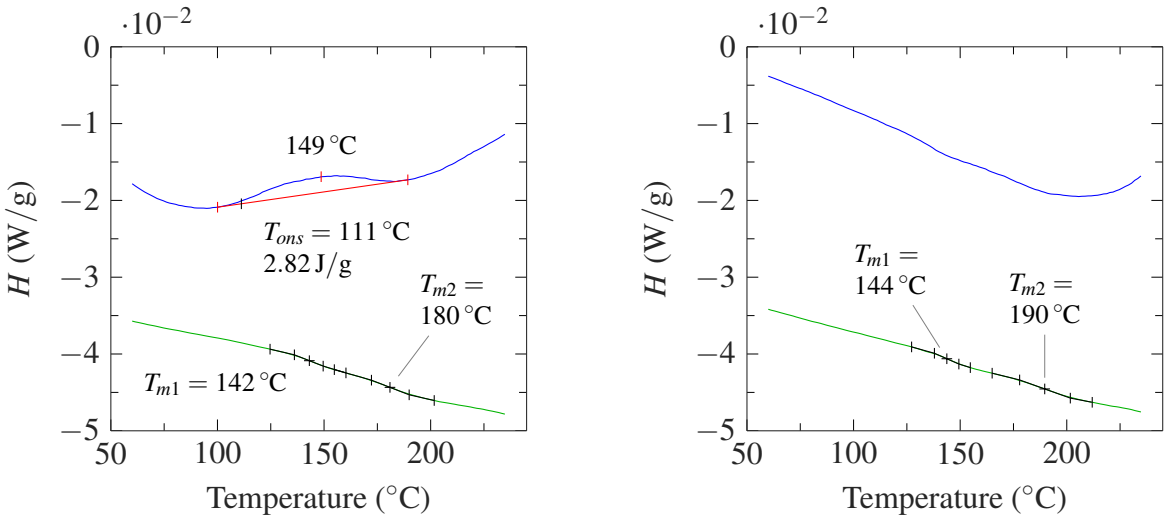

(A) First temperature ramp. (B) Second temperature ramp.

FIGURE 3.35: Reversing heat flow — and nonreversing heat flow — curves from an MDSC ramp at 2 °C min^{-1} ± 1.272 °C every 60 s on the 977-2/baseline adhesive repair (exo up). A residual cure exotherm is visible in the first temperature ramp but not upon reheating. Heat flows are normalized by the sample mass (fibre and resin), m_s = 17.2 mg.

Degree of Cure and T_g

The average MDSC and DMA results are tabulated for the 977-2, 5320 and 9390 in Tables 3.14 and 3.15. The degree of cure computed from the H_{res} results was greater than 97.6 % for all specimens as all residual cure exotherms were small.

In Table 3.14, the MDSC and DMA T_g results both suggest that all prepreg repairs were fully cured, as these values are near those found in the literature for complete cure. There is also good agreement between these repairs and their process controls. Not shown here are the results for the FM300-2M adhesive film used in the prepreg repairs. As this system is reactive at lower temperatures than either 5320 or 977-2, MDSC and DMA T_g's detected for this material suggested the adhesive exceeded 95 % degree of cure in all specimens.

The MDSC and DMA T_g for the 9390 in Table 3.15 however suggest these repairs may have been under cured. The DMA T_g is consistently much lower than the MDSC T_g, which may be due to the 45° stacking sequence of the patch. Specimens with more fibres aligned with the test span are known to have E' curves that are both shifted towards higher modulus and temperature,

TABLE 3.14: Prepreg Repair Degree of Cure and T_g

Quantity	**977-2 Baseline**	**977-2 Embossed**	**977-2 Proc. Ctrl.**	**5320 Baseline**	**5320 Embossed**	**5320 Proc. Ctrl.**
MDSC (H_{res}) Degree of Cure (%)	98.3	99.9	97.6	100.0	99.1	99.9
MDSC T_g (°C)	180	(No data)	190	210	206	212
DMA T_g (°C)	179	182	186	197	193	197
Literature T_g (°C)	195 [90]			212 [35]		
Stacking Sequence	$[45_4]$		$[0]_{10}$	$[45_4]$	$[45_5]$	$[0]_{10}$

TABLE 3.15: Wet Layup Repair Degree of Cure and T_g

Quantity	**Vacuum**	**Vacuum/DVD**	**Rand. Blob**	**Rand. Blob/DVD**
MDSC H_{res} Degree of Cure (%)	99.4	99.0	99.0	99.3
MDSC T_g (°C)	164	156	151	150
DMA T_g (°C)	105	117	120	135
Literature T_g (°C)	174 [50]			
Stacking Sequence	$[45_4]$		$[45_2/0_2/45_2]$	

resulting in a higher T_g [124]–[127]. The surprising effect of fibre orientation on T_g is due mostly to the fibre-matrix interface region.

The wet layup/vacuum sample had contradictory results: the lowest DMA T_g but the highest MDSC degree of cure and T_g. No explanation for the low DMA T_g could be found in the processing data either: steady state in-plane temperature gradients were small, ranging from $-2.2\,^{\circ}\mathrm{C}$ below the control thermocouple to $13.0\,^{\circ}\mathrm{C}$ above. Thermocouples were also placed very near the lower DMA specimen for this patch, with the data plotted in Figure 3.17, which showed the desired cure temperature was reached or exceeded through the thickness. For this repair it was also mentioned that the 121 °C dwell was held for 3 h 51 min rather than the 45 min intended.

3.4 Summary

Prepreg repair processing techniques developed by Préau [32] and wet layup repair processing methods developed in the previous chapter were used to repair a decommissioned composite aircraft structure. These repairs were implemented alongside repairs processed by baseline prepreg and wet layup processing techniques to validate whether quality improvements seen at the lab scale can be achieved in practice.

The embossed/perforated film adhesive yielded no improvement in porosity with the 977-2 prepreg. Several causes were hypothesized for this including the use of intermediate debulks, the higher temperature 977-2 cure cycle, the reduced level of vacuum, possible cold flow of the 977-2 resin and off-gassing. Such autoclave prepregs with 177 °C cure cycles in general do not seem suitable as a repair material. They yield very high patch and bondline void contents with such VBO processes, and the 177 °C cure risks surpassing the parent structure's T_g causing warping or damage.

The embossed/perforated film adhesive yielded a void free bondline with the 5320 semipreg, but was slightly detrimental to the patch void content. With the 5320 semipreg, a good quality repair was achieved even without embossed adhesive: for semipregs with high crimp fibre architectures such as plain weave, the embossed adhesive may not be necessary. The patch void content may have improved with the embossed adhesive had a longer pre-cure vacuum hold been used.

The DVD was the most important factor for the wet layup repairs, significantly reducing porosity for both vacuum and random blob impregnation. While resin impregnation method was less important, the random blob method led to slightly lower porosity than vacuum impregnation both with and without DVD.

Since the elevator's stacking sequence was not suitable for 4-point bending tests, these tests provided no information on the effect of processing variables on strength recovery. However, along with the NDT, these tests showed that the repairs had no major processing induced defects.

Analysis of the degree of cure and T_g through MDSC and DMA testing showed that all prepreg repairs were fully cured. However, the DMA testing of the wet layup repairs suggested some repairs were under-cured, although this was not corroborated by the MDSC results.

Chapter 4

Conclusion

4.1 Conclusions and Contributions

Co-bonded scarf repair process improvements were sought to yield low void content in a robust fashion with minimal adverse affects on process complexity, time and cost. To address current gaps in the understanding of material, processing and quality relationships, wet layup repair was the main focus starting with material and process development at the lab scale. Then improved wet layup, and as a secondary objective prepreg, co-bonded repair procedures were validated on a decommissioned aircraft structure. Overall conclusions and contributions are:

- **Optimal wet layup process** Using Taguchi DOE methods, the effect of many different processing variables on void content was determined to design a robust, low void content process. At the lab scale, this optimal process was predicted and confirmed to yield 1.2 ± 0.8 % void content, a significant improvement over current processes for which 7 % or higher is common. The key factors, in order of importance, were to: reduce the temperature at gelation to 93 °C, impregnate the dry fabric by either the vacuum or random blob techniques, perform a 2 h pre-cure vacuum hold and degas the patch by the DVD technique. Factors with minimal effect on void content were vacuum level (as low as 50 kPa) and repair thickness.

- **Effect of patch void content on strength** A drastic, linear reduction in short beam strength was observed with void content: when void content was decreased from 3.7 % to 0.9 %, short beam strength improved by 37 %.

- **Wet layup resin impregnation technique** At the lab scale, the impregnation technique was the second most important factor to both void content and fibre volume fraction. Only the two

optimal methods, the vacuum and random blob impregnation techniques, were applied to the demonstrator. For the demonstrator this factor proved less important than the DVD process, with the random blob method leading to a slight improvement in void content compared to the vacuum impregnation technique.

- **DVD** In the lab scale Taguchi DOE study, the DVD factor had only a 10 % contribution to void content. However, this was likely a result of poor temperature control: in a follow-up test with the temperature control problem corrected, patch void contents below the predicted optimum (0.68 %) and approaching autoclave quality were achieved. Consequently for the demonstrator the DVD technique proved more important: patch void contents of less than 3 % were achieved when DVD was used compared to 7.5 % or higher without.

- **Effect of embossed and perforated adhesive** The embossed and perforated film adhesive led to a void free bondline when used with semipreg, although provided no improvement in the patch void content. Without this engineered adhesive, a low porosity repair was still achieved with the semipreg, perhaps indicating it is not needed with high crimp (plain weave) semipregs. No improvement in bondline or patch void content was achieved when the engineered adhesive was used in conjunction with the autoclave prepreg. Further experiments would be needed to explain why.

- **Effect of semipreg** Semipregs showed good promise as a repair material, yielding much lower patch and bondline void content than the autoclave prepreg. The lower cure temperature of the semipregs relative to autoclave prepregs can also be beneficial to avoid warping or damaging the parent structure.

- **Real world challenges** The demonstrator implementation also served to highlight typical process deviations experienced in the field: in-plane and through-thickness temperature gradients, hotter and more humid ambient conditions than most controlled laboratory environments and a large variation in vacuum quality due to both available equipment and leaks.

When implemented on the demonstrator, overall the optimized wet layup methods developed in this work and the improved semipreg methods with air breathable adhesive found in the literature led to significant quality and robustness improvements relative to baseline methods. Implementing these new procedures in practice could provide improved mechanical property recovery, durability

and inspectability. This may help address certification challenges with co-bonded repairs and expand their scope to structural repairs currently reserved for less efficient bolted repairs.

4.2 Future Work

The demonstrator served as a first real application for these improved co-bonded repair processes outside of controlled laboratory conditions. As such several areas can be identified for future work:

1. **Demonstrator using low crimp semipreg** A repair demonstrator employing a low crimp or unidirectional semipreg, as might be needed for repairing thick monolithic sections found in modern fuselage and wing structures, would provide a good test of the potential quality improvement using the embossed film adhesive.

2. **Lab scale process development with 977-2** If the autoclave prepreg used here is indeed a preferred repair material, such as for logistical constraints or to facilitate certification, there is potential for significant quality improvement. For instance, after characterizing its viscosity behaviour, a DVD process could be developed to reduce patch porosity. By modifying the process it may be possible to extract air from the bondline using the embossed adhesive.

3. **Physical testing** The static flexure tests performed on the demonstrator repairs provided no useful information due to failure occurring outside of the repairs. Static and fatigue testing of repaired panels would be needed to verify if the observed quality improvements result in improved strength and durability.

4. **Operator variability** This work was performed either by the author or under his close supervision. Studies have shown that much of the variability in co-bonded repair processes is due to different technician experience levels. Therefore the robustness of these techniques to operator variability would need to be assessed.

5. **Wet layup bondline improvement** In this work the standard method of using the laminating resin as the adhesive to bond the patch was employed. Such a bondline has very inconsistent thickness, porosity and likely low strength. To use wet layup repairs in structural applications improved bonding methods or materials may be needed, and would require materials that can also be stored at room temperature.

Appendix A

Random Blob Impregnation and Ply Lay-Up Procedure

A procedure for random blob impregnation of dry fabric and ply lay-up is presented here. These instructions have been written to be cohesive with the CACRC's ARP 5319 [25], "Impregnation of Dry Fabric and Ply Lay-Up". They are meant to supplement, but not replace, this repair document.

A.1 Tools and Materials

A full list of tools and materials is available in ARP 5319. The tools and materials used in this appendix are listed and defined here.

A.1.1 Tools

- Scale: An electronic scale accurate to ± 0.1 g.
- Rigid plate: A thin, rigid plate larger than the largest repair ply, to be placed on the scale.
- Marking pen: A permanent marker that will not contaminate the resin.

A.1.2 Consumable Materials

- Wooden tongue depressor: Any wooden tongue depressor.
- Parting film: A release film, such as fluorinated ethylene propylene (FEP) film, with film thickness of 50 µm or thicker. The film should be translucent and colored.

- Drawing film: A nylon vacuum bagging film which ply outlines may be drawn onto. The film thickness should be 50 µm or thicker.
- Release film: A release film such as fluorinated ethylene propylene (FEP) film, any thickness.
- Thermoplastic film tape: Commonly known as flashbreaker tape, a tape used to cover areas where resin may bleed. Commonly polyester film, coated on one side with pressure sensitive adhesive.
- Brush: A short bristled brush with natural bristles. Typically a 25 mm wide brush with 12 mm long bristles.
- Container: A clean, disposable plastic container to contain the resin during measuring and mixing. Typically translucent high density polyethylene (HDPE) or polypropylene (PP) is used, with a height to diameter ratio of one.

A.2 Preparation of the Repair Area

Before starting ply impregnation, follow the instructions of ARP 5319 [25], section 6 “Preparation of the repair area”. These instructions are briefly summarized here.

It is assumed that the repair area has been abraded for a scarf, step or scab repair. Refer to ARP 5319 for instructions on cleaning and drying the repair area. The repair area should then be prepared as shown in Figure A.1a. Normally the area adjacent to the repair is masked with thermoplastic film tape. Either outside the repair area or on the thermoplastic tape two axes are drawn: the primary axis in the 0° direction of the part, and the secondary axis in part’s 90° direction. These axes are used for aligning plies during lay-up.

Refer to ARP 5319 for instructions on preparing ply templates out of transparent drawing film. They should look as shown in Figure A.1b, with the following information: primary and secondary axes, fabric warp direction and ply number.

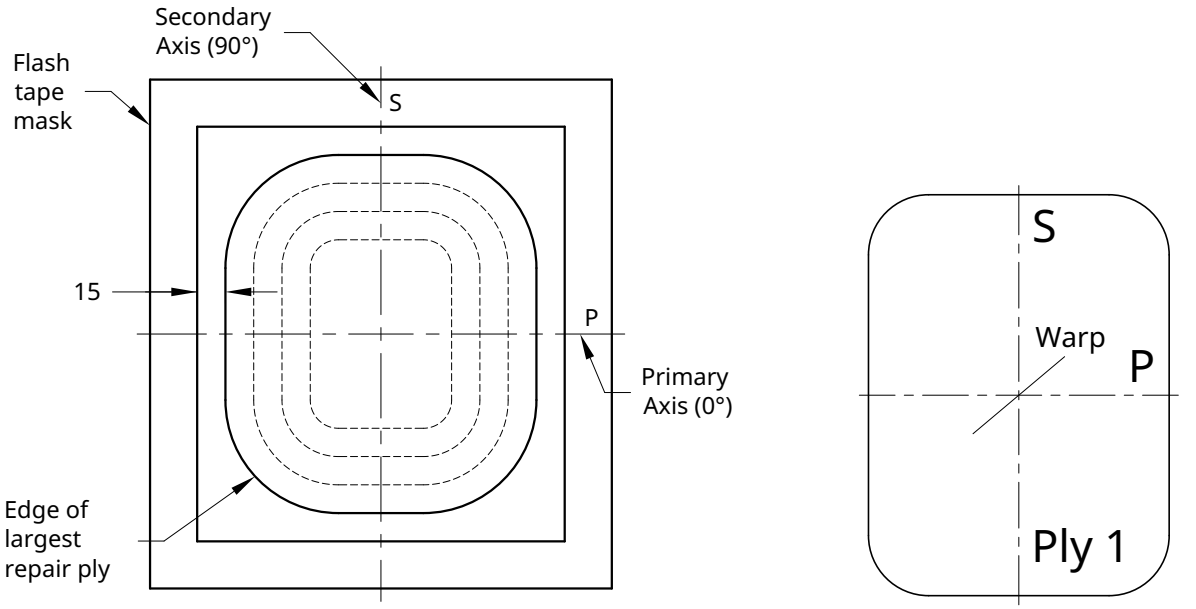

(A) Preparation of the repair area. (B) Ply template preparation.

FIGURE A.1: Preparatory work as instructed by ARP 5319. Dimensions in mm.

A.3 Preparation for Ply Impregnation

A.3.1 Drawing Film and Dry Fabric Cutting

Follows these instructions rather than section 7 of ARP 5319.

1. Cut a piece of drawing film large enough to fit all the ply templates, no wider than the fabric roll width (fabric weft direction).

2. Indicate the fabric warp direction by marking a line on the drawing film as illustrated in Figure A.2a.

3. Arrange the ply templates on the drawing film, leaving approximately 12 mm between any two templates and to the drawing film edge. Make sure to align the warp direction of the ply templates with the warp axis on the drawing film.

4. Trace the ply outline from each template onto the drawing film. Place the templates aside.

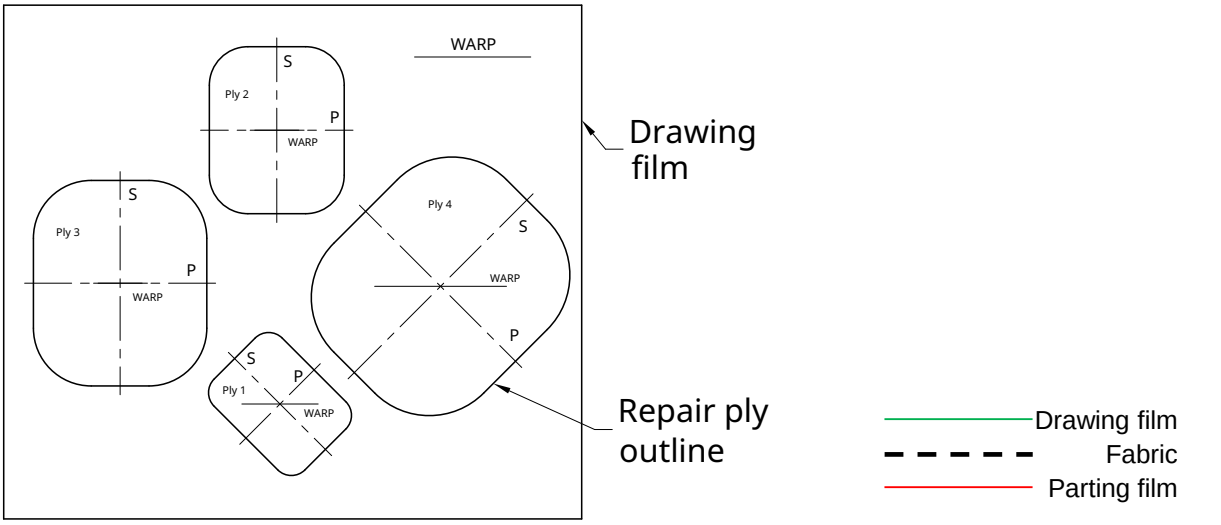

(A) Drawing film.

(B) Dry fabric is protected from contamination by two films.

FIGURE A.2: Preparation of drawing film with ply outlines and placement of drawing film over dry fabric.

5. On the drawing film, within each repair ply outline, draw lines for the fabric warp direction, primary and secondary axes. Write the ply information (primary axis, secondary axis, fabric warp direction and ply number) within the boundary of each ply on the drawing film as well.

6. The prepared drawing film should now appear as shown in Figure A.2a.

7. Cut a piece of parting film to the same dimensions as the drawing film.

8. Cut the dry fabric to the same dimensions as the drawing film, making sure the warp direction of the fabric coincides with the warp direction indicated on the drawing film.

9. Sandwich the dry fabric between the parting film and drawing film as indicated in Figure A.2b. These films help to prevent contamination, weave distortion and fibre bundle fraying during subsequent operations.

10. Cut each ply, making sure to keep the cut plies between the drawing and parting films.

TABLE A.1: Dry Fabric and Impregnated Fabric Mass for Each Ply, $m_f = X.XX$

	Ply 1	**Ply 2**	**Ply 3**	**...**
Dry fabric mass M_f (g)				...
Impregnated fabric mass $M_c = M_f/m_f$ (g)				...

A.3.2 Resin Quantity Calculation

To determine the quantity of resin required for each ply, first select a desired fiber volume fraction v_f. A fibre volume fraction of 0.50 to 0.55 was found to be effective for 3k plain weave. Using this volume fraction, the mixed resin density ρ_r and the fibre density ρ_f, calculate the fibre mass fraction m_f as per Equation A.1. For a given mass of dry fabric M_f, the mass of impregnated fabric M_c can be computed as per Equation A.2.

$$m_f = \frac{\rho_f v_f}{(1-v_f)\rho_r + v_f \rho_f} \tag{A.1}$$

where:

m_f is the fibre mass fraction

ρ_f, ρ_r are the fibre and resin density respectively ($\mathrm{g\,m^{-3}}$)

v_f is the fibre volume fraction desired (0.50 to 0.55 typically)

$$M_c = \frac{1}{m_f} M_f \tag{A.2}$$

where:

M_f is the mass of a ply of dry fabric (g)

M_c is the mass of an impregnated ply (g)

The mass of each impregnated ply will be determined by weighing each ply of dry fabric in the next section. Prepare a table as shown in Table A.1 for your number of plies, indicating the calculated m_f.

A.4 Random Blob Impregnation and Lay-up

A.4.1 Impregnation

1. Setup a scale on a rigid surface as shown in Figure A.3a. The scale should be accurate to ± 0.1 g. Place a clean, thin rigid plate larger than the largest repair ply on top of the scale as shown. Tape a piece of release film to the plate to prevent contamination and facilitate clean-up of any spilt resin during the impregnation process.

2. Cut a wooden tongue depressor longitudinally in two. Place aside.

3. Mix the resin. Refer to ARP 5256 [24]. Record the time when mixing is complete for control of residual pot life. An adequate quantity should be mixed to impregnate all plies, wet the bondline and account for losses. To minimize heat build-up do not mix quantities greater than 250 g in any one container.

4. Zero the scale.

5. Place the first ply on the scale, with the drawing film side directly on the scale and removing the parting film as shown in Figure A.3a.

6. Record the mass indicated as the *dry fabric mass* in Table A.1 for ply 1. (This includes the mass of the drawing film which can be considered negligible here).

7. Calculate the impregnated fabric mass as per Equation A.2 and enter in Table A.1 for ply 1.

8. Coat the tip of the wooden tongue depressor from step (2) with a small quantity mixed resin. Using the sharp point of the tongue depressor, gently place a small drop of resin on the ply, as shown in Figure A.3b. Place drops of resin uniformly over the ply in this way, until the impregnated mass M_c for the ply is reached.

9. Remove the impregnated ply from the scale and place aside on a clean surface, with the impregnated side facing up as shown in Figure A.4.

10. Repeat steps (4) to (9) to impregnate the remaining plies.

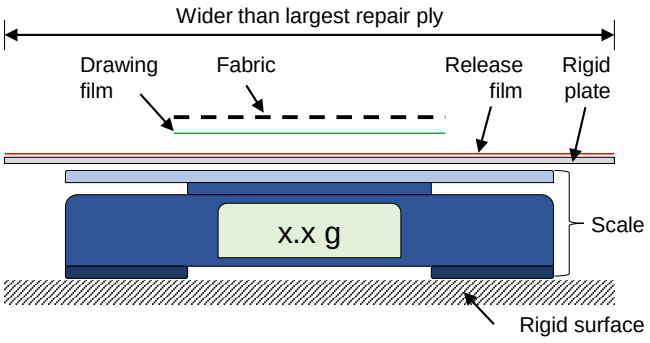

(A) Scale set up for random blob impregnation.

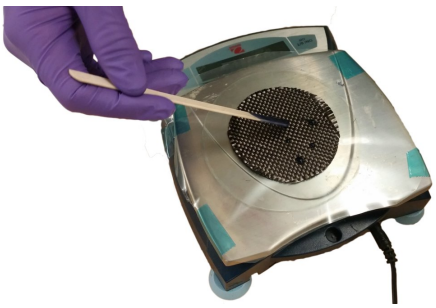

(B) Ply impregnation with wooden tongue depressor.

FIGURE A.3: Each ply of dry fabric is weighed, then resin is added in uniformly spaced drops.

A.4.2 Ply Lay-Up

1. Brush a thin coat of laminating resin onto the entire repair area as shown in Figure A.5a. Use the minimum quantity necessary to fully wet the surface, taking care to work the resin into the surface of the bond area.

2. Pick up the first ply, pinching the edges of the impregnated fabric and the drawing film. As the fabric is minimally impregnated, both the impregnated fabric and drawing film need to be held together when transferring to the repair area.

3. Lightly place the ply, with the exposed side facing down, onto the repair area, taking care to align the primary and secondary axes of the drawing film with those on the component.

4. Remove the drawing film. Do not attempt to compact the ply.

5. Laminate the remaining plies following steps (2) to (4). Count the drawing films to make sure none are left in the patch.

6. Vacuum bag the repair area. Refer to ARP 5143, Method 1 (Vertical Bleed) [20].

7. Apply vacuum to the bag, using the maximum vacuum that is available.

8. Cure the repair following the desired cure cycle.

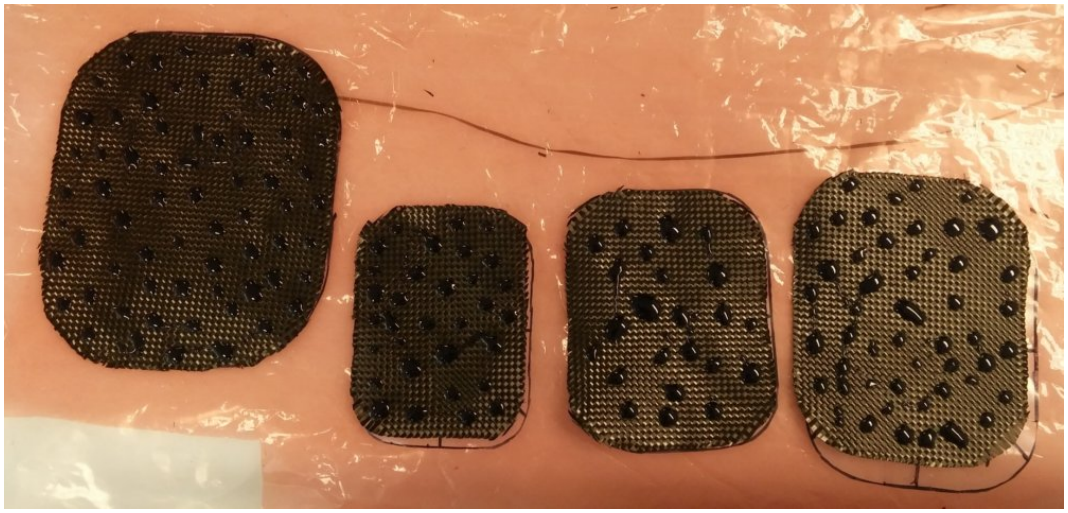

FIGURE A.4: Plies impregnated by the random blob process. Note the drawing film kept underneath each ply.

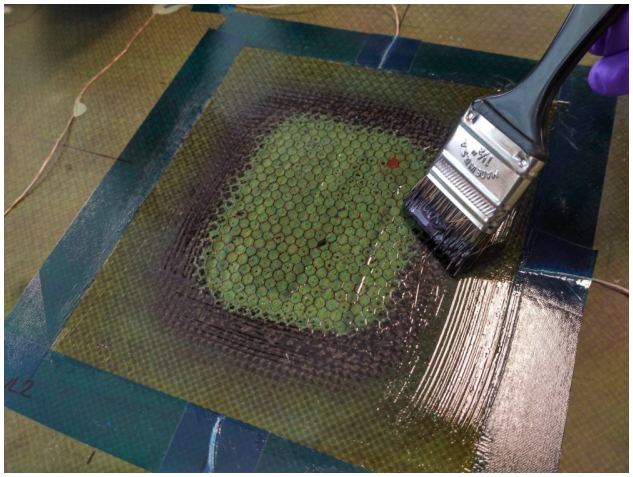

(A) Resin application with a brush onto the repair area.

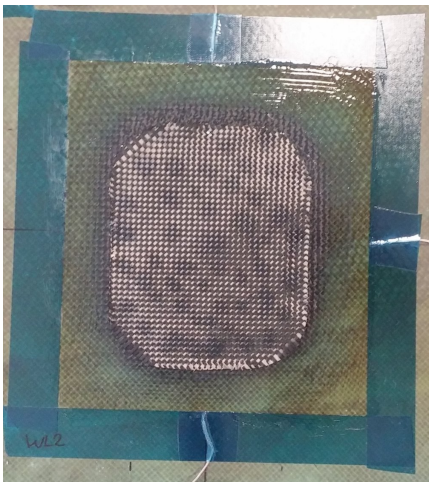

(B) Plies are laminated with drops of resin facing downward.

FIGURE A.5: Bondline wetting and ply lay-up.

Bibliography

[1] A. MacLean, D. Casari, and P. Hubert, "Wet Layup Composite Bonded Scarf Repairs: Effect of Processing Variables on Porosity", in *SAMPE TECHNICAL CONF. Proc.*, Long Beach, CA, 2016.

[2] B. Hartunian, "Speaking Out: ACEE, the NASA program that almost didn't get composites on commercial jets", *Composites World*, May 2007.

[3] D. V. Chovil, S. T. Harvey, J. E. McCarty, O. E. Desper, E. S. Jamison, and H. Syder, "Advanced Composite Elevator for Boeing 727 Aircraft - Volume I - Technical Summary", Boeing Commercial Airplane Company, Seattle, WA, NASA Contractor Report 3290, Nov. 1981.

[4] C. Soutis, "Carbon fiber reinforced plastics in aircraft construction", *Materials Science and Engineering: A*, International Conference on Recent Advances in Composite Materials, vol. 412, no. 1–2, pp. 171–176, Dec. 2005. DOI: 10.1016/j.msea.2005.08.064.

[5] A. Lewis, "Making Repairs to the 787", *AERO*, 2014.

[6] V. Faivre and E. Morteau, "Damage Tolerant Composite Fuselage Sizing: Characterisation of Accidental Damage Threat", *Flight Airworthiness Support Technology*, no. 48, Aug. 2011.

[7] G. Marsh, "The challenge of composite fuselage repair", *Reinforced Plastics*, vol. 56, no. 3, pp. 30–35, May 2012. DOI: 10.1016/S0034-3617(14)70085-2.

[8] F. C. Campbell, "The Case Against Honeycomb Core", in *Proc. International SAMPE Symposium and Exhibition*, Long Beach, CA, 2004.

[9] J. H. Fogarty, "Steam pressure induced delamination of honeycomb core sandwich panels", in *Proc. SAMPE Fall Technical Conference 37th ISTC*, Seattle, WA, 2005.

[10] L. Dorworth, "Composite repair: Lessons learned, challenges and opportunities, Part I", *Composites World*, Oct. 2016.

[11] K. B. Armstrong, L. G. Bevan, and W. F. Cole, *Care and Repair of Advanced Composites*, English. Warrendale, Pa.: SAE International, 2005.

[12] J. Berner, *Bolted Repair in Composite Structure*, 2009.

[13] F. C. Campbell, *Manufacturing Processes for Advanced Composites*. Oxford, UK: Elsevier, 2004.

[14] M. Gubisch, *MRO Europe: Airbus cautious about bonded structural repairs on A350*, https://www.flightglobal.com/news/articles/mro-europe-airbus-cautious-about-bonded-structural-repairs-on-a350-377511/, Oct. 2012. (visited on 05/19/2017).

[15] B. Whittingham, A. A. Baker, A. Harman, and D. Bitton, "Micrographic studies on adhesively bonded scarf repairs to thick composite aircraft structure", *Composites Part A: Applied Science and Manufacturing*, Special Issue: Repair, vol. 40, no. 9, pp. 1419–1432, Sep. 2009. DOI: 10.1016/j.compositesa.2008.12.011.

[16] ARP 4916 (2011), *Masking and Cleaning of Epoxy and Polyester Matrix Thermosetting Composite Materials*, 2011, [Online]. Available: https://saemobilus.sae.org/content/ARP4916.

[17] C. H. Wang and A. J. Gunnion, "On the design methodology of scarf repairs to composite laminates", *Composites Science and Technology*, vol. 68, no. 1, pp. 35–46, Jan. 2008. DOI: 10.1016/j.compscitech.2007.05.045.

[18] M. Préau and P. Hubert, "Processing of co-bonded scarf repairs: Void reduction strategies and influence on strength recovery", *Composites Part A: Applied Science and Manufacturing*, vol. 84, pp. 236–245, May 2016. DOI: 10.1016/j.compositesa.2016.01.016.

[19] ARP 4977 (2006), *Drying of Thermosetting Composite Materials*, 2006, [Online]. Available: https://saemobilus.sae.org/content/ARP4977.

[20] ARP 5143 (2011), *Vacuum Bagging of Thermosetting Composite Repairs*, 2011, [Online]. Available: https://saemobilus.sae.org/content/arp5143.

[21] ARP 5144A (2017), *Heat Application for Thermosetting Resin Curing*, 2017, [Online]. Available: https://saemobilus.sae.org/content/ARP5144A.

[22] M. Lane, A. Poursartip, G. Fernlund, K. Willden, and K. Nelson, "Robust Processing of Composite Structures", in *SAMPE TECHNICAL CONF. Proc.*, Seattle, WA, 2010.

[23] *Composite Materials Handbook Volume 3: Polymer Matrix Composites Materials, Usage, Design and Analysis*, ser. Composite Materials Handbook CMH-17. SAE International, Jul. 2012, vol. 3.

[24] ARP 5256 (2014), *Mixing Resins, Adhesives and Potting Compounds*, 2014, [Online]. Available: `https://saemobilus.sae.org/content/arp5256`.

[25] ARP 5319 (2011), *Impregnation of Dry Fabric and Ply Lay-Up*, 2011, [Online]. Available: `https://saemobilus.sae.org/content/arp5319`.

[26] L. K. Grunenfelder, T. Centea, G. Riddle, and S. R. Nutt, "The Influence of Prepreg Architecture on Part Quality for Vacuum Bag Only Processing", in *SAMPE TECHNICAL CONF. Proc.*, Baltimore, MD, 2015.

[27] C. Seaton and S. Richter, "Nonconforming Composite Repairs: Case Study Analysis", US Department of Transportation Federal Aviation Administration, Tech. Rep. DOT/FAA/TC-14/20, Nov. 2014.

[28] G. Gardiner, "Aircraft composites repair moves toward maturity", *Composites World*, Feb. 2016.

[29] F. C. Campbell, A. R. Mallow, and C. E. Browning, "Porosity in Carbon Fiber Composites - An Overview of Causes", *Journal of Advanced Materials*, vol. 26, no. 4, pp. 18–33, 1995.

[30] J. Tomblin and L. Salah, "Lessons Learned from CACRC Depot Bonded Repair Round Robin Investigation", in *Proc. 2015 FAA/Bombardier/TCCA/EASA/Industry Composite Transport Damage Tolerance and Maintenance Workshop*, 2015.

[31] D. W. Hempe, "Composite Aircraft Structure", US Department of Transportation Federal Aviation Administration, Tech. Rep. AC 20-107B, Sep. 2009.

[32] M. Préau, "Defect Management in Vacuum Bag Only Semipreg Processing of Co-bonded Composite Repairs", Ph.D. thesis, McGill University, Montreal, QC, Jun. 2016.

[33] K. Bujun, "Processing Study of in-situ Bonded Scarf Repairs for Composite Structures", Master's thesis, McGill University, Montreal, QC, Aug. 2014.

[34] N. H. Auda, "The Effect of Pre-Bond Moisture on In-Service Composite Bonded Repairs", Master's thesis, McGill University, Montreal, QC, Apr. 2015.

[35] J. Kratz, K. Hsiao, G. Fernlund, and P. Hubert, "Thermal models for MTM45-1 and Cycom 5320 out-of-autoclave prepreg resins", *Journal of Composite Materials*, vol. 47, no. 3, pp. 341–352, Feb. 2013. DOI: 10.1177/0021998312440131.

[36] D. Casari, "Out-of-Autoclave Bonded Repairs for Composite Structures in Aircrafts", Master's thesis, McGill University, Montreal, QC, Mar. 2016.

[37] T. Centea and P. Hubert, "Measuring the impregnation of an out-of-autoclave prepreg by micro-CT", *Composites Science and Technology*, vol. 71, no. 5, pp. 593–599, Mar. 2011. DOI: 10.1016/j.compscitech.2010.12.009.

[38] T. A. Cender, P. Simacek, and S. G. Advani, "Gas Permeability of Partially Saturated Fabrics", in *Proc. 19th International Conf. Composite Materials*, Montreal, QC, 2013.

[39] F. C. Campbell, "Chapter 2 - Fibers and Reinforcements: The String That Provides the Strength", in *Manufacturing Processes for Advanced Composites*, Amsterdam, NL: Elsevier, 2004, pp. 39–62.

[40] L. K. Grunenfelder and S. R. Nutt, "Void formation in composite prepregs – Effect of dissolved moisture", *Composites Science and Technology*, Metal Matrix Composites Reinforced with Nano-sized Reinforcements, vol. 70, no. 16, pp. 2304–2309, Dec. 2010. DOI: 10.1016/j.compscitech.2010.09.009.

[41] K. R. Bernetich, T. J. Gonze, G. N. Bachman, and L. D'Astuto, "Out-of-Autoclave Materials, Applications for Composite Laminate Repair", in *SAMPE TECHNICAL CONF. Proc.*, Baltimore, MD, 2012.

[42] M. Préau and P. Hubert, "Bonded Repairs of Honeycomb Sandwich Structures: Process Monitoring and Quality Assessment", in *Proc. 20th International Conf. on Composite Materials*, Copenhagen, DK, Jul. 2015.

[43] *CYCOM 5320 Toughened Epoxy Information Sheet*, 2009.

[44] "Curable prepregs with surface openings", pat. US20140174632A1, Dec. 2013. (visited on 03/09/2017).

[45] J. Kratz and P. Hubert, "Anisotropic air permeability in out-of-autoclave prepregs: Effect on honeycomb panel evacuation prior to cure", *Composites Part A: Applied Science and Manufacturing*, vol. 49, pp. 179–191, Jun. 2013. DOI: 10.1016/j.compositesa.2013.02.013.

[46] *CYCOM 977-2 Toughened Epoxy Resin Technical Datasheet*, 1995.

[47] A. Jumahat, C. Soutis, F. R. Jones, and A. Hodzic, "Fracture mechanisms and failure analysis of carbon fibre/toughened epoxy composites subjected to compressive loading", *Composite Structures*, vol. 92, no. 2, pp. 295–305, Jan. 2010. DOI: 10.1016/j.compstruct.2009.08.010.

[48] *FM 300-2 Film Adhesive Technical Datasheet*, 2011.

[49] *Epocast 52 A/B Epoxy Laminating System Datasheet*, 2006.

[50] *Loctite EA 9390 Aero Epoxy Paste Adhesive Datasheet*, 2013.

[51] R. Cochran, R. Traboco, P. A. Mehrkam, and M. DiBerardino, "Field Repair Materials for Naval Aircraft", in *Proc. 79th Meeting of the AGARD Structures and Materials Panel on Composite Repair of Military Aircraft Structures*, Seville, Spain, 1994.

[52] AMS2980 (2000), *Technical Specification: Carbon Fiber Fabric and Epoxy Resin Wet Lay-Up Repair Material*, 2000, [Online]. Available: https://saemobilus.sae.org/content/AMS2980.

[53] *Composite Materials Handbook Volume 2: Polymer Matrix Composites Material Properties*, ser. Composite Materials Handbook CMH-17. SAE International, 2012, vol. 2.

[54] L. J. Buckley, R. E. Trabocco, and E. L. Rosenzweig, "Non-Autoclave Processing for Composite Material Repair", Naval Air Warfare Center, Warminster, PA, Tech. Rep. NADC-83084-60, 1983.

[55] M. F. Diberardino, J. Dominguez, and R. Cochran, "Bonded Field Repair Concepts Using Ambient Storable Materials", in *Closed Proc. 34th SAMPE Symposium*, Reno, NV, 1989.

[56] G. R. Sherwin, "Non-autoclave processing of advanced composite repairs", *International Journal of Adhesion and Adhesives*, vol. 19, no. 2, pp. 155–159, Apr. 1999. DOI: 10.1016/S0143-7496(98)00030-X.

[57] P. H. Wang, "The Comparison of Composite Aircraft Field Repair Method (CAFRM) with Traditional Aircraft Repair Technologies", Ph.D. thesis, Purdue University, 2013.

[58] T. Hou and B. Jensen, "Double-vacuum-bag technology for volatile management in composite fabrication", en, *Polymer Composites*, vol. 29, no. 8, pp. 906–914, Aug. 2008. DOI: 10.1002/pc.20475.

[59] M. W. Evens, K. E. Nelson, J. F. Spalding Jr., J. D. Chanes, J. P. Baldwin, and P. S. Rutherford, "Systems and Methods for On-Aircraft Composite Repair Using Double Vacuum Debulking", pat. US8986479B2, Sep. 2010. (visited on 05/24/2017).

[60] B. Rutan, *Moldless Composite Homebuilt Sandwich Aircraft Construction*, 3rd edition. Mojave, CA: Rutan Aircraft Factory Inc., 1983.

[61] F. Aird, *Fiberglass & composite materials: An enthusiast's guide to high performance nonmetallic materials for automotive racing and marine use*, English. New York: HP Books, 1996, OCLC: 33104613.

[62] L. G. Stringer, "Optimization of the wet lay-up/vacuum bag process for the fabrication of carbon fibre epoxy composites with high fibre fraction and low void content", *Composites*, vol. 20, no. 5, pp. 441–452, Sep. 1989. DOI: 10.1016/0010-4361(89)90213-9.

[63] D. Cripps, T. J. Searle, and J. Summerscales, "2.21 - Open Mold Techniques for Thermoset Composites", in *Comprehensive Composite Materials*, A. Kelly and C. Zweben, Eds., Oxford: Pergamon, 2000, pp. 737–761. DOI: 10.1016/B0-08-042993-9/00188-1.

[64] B. A. Burroughs, R. L. Hunziker, T. McGann, G. Hanneman, and J. Rosenthal, "Manufacturing Technology for Nonautoclave Fabrication of Composite Structures", Rockwell International, Los Angeles, CA, Tech. Rep. NA-85-1212L, 1985.

[65] T. Harris, *Commercial Aircraft Composite Repair Committee (CACRC) ATA/IATA/SAE*.

[66] ARP 4991A (2014), *Core Restoration of Thermosetting Composite Components*, 2014, [Online]. Available: https://saemobilus.sae.org/content/ARP4991A.

[67] ARP 5089 (2011), *Composite Repair NDT/NDI Handbook*, 2011, [Online]. Available: https://saemobilus.sae.org/content/ARP5089.

[68] AMS3970A (2016), *Carbon Fiber Fabric Repair Prepreg,* 120°*C Vacuum Curing Part*, 2016, [Online]. Available: https://saemobilus.sae.org/content/AMS3970A.

[69] J. Tomblin, L. Salah, J. M. Welch, and M. D. Borgman, "Bonded repair of aircraft composite sandwich structures", U.S. Department of Transportation - Federal Aviation Administration, Washington, DC, Tech. Rep. DOT/FAA/AR-03/74, 2004.

[70] R. S Davé and A. C Loos, Eds., *Processing of composites*, English. Munich; Cincinnati: Hanser Publishers ; Hanser/Gardner Publications, 2000.

[71] R. K. Roy, *A primer on the Taguchi method*, English. Dearborn, MI: Society of Manufacturing Engineers, 2010, OCLC: 551122799.

[72] K. Dehnad, *Quality control, robust design, and the Taguchi method*, English. Pacific Grove, Calif.: Wadsworth & Brooks/Cole Advanced Books & Software, 1989, OCLC: 581846118.

[73] D. S. Moore and G. P. McCabe, *Introduction to the practice of statistics*, English. New York: Freeman, 1993, OCLC: 26129272.

[74] T. Sellke, M. J. Bayarri, and J. O. Berger, "Calibration of p values for testing precise null hypotheses", *American Statistician*, vol. 55, no. 1, pp. 62–71, Feb. 2001. DOI: 10.1198/000313001300339950.

[75] R. K. Roy, *Design of experiments using the Taguchi approach: 16 steps to product and process improvement*, English. New York: Wiley, 2001, OCLC: 43894329.

[76] *Composite Materials Handbook Volume 1: Polymer Matrix Composites Guidelines for Characterization of Structural Materials*, ser. Composite Materials Handbook CMH-17. SAE International, Jul. 2012, vol. 1.

[77] J. L. Kardos, "Chapter 6: Void Growth and Dissolution", in *Processing of Composites*, R. S Davé and A. C Loos, Eds., Cincinnati, OH: Hanser/Gardner Publications, Inc., 2000.

[78] M. R. Wisnom, T. Reynolds, and N. Gwilliam, "Reduction in interlaminar shear strength by discrete and distributed voids", *Composites Science and Technology*, vol. 56, no. 1, pp. 93–101, Jan. 1996. DOI: 10.1016/0266-3538(95)00128-X.

[79] M. L. Costa, S. F. M. de Almeida, and M. C. Rezende, "The influence of porosity on the interlaminar shear strength of carbon/epoxy and carbon/bismaleimide fabric laminates", *Composites Science and Technology*, vol. 61, no. 14, pp. 2101–2108, Nov. 2001. DOI: 10.1016/S0266-3538(01)00157-9.

[80] P. Olivier, J. P. Cottu, and B. Ferret, "Effects of cure cycle pressure and voids on some mechanical properties of carbon/epoxy laminates", *Composites*, vol. 26, no. 7, pp. 509–515, Jul. 1995. DOI: 10.1016/0010-4361(95)96808-J.

[81] ASTM D2344-16 (2016), *Standard Test Method for Short-Beam Strength of Polymer Matrix Composite Materials and Their Laminates*, West Conshohocken, PA, 2016, [Online]. Available: www.astm.org.

[82] M. Xie and D. F. Adams, "Study of three- and four-point shear testing of unidirectional composite materials", *Composites*, vol. 26, no. 9, pp. 653–659, Sep. 1995. DOI: 10.1016/0010-4361(95)98914-7.

[83] W. R. Broughton, "8 - Through-thickness testing", in *Mechanical Testing of Advanced Fibre Composites*, ser. Woodhead Publishing Series in Composites Science and Engineering, J. M. Hodgkinson, Ed., Woodhead Publishing, 2000, pp. 143–169. DOI: 10.1533/9781855738911.143.

[84] R. Thévenin, *Airbus Composite Structures: Perspectives on safe maintenance practice*, Amsterdam, NL, May 2007.

[85] A Kelly and C. H. Zweben, *Comprehensive composite materials*, English. Amsterdam; New York: Elsevier, 2000.

[86] ASTM D7028-07 (2015), *Standard Test Method for Glass Transition Temperature (DMA Tg) of Polymer Matrix Composites by Dynamic Mechanical Analysis (DMA)*, West Conshohocken, PA, 2015, [Online]. Available: www.astm.org.

[87] C. Blohm, *Lufthansa Perspectives on Safe Composite Maintenance Practices*, May 2007.

[88] A. J. Gunnion and I. Herszberg, "Parametric study of scarf joints in composite structures", *Composite Structures*, Thirteenth Int. Conf. Composite Structures, vol. 75, no. 1–4, pp. 364–376, Sep. 2006. DOI: 10.1016/j.compstruct.2006.04.053.

[89] *FM 410-1 Core Splice Foam Technical Datasheet*, 2010.

[90] S. M. Sabzevari, S. Alavi-Soltani, and B. Minaie, "New method for estimating the extent of curing of thermosetting prepregs", en, *Journal of Applied Polymer Science*, vol. 121, no. 2, pp. 883–891, Jul. 2011. DOI: 10.1002/app.33616.

[91] S. Alavi-Soltani, S. Sabzevari, H. Koushyar, and B. Minaie, "Thermal, rheological, and mechanical properties of a polymer composite cured at different isothermal cure temperatures", English, *Journal of Composite Materials*, vol. 46, no. 5, pp. 575–587, Mar. 2012. DOI: 10.1177/0021998311415443.

[92] A. N. Rider, C. H. Wang, and P. Chang, "Bonded repairs for carbon/BMI composite at high operating temperatures", *Composites Part A: Applied Science and Manufacturing*, vol. 41, no. 7, pp. 902–912, Jul. 2010. DOI: 10.1016/j.compositesa.2010.03.006.

[93] G. S. Springer and S.-H. Ahn, "Repair of Composite Laminates", US Department of Transportation Federal Aviation Administration, Washington, DC, Tech. Rep. DOT/FAA/AR-00/46, 2000.

[94] R. B. Pipes and D. W. Adkins, "Strength and Mechanics of Bonded Scarf Joints for Repair of Composite Materials", Tech. Rep., Dec. 1982. (visited on 11/18/2016).

[95] J. Tomblin, L. Salah, C. Davies, and L. Pham, "CACRC Depot Bonded Repair Investigation - Round Robin Testing", in *FAA JOINT ADVANCED MATERIALS & Structures (JAMS) Center of Excellence 8th Annual Technical Review Meeting*, Baltimore, MD, Apr. 2012.

[96] ASTM D3518-13 (2013), *Standard Test Method for In-Plane Shear Response of Polymer Matrix Composite Materials by Tensile Test of a +/- 45 degree Laminate*, West Conshohocken, PA, 2013, [Online]. Available: www.astm.org.

[97] ASTM D7249-12 (2015), *Standard Test Method for Facing Properties of Sandwich Constructions by Long Beam Flexure*, West Conshohocken, PA, 2015, [Online]. Available: www.astm.org.

[98] W. Rust, *Non-linear finite element analysis in structural mechanics*, English. 2015, OCLC: 903685469.

[99] R. Hilgers, *Substantiation of Damage Growth within Sandwich Structures*, Tokyo, JP, Jun. 2009.

[100] R. R. Butukuri, V. P. Bheemreddy, K. Chandrashekhara, T. R. Berkel, and K. Rupel, "Evaluation of skin-core adhesion bond of out-of-autoclave honeycomb sandwich structures", English, *Journal of Reinforced Plastics and Composites*, vol. 31, no. 5, pp. 331–339, Mar. 2012, WOS:000300496700006. DOI: 10.1177/0731684412437267.

[101] S. M. Grove, E. Popham, and M. E. Miles, "An investigation of the skin/core bond in honeycomb sandwich structures using statistical experimentation techniques", *Composites Part A: Applied Science and Manufacturing*, vol. 37, no. 5, pp. 804–812, May 2006. DOI: 10.1016/j.compositesa.2005.07.005.

[102] R. Okada and M. T Kortschot, "The role of the resin fillet in the delamination of honeycomb sandwich structures", *Composites Science and Technology*, vol. 62, no. 14, pp. 1811–1819, Nov. 2002. DOI: 10.1016/S0266-3538(02)00099-4.

[103] S. S. Tavares, N. Caillet-Bois, V. Michaud, and J. A. E. Månson, "Vacuum-bag processing of sandwich structures: Role of honeycomb pressure level on skin–core adhesion and skin quality", *Composites Science and Technology*, vol. 70, no. 5, pp. 797–803, May 2010. DOI: 10.1016/j.compscitech.2010.01.015.

[104] J. Rion, Y. Leterrier, and J.-A. E. Månson, "Prediction of the adhesive fillet size for skin to honeycomb core bonding in ultra-light sandwich structures", *Composites Part A: Applied Science and Manufacturing*, vol. 39, no. 9, pp. 1547–1555, Sep. 2008. DOI: 10.1016/j.compositesa.2008.05.022.

[105] L. C. Thomas, "Modulated DSC Paper 5 - Measurement of Glass Transitions and Enthalpic Recovery", TA Instruments, New Castle, DE, Tech. Rep. TP 010, 2005.

[106] M. J. Parker, "5.09 - Test Methods for Physical Properties", in *Comprehensive Composite Materials*, A. Kelly and C. Zweben, Eds., Oxford: Pergamon, 2000, pp. 183–226. DOI: 10.1016/B0-08-042993-9/00074-7.

[107] P. S. Gill, S. R. Sauerbrunn, and M. Reading, "Modulated differential scanning calorimetry", *Journal of Thermal Analysis*, vol. 40, no. 3, pp. 931–939, 1993. DOI: 10.1007/BF02546852.

[108] A. A. Lacey, C. Nikolopoulos, and M. Reading, "A mathematical model for Modulated Differential Scanning Calorimetry", *Journal of thermal analysis*, vol. 50, no. 1, pp. 279–333, 1997. DOI: 10.1007/BF01979568.

[109] ASTM E1356-08 (2014), *Standard Test Method for Assignment of the Glass Transition Temperatures by Differential Scanning Calorimetry*, West Conshohocken, PA, 2014, [Online]. Available: www.astm.org.

[110] K. Bujun and P. Hubert, "Analytical Heat Transfer Modelling for In-Situ Bonded Scarf Repairs of Monolithic Composite Panels", in *SAMPE TECH. Conf. Proc.*, Seattle, WA, 2014.

[111] T. A. Bogetti and J. W. Gillespie, "Process-Induced Stress and Deformation in Thick-Section Thermoset Composite Laminates", *Journal of Composite Materials*, vol. 26, no. 5, pp. 626–660, Mar. 1992. DOI: 10.1177/002199839202600502.

[112] G. Fernlund, N. Rahman, R. Courdji, M. Bresslauer, A. Poursartip, K. Willden, and K. Nelson, "Experimental and numerical study of the effect of cure cycle, tool surface, geometry, and lay-up on the dimensional fidelity of autoclave-processed composite parts", *Composites Part A-Applied Science and Manufacturing*, vol. 33, no. 3, pp. 341–351, 2002. DOI: 10.1016/S1359-835X(01)00123-3.

[113] J. Kratz, M. Genest, M. Préau, and P. Hubert, "Vacuum-Bag-Only Prepreg Processing of Honeycomb Structures: From Lab-Scale Experiments to an Aircraft Demonstrator", in *Proc. SAMPE Conf. and Exhibition*, Seattle, WA, 2014.

[114] J. Kratz and P. Hubert, "Vacuum Bag Only Manufacturing of Honeycomb Sandwich Panels", in *Int. Conf. Composite Materials (ICCM) 19*, Montreal, QC, 2013.

[115] ——, "Vacuum-bag-only co-bonding prepreg skins to aramid honeycomb core. Part II. In-situ core pressure response using embedded sensors", English, *Composites Part a-Applied Science and Manufacturing*, vol. 72, pp. 219–227, May 2015. DOI: 10.1016/j.compositesa.2014.11.030.

[116] K. M. Nelson, K. S. Willden, A. Poursartip, and M. D. Lane, "Collection of Process Data Using In-Situ Sensors", pat. US 8,833,144 B2, Sep. 2014.

[117] J. Kratz and P. Hubert, "Vacuum bag only co-bonding prepreg skins to aramid honeycomb core. Part I. Model and material properties for core pressure during processing", English, *Composites Part a-Applied Science and Manufacturing*, vol. 72, pp. 228–238, May 2015. DOI: 10.1016/j.compositesa.2014.11.026.

[118] R. Adams and P. Cawley, "A Review of Defect Types and Nondestructive Testing Techniques for Composites and Bonded Joints", English, *Ndt International*, vol. 21, no. 4, pp. 208–222, Aug. 1988, WOS:A1988P549700002. DOI: 10.1016/0308-9126(88)90333-1.

[119] C. H. Wang and C. N. Duong, "Chapter 10 - Non-destructive evaluation of bond quality", in *Bonded Joints and Repairs to Composite Airframe Structures*, Oxford: Academic Press, 2016, pp. 265–285. DOI: 10.1016/B978-0-12-417153-4.00010-4.

[120] B. R. Tittmann and R. L. Crane, "5.12 - Ultrasonic Inspection of Composites", in *Comprehensive Composite Materials*, A. Kelly and C. Zweben, Eds., Oxford: Pergamon, 2000, pp. 259–320. DOI: 10.1016/B0-08-042993-9/00201-1.

[121] S. S. Tavares, N. Caillet-Bois, V. Michaud, and J. A. E. Månson, "Non-autoclave processing of honeycomb sandwich structures: Skin through thickness air permeability during cure", *Composites Part A: Applied Science and Manufacturing*, vol. 41, no. 5, pp. 646–652, May 2010. DOI: 10.1016/j.compositesa.2010.01.013.

[122] C. Kassapoglou, S. Fantle, and J. Chou, "Wrinkling of Composite Sandwich Structures Under Compression", *Journal of Composites Technology & Research*, vol. 17, no. 4, pp. 308–316, Oct. 1995, WOS:A1995TC99400004.

[123] H. Ullah, A. R. Harland, R. Blenkinsopp, T. Lucas, D. Price, and V. V. Silberschmidt, "Analysis of nonlinear shear deformations in CFRP and GFRP textile laminates", in *Advances in Experimental Mechanics Viii*, R. L. Burguete, M. Lucas, E. A. Patterson, and S. Quinn, Eds., vol. 70, Durnten-Zurich: Trans Tech Publications Ltd, 2011.

[124] J. Jankowsky, D. Wong, M. Diberardino, and R. Cochran, "Evaluation of Upper Use Temperature of Toughened Epoxy Composites", in *Assignment of the Glass Transition*, R. J. Seyler, Ed., vol. 1249, West Conshohocken, PA: American Society for Testing and Materials, 1994, pp. 277–292.

[125] M. Akay, "Aspects of Dynamic Mechanical Analysis in Polymeric Composites", *Composites Science and Technology*, vol. 47, no. 4, pp. 419–423, 1993. DOI: 10.1016/0266-3538(93)90010-E.

[126] J. L. Thomason, "Investigation of composite interphase using dynamic mechanical analysis: Artifacts and reality", *Polymer Composites*, vol. 11, no. 2, pp. 105–113, Apr. 1990. DOI: 10.1002/pc.750110206.

[127] P. S. Theocaris and G. C. Papanicolaou, "Variation of glass transition temperature with direction in unidirectional glass fiber-reinforced composites", *Colloid and Polymer Science*, vol. 258, no. 9, pp. 1044–1051, Sep. 1980. DOI: 10.1007/BF01382400.